EFFECTS OF SHAPE AND MATERIAL MISMATCH ON 2D FINITE DOMAINS CONTAINING INCLUSIONS

by

Chunlin Pan

Bachelor in Engineering, Harbin Institute of Engineering, 2005

Master in Science, Tsinghua University, 2011

Submitted to the Graduate Faculty of

Swanson School of Engineering in partial fulfillment

of the requirements for the degree of

Doctor of Philosophy

University of Pittsburgh

2016

UNIVERSITY OF PITTSBURGH

SWANSON SCHOOL OF ENGINEERING

This dissertation was presented

by

Chunlin Pan

It was defended on

November 1, 2016

and approved by

Qiang Yu, Ph.D., Assistant Professor,

Department of Civil and Environmental Engineering, University of Pittsburgh

Jeen-Shang. Lin, Sc.D., Associate Professor,

Department of Civil and Environmental Engineering, University of Pittsburgh

Albert To, Ph.D., Associate Professor,

Department of Mechanical Engineering and Material Science, University of Pittsburgh

Luis Vallejo, Ph.D., Professor,

Department of Civil and Environmental Engineering, University of Pittsburgh

Dissertation Director: Qiang Yu, Ph.D., Assistant Professor,

Department of Civil and Environmental Engineering, University of Pittsburgh

EFFECTS OF SHAPE AND MATERIAL MISMATCH ON 2D FINITE DOMAINS CONTAINING INCLUSIONS

Chunlin Pan, PhD

University of Pittsburgh, 2016

To develop a sustainable built environment, a realistic prediction of critical structures residing on a microstructure-based approximation of the material behavior is of great importance. Characterization of the elastic fields inside representative volume elements (RVEs) is the key to accomplish this approximation. In this research, an investigation is carried out to seek for the solutions of 2D bounded RVEs containing homogeneous and inhomogeneous inclusions. Based on the fundamental works by Muskhelishvilli (1953) on Riemann Hilbert Problem, the complex potential formulation is employed to analytically investigate the disturbance inside the finite domain induced by the material mismatch or eigenstrains. According to Sokhotski-Plemelj Theorem, the potentials in the inclusions and the matrix are constructed in the form of Laurent series at the center of each corresponding domain. Then with the help of the independence of the linear group of exponential terms, the interfacial condition of continuity and equilibrium between the inclusions and the matrix, as well as the exterior Dirichlet boundary conditions, can be explicitly expressed as algebraic equations, which lead to the identification of the coefficients in the Laurent series. The shape effect of the bounded matrix is also captured by coupling this approach with conformal mapping strategy. To study the complicatedly shaped inclusions, the singly connected curves of interfaces are replaced with piecewise straight lines to simplify the evaluation of boundary integrals. The analytical solution obtained can provide a deep understanding of the RVEs on capturing the local elastic fields at the micro-scale as well as on

estimating the overall effective elastic moduli at the macro-scale. The obtained solutions are documented in this dissertation and can be applied directly in a wide variety of engineering applications, which include the homogeneous inclusions with arbitrary shapes and inhomogeneous inclusions with multi-layers structure.

TABLE OF CONTENTS

LIST OF TABLES

LIST OF FIGURES

PREFACE

Thanks to my advisor and chair of my graduate committee Dr. Qiang Yu for his consistent help and unbelievable patience during my PhD study at PITT.

Great appreciation to Dr. Albert To, Dr. Jeen-Shang Lin and Dr. Luis Vallejo for their inspiring suggestions on my research and service in my graduate committee.

Thanks to the deepest love from my mother.

1.0 INTRODUCTION

Inclusion problem, as one of the fundamental problems in contemporary composite mechanics and micromechanics, has been attracting increasing attentions in a wide range of engineering applications with the advances in nano-science and nano-technologies. The physical phenomena, which stem from the inclusion problem, are not rare in engineering practice. For example, a certain region of a continuum undergoes a spontaneous change, which could be trigged by either material properties or eigenstrains representing manufacturing defects, thermal expansion or plastic flow. This region would deform freely. Because of the presence of the surrounding intact material, the distortion of elastic fields will appear both inside and outside the region. It seems like the elastic fields are disturbed by the initial change inside the region, which is generally named as an inclusion. In general, the inclusion problem is about the disturbance of the elastic fields. This study is dedicated to developing a systematic approach to solve this problem in 2D domains despite the complex geometry and severe material mismatch. Built upon the systematical framework, some possible applications of the analytical solutions will be discussed as well.

1.1 MOTIVATION AND BACKGROUND

In engineering applications, when modeling the behavior of composite materials, two approaches are in general widely adopted. One analyzes material elements at macroscale that is sufficiently large compared to the microstructural length scale and therefore it treats the material as a homogeneous one with spatially constant average or overall properties. For example, based on Hashin and Shtrikman's variational principle (1962a, b), the upper and lower bounds on the overall constitutive modulus can be obtained. This approach works well for the evaluation of the global behavior of composite materials but cannot lead to the accurate solution of the elastic fields in the Representative Volume Elements (RVEs), which are critical for the prediction of structural response under different loadings. For example, for concrete creep, the macroscale approach is not able to capture the essential physical mechanisms within concrete microstructure. On the contrary, the other approach is focused on the analysis of the strongly heterogeneous microstructures of composite materials. In order to avoid the tedious specimen-specific calculations, the microstructures of composite materials are idealized as a homogeneous matrix containing homogeneous or inhomogeneous inclusions, and sometimes even as simple as a RVE with a single inclusion; e.g., see Figure 1.1:

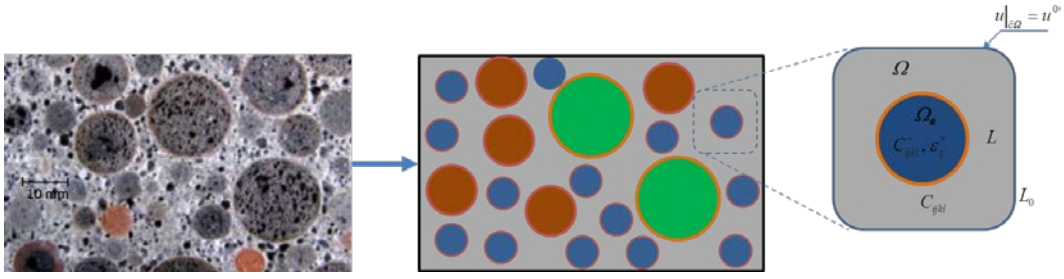

Figure 1.1. Concrete Mesostructure and its idealization

In order to capture the real response of the RVE, it is essential to solve the disturbance of the elastic fields induced by the inclusions and inhomogeneities inside it. As one of the fundamental problems in contemporary composite mechanics and micromechanics, it has been attracting increasing attentions in diverse areas and problems of physical science. Following the nomenclature introduced by Mura (1987), there are two types of problems for the disturbance in the RVEs.

Eshelby's first problem: The inclusion and the surrounding matrix share the same elastic properties and the disturbance is induced by the eigenstrain within the inclusion (Figure 1.2a). The eigenstrain can be triggered by a variety of mechanical and physical activations, for example, thermal expansion, plastic strain, magnetomechanical and optical excitation, lattice mismatch, to name a few. Conventionally, this is also called inclusion problem; and

Eshelby's second problem: The inclusion and its hosting matrix have different elastic properties and the inclusion is now referred as an inhomogeneity. The sources of inhomogeneity include material mismatch, cavity, defects, crack, and so forth. In this work, the inhomogeneity problem is limited to material mismatch. If an eigenstrain resulting from the physical changes listed in the Eshelby's first problem is allowed within the inhomogeneity, then the problem is also referred as inhomogeneous inclusion problem (Figure 1.2b).

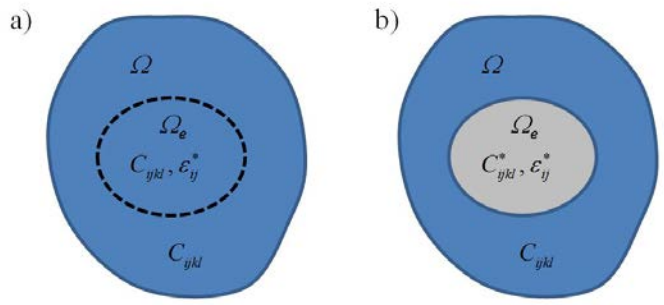

Figure 1.2. a) Inclusion problem and b) inhomogeneous inclusion problem

The inclusion problem was initially examined by Mott and Nabarro (1940) and Frenkel (1946), but the real breakthrough was made by Eshelby (1957), who, by using what has been called Point Force method, determined the elastic field of an ellipsoidal inclusion embedded in an unbounded ambient space. In Eshelby's ellipsoidal inclusion solution, the disturbance in both the matrix and inclusion can be elegantly expressed by the eigenstrain based on the classical Eshelby's tensor (Eshelby 1957, 1959, 1962). Since this pioneer and inspirational work, significant progress has been made in understanding the elastic inclusion problem in an infinite domain by taking into account the inclusion shape, anisotropy, non-uniform eigenstrain, and bond slip (Jaswon and Bhargava 1958, List and Silberstein 1966, Nozaki and Taya 1997, 2001, Mura et al. 1985, Rodin 1996, Ru 2003, Luo and Weng 1987).

With the advance in materials science, nano-technology and micromechanics, the Eshelby's formulation based on Green's function and its extension are penetrating into the regime of nano-scale to analyze the disturbance in nanocomposite solids. Makeev et al (2003) found that the inclusion strain obtained by linear elasticity theory coincides with the atomistic calculation if the inclusion size exceeds 5 interatomic distances. Then Sharma and Ganti (2004)

refined Eshelby's solution by considering the surface-interface stress which is prominent for nano-sized inclusions. In addition, the shape effect of the nano-sized inclusion is extensively investigated for an unbounded domain (Andreev and O'Reilly 2000).

However, Eshelby's formulation is effective only when the surrounding matrix is unbounded or the volume of the inclusion is negligible when compared to the size of the RVE. In real applications, there is no infinite RVE, and in many cases including the nanocomposites, the volume ratio of the inclusion to the RVE is not negligible. As a result of the finite volume fraction ratio of the inclusion to matrix, the solutions derived from an infinite RVE cannot realistically capture the disturbance induced by the inclusion and correspondingly, the elastic field determined is no longer accurate. This limitation obstructs calculation of mechanical strength, determination of local response and prediction of damage initiation. Furthermore, the important homogenization schemes including the Mori-Tanaka method (Mori and Tanaka 1973, Weng 1990) and the self-consistent method (Hill 1965, Huang et al. 1994) can no longer be directly used to estimate the global properties and responses of the composite solids.

To circumvent this obstacle, analytical solutions of the inclusion problem in a finite domain are indispensible. The initial attempts, including the work by Kinoshita and Mura (1984), Kröner (1986, 1990), and Kirchner and Ni (1993), were focused on Green's function in a finite domain. Unfortunately, their effort leads to no analytical solution because of the formidable nature of solving the Green's function in a finite domain. Alternatively, Jaswon and Bhargava (1960) as well as List and Silberstein (1967) switched to the complex potential method to bypass the mathematical difficulty presented in Green's function. They examined the 2D elastic inclusion problem, but did not give any explicit expression for the elastic field of a finite domain. Recently, a modified Eshelby's tensor for a finite domain has been proposed by Li and his

coworkers (Li et al 2005, Wang et al 2005, Li et al 2007a, b) by taking advantage of the Somigliana's identity and Green's function in an infinite domain in their analytical derivation. Similar Eshelby's tensor for a finite domain was subsequently obtained by Gao and his colleague (2010, 2011) using strain gradient elasticity theory. In the solutions by Li et al (2005, 2007a, b) and Wang et al (2005), an inventive hypothesis has been adopted that the circumference basis of the Eshelby's tensor of an isotropic finite domain is similar to that of the Eshelby's tensor in an isotropic infinite domain. This postulate, which enables solving the Fredholm type integral equation in an analytic way, is later found only effective for the concentric configuration. It will not hold when the RVE is no longer displaying geometrical characteristics similar to a concentric configuration, and thus cannot be extended to a finite RVE of arbitrary shape, e.g., a squared RVE, a hexagonal RVE or a polygonal inclusion.

Compared to inclusion problem, the inhomogeneity problem is more challenging because it can be deemed as a more general case of inclusion problem. For infinite domain, the primary difficulty in solving inhomogeneity problem is to construct a proper equivalent eigenstrain within the domain occupied by the inhomogeneity. Based on Eshelby's conjecture, in an unbounded domain, the strain and stress in an ellipsoidal inclusion is uniform for an arbitrary uniform eigenstrain. Therefore, there is no theoretical difficulty to treat the inhomogeneity problem as an inclusion problem by using equivalent inclusion method (EIM) as long as the inhomogeneity is ellipsoidal and the surrounding matrix is unbounded (Eshelby 1957, Mura 1987). If the inhomogeneity size is approaching nano-scale, the effectiveness of EIM will be further narrowed to inclusions with a constant curvature (e.g., sphere in 3D and cylinder in 2D) because of the surface-interface stress (Sharma and Ganti 2004). For those without constant curvature, only approximate solutions are available (Sharma and Wheeler 2007). Therefore, for

inhomogeneities of complex shape, EIM is generally not effective even for unbounded domain because uniform equivalent eigenstrain and stress is not available (Waldvogel 1979, Rodin 1996, Nozaki and Taya, 2001). Therefore, more complicated methods based on Green's function combined with surface/volume integral evaluation of harmonic and bi-harmonic potentials (Kuvshinov 2008) or dislocation loop (Li and Anderson 2001) have to be employed.

If the RVE is bounded, the Eshelby's conjecture may not hold even for ellipsoidal inclusions due to the influence of complicated boundary conditions. In this case, the size and shape of the RVE must be taken into account in formulating the solution to the boundary value problems of the RVE, which is a formidable challenge for analytical approaches residing on Green's function and integral evaluation. There is very limited information about the elastic fields of inhomogeneity problem in a finite domain, except for some extremely special cases, e.g., a concentric configuration under hydrostatic eigenstrain or loading. Therefore, FEM and other numerical approaches are frequently employed to handle inclusion and inhomogeneity problems in finite domains (Shodja et al. 2006). However, numerical approach, effective for individual analysis, is not capable of providing the basic physical insights of the fundamentals governing the local and global property and response of the composite solids, which are essential for developing innovative composites.

In view of the challenges existing in Eshelby's formulation, increasing efforts are invested in seeking for alternative approaches that are capable of tackling the mathematical difficulties brought up by the geometry of the RVE. For example, following the specified stress function formulation proposed by Christensen and Lo (1979), Luo and Weng (1987) formulated the elastic fields for a 3-phase 3D inclusion problem with the third phase (i.e., the exterior matrix) being unbounded. This implicitly provides analytical solutions for inhomogeneity

problem in a finite domain of the 2 interior phases forming a concentric configuration in 2 limiting cases: 1) free boundary if the third phase is infinitely soft and 2) fixed boundary if the third phase is perfectly rigid. Then Ru (1999, 2000, 2001) worked on 2D inclusions of complex shape in infinite domain based on complex potential method. Recently, Zou et al (2012) further analyzed the inclusion problem in a finite domain based on complex potential method for a circular RVE. However, for Zou et al's solutions, a suspicious displacement/stress singularity exists when a point is approaching the origin ($z = 0$). This is due to the fact that in their solutions, terms of 1/z appear in the governing potentials. In addition, the analytical solutions of inclusion problems for 2D RVEs of shapes other than circle are still not available. Further limited information exists for inhomogeneity problem in a finite domain.

Based on the discussion above, the primary aim of this research is set to advance the basic science behind the fundamental rules governing the disturbance induced by inclusion and inhomogeneity in a finite RVE of specific shape. Thus, the objectives are all built toward searching for mathematical tools to establish a theoretical platform for complicatedly shaped domains.

To accomplish the proposed goal, complex potential method is first selected to analyze the 2D inclusion and inhomogeneity problems. Due to its efficiency shown in handling various boundary value problems (Ru 1999, 2000, 2001, Zou et al. 2012), the complex potential method is powerful in tackling 2D elastic problems if the potential functions are correctly constructed. The work by Pan and Yu (2014, 2015) shows that without any postulate on the geometrical property of RVE boundary, the complex potential method reproduces the analytical solutions for inclusion problem proposed by Li and his coworkers (Li et al 2005) based on Green’s function formulation, for which a hypothesis only effective for concentric configuration must be used. In

the rest part of this research, this theoretical framework of analysis will be further developed to handle the problems have inhomogeneous inclusions, multi-phases RVEs, interactions among the spatially separated multiple inclusions and complicatedly shaped boundaries. The conformal mapping strategy will be employed to simplify the investigation of the boundary conditions.

In summary, the boundary value problems brought up by the geometry of the finite RVE will be tackled by complex potential functions in 2D domain. The current work shows promising results for 2D finite domain problems, and great potentials to be extended for multi-inhomogeneity problems in finite domains.

1.2 COMPLEX POTENTIAL METHOD

In this section, the mathematical fundament of this research, the complex potential method will be briefly explained. The complex potential method refers to the construction of governing potential functions depending on a single complex variable *z*, which uses its real and imaginary parts to represent a point in the 2D domain. In fact, the driving force behind many of the applications of complex potential method is the notable connection between complex functions and the solutions of the planar Laplace equations. For example, in plane theory of elasticity, the stress field can be expressed by means of a single Airy stress function ϕ, which is the solution of a Laplace equation and in general biharmonic. Theoretically, every biharmonic function of the two variables *x* and *y* may be represented in a simpler manner with the help of two complex functions φ and ψ, which are conventionally denoted as complex potentials. Then the Airy stress function is written as

$$\phi = \mathrm{Re}\left\{\overline{z}\varphi(z) + \chi(z)\right\} \tag{1.1}$$

where $z = x + iy$, $\chi(z)$ is an artificial complex function related to $\psi(z)$ by $\psi(z) = \frac{d\chi}{dz}$, and Re means the real part of a complex number. Consequently, the elastic fields within the 2D domain can be expressed in the form of complex potentials as follows:

$$u + iv = \frac{1}{2\mu}\left(\kappa\varphi(z) - z\overline{\varphi'(z)} - \overline{\psi(z)}\right) \tag{1.2}$$

where *u* and *v* are displacement in *x* and *y* direction, respectively; μ is the shear modulus and κ is the Kolosov constant defined as $3-4\nu$ for plain strain and $(3-\nu)/(1+\nu)$ for plain stress problem. The notation will be used in the following sections and chapters.

For plane elastic problem, writing the displacement field in the form of Eq. (1.2) is of great importance in that some characteristics of the complex functions are well known and can be employed directly. For example, for the inclusion problems in a finite domain, the complex potentials are in general sectionally holomorphic in the inclusion and the matrix with a pre-described gap at the interface determined by the given eigenstrain ε_{ij}^{*}. Fortunately this problem has been studied in the Hilbert Problem based on complex functions (Sherman 1940).

The Hilbert Problem is to find out the sectionally holomorphic function $F(z)$ with the line of discontinuity *L* (here the interface between the inclusion and matrix), the boundary values of which from the positive side and the negative side (here from the inside and from the outside) satisfy the following condition on *L* (except the ends)

$$F^{+}(t) = G(t)F^{-}(t) + f(t) \tag{1.3}$$

where $G(t)$ and $f(t)$ are functions given on L and $G(t) \neq 0$ everywhere on L. Note that given $G(t)=1$, it simplifies Eq. (1.3) to $F^{+}(t)-F^{-}(t)=f(t)$ on L, and that L could be treated as the contour enclosing the inclusion. Therefore, the solution of the simplified Hilbert Problem is actually the complex potentials sought in the finite domain inclusion problem, if $f(t)$ is assigned to be the gap at interface according to the given eigenstrain. Now, such a sectionally holomorphic function in a finite domain could be expressed as

$$F(z)=\frac{1}{2\pi i}\int_{L}\frac{f(t)}{t-z}dt+F^{*}(z) \tag{1.4}$$

where $F^{*}(z)$ is a holomorphic function in the whole finite domain. Now, it can be seen that the solution of the Hilbert Problem in a finite domain can be evaluated in the form of Cauchy Integral.

It is critical to evaluate the contour integral in Eq. (1.4) for obtaining the solution of the simplified Hilbert Problem, which governs the construction of the complex potentials. According to Cauchy's residue theorem (Priestley 2003), this integral can be expressed in the form of the combination of residues at poles inside. It is in general stated as:

$$\frac{1}{2\pi i}\int_{\gamma}g(z)dz=\sum_{k=1}^{N}\operatorname{res}\{g(z);a_{k}\} \tag{1.5}$$

where g(z) is a holomorphic function inside and on a positively oriented contour γ except for a finite number N of poles, $a_1,\cdots,a_N$, and $\operatorname{res}\{g(z);a_k\}$ denotes the residue of g at a_k. Once the evaluation is finished, the complex potentials in Eq. (1.2) are constructed.

1.3 RESEARCH TOPICS IN THIS DISSERTATION

Following the methodology discussed above, this research is started with some simple and fundamental problems. The homogeneous inclusion problem with a concentric configuration will be investigated at the next chapter. Based on the similar formulation, the shape effect of the matrix and the inclusion will be further discussed in the following two chapters. The inhomogeneous inclusion problem will then be dealt with, and the multiphase inhomogeneities will be analyzed with the help of the same framework.

Based on the analytical solutions obtained, some possible applications in engineering will also be discussed, with a demonstration included before the end of this dissertation.

2.0 HOMOGENEOUS CONCENTRIC CIRCULAR RVE

Obviously, the shape of the finite matrix has a significant effect on the final distribution of the disturbance induced by the eigenstrain in the inclusion. To demonstrate the effectiveness of the complex potential method, here a RVE of a simple geometrical configuration is examined. As illustrated in Figure 2.1, a circular inclusion Ω_e with radius r is embedded at the center of Ω to form a circularly concentric RVE.

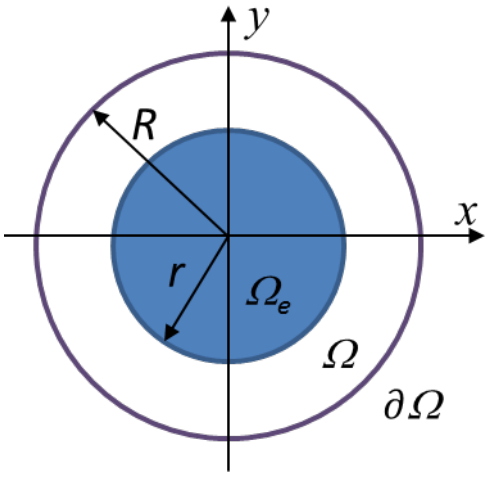

Figure 2.1. A concentric RVE consists of a circular matrix and a circular inclusion

Both the inclusion and the matrix are isotropic, homogeneous, and share same elastic constants. Due to certain physical changes, a uniform eigenstrain is induced in the inclusion and can be expressed as

$$\varepsilon_{ij}^{*}(\mathbf{x}) = \begin{cases} \varepsilon_{ij}^{*} & \mathbf{x} \in \Omega e \\ 0 & \mathbf{x} \in \Omega / \Omega e \end{cases} \tag{2.1}$$

Here **x** represents any point within the RVE. Note that the theoretical formulations presented here are based on the condition of plane strain, although there is no mathematical obstacle preventing their extension to plane stress in complex potential approach.

Following the work by Li and his coworkers (Li et al 2005, Li et al 2007), two types of boundary conditions will be prescribed on the boundary of the RVE. The first one is the displacement (Dirichlet) boundary condition imposed by the governing strain field at the remote region far away from the RVE; and the second one is the traction (Neumann) boundary condition dictated by the remote stress field. If the disturbed displacement field is expressed as u^d and the corresponding strain as ε^d, the first boundary condition imposed on the RVE leads to the following boundary value problem:

$$u_i^d = 0, \forall\, \mathbf{x} \in \partial\Omega \tag{2.2}$$

Based on Eqs (2.1) and (2.2), the disturbance field can be characterized by alternatively solving the problem described by Figure 2.1, in which the boundary of Ω is fixed and a constant eigenstrain ε^* exists in the inclusion.

Similarly, the boundary value problem based on the Neumann boundary condition can be expressed as

$$t_i^d = 0, \forall\, \mathbf{x} \in \partial\Omega \tag{2.3}$$

Again, the disturbance field can be obtained by solving the problem demonstrated in Figure 2.1, in which the boundary of Ω is free and a constant eigenstrain ε^* exists in the inclusion.

2.1 GENERAL FORMULATION FOR A CONCENTRIC RVE

Following Eshelby (1957), the inclusion problem may be decomposed into three sequential steps. As shown in Figure 2.2a, first the inclusion undergoes stress-free deformation according to the given eigenstrain ε_{ij}^{*}. At this stage, no constraints are applied on the inclusion boundary L. Then surface traction is applied to bring the inclusion back to its original shape (strain-free state) as shown in Figure 2.2b. The last step is critical. The inclusion and the matrix are welded together and undergo deformation under the prescribed constraints on matrix boundary L_0 as well as a surface traction on L, which is equal in magnitude to what is applied in the second step but in an opposite direction (Figure 2.2c). Obviously, only the last two steps are related to the elastic deformation of interest.

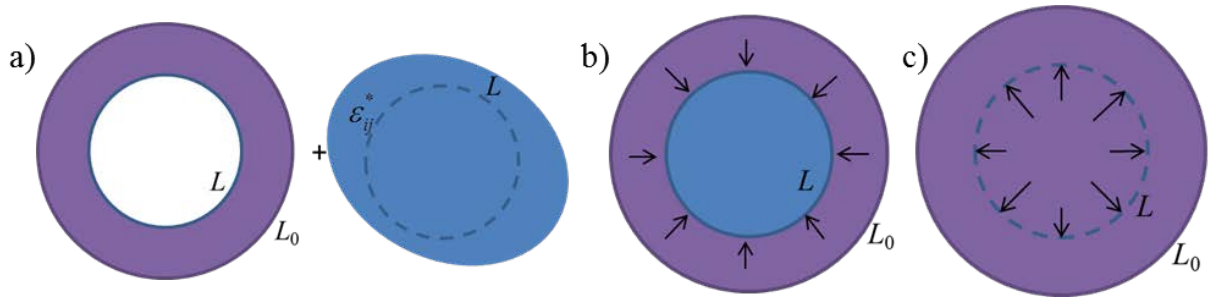

Figure 2.2. a) stress-free deformation induced by given eigenstrain, b) strain-free state recovered, c) deformation induced by opposite traction

In Eshelby's derivation, the point-force result, which is in agreement with Green's function in infinite domain, is successfully adopted in order to solve the key step as shown in Figure 2.2c. However, when facing the finite domain problem, this classical solution might not be implemented due to the lack of Green's function solutions for a finite domain. As mentioned

above, to circumvent this mathematical obstacle, complex potentials for a finite domain are constructed alternatively to describe the elastic field, and the details of them could be found below.

In the RVE under plane strain, a uniform eigenstrain $\left[\varepsilon_1^* \quad \varepsilon_2^* \quad \gamma_{12}^*\right]^T$ is induced in the inclusion due to some physical changes. The displacement field induced by the stress-free deformation of the inclusion, which is visualized in Figure 2.2a, can be expressed as:

$$u_* = \varepsilon_1^* x + \left(\frac{\gamma_{12}^*}{2} + d^*\right) y;\ v_* = \left(\frac{\gamma_{12}^*}{2} - d^*\right) x + \varepsilon_2^* y \tag{2.4}$$

where d^* is an arbitrary constant representing the rigid body rotation.

Here we ignore the rigid body translation and rotation because they do not cause elastic deformation. If a surface traction is applied to bring the inclusion back to its original shape, the boundary of inclusion must undergo displacement equal to $-u_*(t) - iv_*(t)$, where $t \in L$. Then at the strain-free state, the difference of displacement related to the elastic deformation between the inclusion and matrix should be $-u_*(t) - iv_*(t)$ along the interface L. This difference must be maintained in the final key step. Based on Eq. (1.2), this gap along the interface L should be constructed in the complex potential functions.

It is convenient to denote $g(t) = -u_*(t) - iv_*(t)$ and $h(t) = -\overline{g(t)} - \bar{t}g'(t)$ because the interface L is a circle with a radius = r. Then it gives

$$g(t) = -\frac{t}{2}\left(\varepsilon_1^* + \varepsilon_2^* - 2id^*\right) - \frac{r^2}{2t}\left(\varepsilon_1^* - \varepsilon_2^* + i\gamma_{12}^*\right) \tag{2.5}$$

and

$$h(t)=\frac{t}{2}\left(\varepsilon_1^*-\varepsilon_2^*-i\gamma_{12}^*\right)+\frac{r^2}{t}\left(\varepsilon_1^*+\varepsilon_2^*\right)-\frac{r^4}{2t^3}\left(\varepsilon_1^*-\varepsilon_2^*+i\gamma_{12}^*\right) \tag{2.6}$$

To maintain the gap on the interface, the complex potentials representing the whole finite domain can be constructed in a way similar to what proposed by Muskhelishvili (1963):

$$\varphi^+(t)-\varphi^-(t)=\frac{2\mu g(t)}{\kappa+1};\ \psi^+(t)-\psi^-(t)=\frac{2\mu h(t)}{\kappa+1} \tag{2.7}$$

here t is on L, and κ and μ are material parameters same as those in Eq. (1.2).

Using Eqs. (1.3) and (1.4) for Hilbert Problem in a finite domain, the following expression is obtained for the complex potentials:

$$\varphi(z)=\varphi_0(z)+\frac{\mu}{\pi i(\kappa+1)}\int_L\frac{g(t)dt}{t-z};\ \psi(z)=\psi_0(z)+\frac{\mu}{\pi i(\kappa+1)}\int_L\frac{h(t)dt}{t-z} \tag{2.8}$$

where $\varphi_0(z)$ and $\psi_0(z)$ are holomorphic functions in the finite domain, which can be further expressed in the form of power series:

$$\varphi_0(z)=\sum_{n=0}^{+\infty}a_n z^n;\ \psi_0(z)=\sum_{n=0}^{+\infty}b_n z^n \tag{2.9}$$

here n must be nonnegative because the domain contains the origin (0, 0) of the coordinate system. Denoting $\varphi_*(z)=\frac{\mu}{\pi i(\kappa+1)}\int_L\frac{g(t)dt}{t-z}$ and $\psi_*(z)=\frac{\mu}{\pi i(\kappa+1)}\int_L\frac{h(t)dt}{t-z}$, and using Eqs. (2.5) and (2.6), one may obtain the following expressions:

$$\varphi_*(z)=\begin{cases}-\dfrac{\mu}{\kappa+1}z\left(\varepsilon_1^*+\varepsilon_2^*-2id^*\right) & |z|<r\\ \dfrac{\mu}{\kappa+1}\dfrac{r^2}{z}\left(\varepsilon_1^*-\varepsilon_2^*+i\gamma_{12}^*\right) & |z|>r\end{cases} \tag{2.10}$$

$$\psi_*(z)=\begin{cases}\dfrac{\mu}{\kappa+1}z\left(\varepsilon_1^*-\varepsilon_2^*-i\gamma_{12}^*\right) & |z|<r\\ -\dfrac{\mu}{\kappa+1}\dfrac{2r^2}{z}\left(\varepsilon_1^*+\varepsilon_2^*\right)+\dfrac{\mu}{\kappa+1}\dfrac{r^4}{z^3}\left(\varepsilon_1^*-\varepsilon_2^*+i\gamma_{12}^*\right) & |z|>r\end{cases} \tag{2.11}$$

Now, the explicit expressions of $\varphi_*(z)$ and $\psi_*(z)$ describing the RVE are established. To identify the only unknown coefficients a_n and b_n, the boundary condition on the exterior boundary of matrix L_0 must be enforced. Next, two types of boundary conditions are considered.

2.2 SOLUTION FOR TWO DIFFERENT TYPES OF BOUNDARY CONDITIONS

2.2.1 Dirichelet Boundary Conditions

As stated in Eq. (2.2), this boundary value problem can be solved alternatively in the form of the disturbed displacement fields. For the complex potentials representing the disturbed displacement fields, namely, $\varphi=\varphi_0+\varphi_*$, $\psi=\psi_0+\psi_*$, the fixed boundary condition can be described based on Eqs. (1.2) and (2.2):

$$\kappa\left(\varphi_0(t)+\varphi_*(t)\right)-t\left(\overline{\varphi_0'(t)}+\overline{\varphi_*'(t)}\right)-\left(\overline{\psi_0(t)}+\overline{\psi_*(t)}\right)=0,\ t\in L_0, \tag{2.12}$$

Since φ_* and ψ_* have to be in the forms given in Eqs. (2.10) and (2.11), the complete solution will be obtained once the coefficients a_n and b_n are found to guarantee Eq. (2.12), which leads to

$$\kappa\sum_{n=0}^{\infty}a_nt^n-t\sum_{n=0}^{\infty}n\overline{a}_n\overline{t}^{n-1}-\sum_{n=0}^{\infty}\overline{b}_n\overline{t}^n=-\kappa\varphi_*(t)+t\overline{\varphi_*'(t)}+\overline{\psi_*(t)} \tag{2.13}$$

Since on L_0, $t = R\mathrm{e}^{i\theta}$, the equation can further be written as:

$$\begin{aligned}\kappa\sum_{n=0}^{\infty}a_n R^n e^{in\theta} - \sum_{n=0}^{\infty}nR^n\overline{a}_n e^{-i(n-2)\theta} - \sum_{n=0}^{\infty}R^n\overline{b}_n e^{-in\theta} = &-\frac{\kappa\mu}{\kappa+1}\frac{r^2}{R}\left(\varepsilon_1^* - \varepsilon_2^* + i\gamma_{12}^*\right)e^{-i\theta} \\ &-\frac{\mu}{\kappa+1}\frac{2r^2}{R}\left(\varepsilon_1^* + \varepsilon_2^*\right)e^{i\theta} \\ &+\frac{\mu}{\kappa+1}\frac{r^2}{R}\left(\frac{r^2}{R^2}-1\right)\left(\varepsilon_1^* - \varepsilon_2^* - i\gamma_{12}^*\right)e^{i3\theta}\end{aligned} \tag{2.14}$$

Because of the linear independency of the basis $e^{in\theta}$, $n = 0,1,\cdots\infty$, Eq. (2.14) leads to the following conclusions: $a_n = 0$, and $b_n = 0$ except that

$$\begin{aligned}a_1 &= -\frac{\mu}{\kappa^2-1}\frac{2r^2}{R^2}\left(\varepsilon_1^* + \varepsilon_2^*\right) \\ a_3 &= \frac{\mu}{\kappa\left(\kappa+1\right)}\frac{r^2}{R^4}\left(\frac{r^2}{R^2}-1\right)\left(\varepsilon_1^* - \varepsilon_2^* - i\gamma_{12}^*\right) \\ b_1 &= \frac{\kappa\mu}{\kappa+1}\frac{r^2}{R^2}\left(\varepsilon_1^* - \varepsilon_2^* - i\gamma_{12}^*\right) - \frac{3\mu}{\kappa\left(\kappa+1\right)}\frac{r^2}{R^2}\left(\frac{r^2}{R^2}-1\right)\left(\varepsilon_1^* - \varepsilon_2^* - i\gamma_{12}^*\right)\end{aligned} \tag{2.15}$$

Once the coefficients are determined, φ_0 and ψ_0 are obtained subsequently. It should be noted that the solution described here is only related to the elastic deformation of the last two steps in the Figure.2.2. As for the final solution of the inclusion problem, the simple stress-free state shown in Eq. (2.4) should be added to the solution obtained above. This gives

$$\varphi\left(z\right) = \begin{cases} -\dfrac{\mu}{\kappa+1}z\left(\varepsilon_1^* + \varepsilon_2^* - 2id^*\right) + a_1 z + a_3 z^3 & \left|z\right| < r \\ \dfrac{\mu}{\kappa+1}\dfrac{r^2}{z}\left(\varepsilon_1^* - \varepsilon_2^* + i\gamma_{12}^*\right) + a_1 z + a_3 z^3 & \left|z\right| > r \end{cases} \tag{2.16}$$

$$\psi\left(z\right) = \begin{cases} \dfrac{\mu}{\kappa+1}z\left(\varepsilon_1^* - \varepsilon_2^* - i\gamma_{12}^*\right) + b_1 z & \left|z\right| < r \\ -\dfrac{\mu}{\kappa+1}\dfrac{2r^2}{z}\left(\varepsilon_1^* + \varepsilon_2^*\right) + \dfrac{\mu}{\kappa+1}\dfrac{r^4}{z^3}\left(\varepsilon_1^* - \varepsilon_2^* + i\gamma_{12}^*\right) + b_1 z & \left|z\right| > r \end{cases} \tag{2.17}$$

and

$$u^d + iv^d = \begin{cases} \dfrac{1}{2\mu}\left(\kappa\varphi(z) - z\overline{\varphi'(z)} - \overline{\psi(z)}\right) + u_* + iv_* & |z| < r \\ \dfrac{1}{2\mu}\left(\kappa\varphi(z) - z\overline{\varphi'(z)} - \overline{\psi(z)}\right) & |z| > r \end{cases} \tag{2.18}$$

In a matrix form (here both A and B are degenerated to 2 by 3 matrices because of plane strain), it is convenient to write the disturbed displacement field as:

$$\mathbf{u}^d = \begin{cases} \mathbf{A}\boldsymbol{\varepsilon}^* & |z| < r \\ \mathbf{B}\boldsymbol{\varepsilon}^* & |z| > r \end{cases} \tag{2.19}$$

where $\mathbf{u}^d = \begin{bmatrix} u^d & v^d \end{bmatrix}^T$ and $\boldsymbol{\varepsilon}^* = \begin{bmatrix} \varepsilon_1^* & \varepsilon_2^* & \gamma_{12}^* \end{bmatrix}^T$.

The first components of the 2 by 3 matrices are listed here for simplicity

$$\begin{aligned} A_{11} = &-\frac{1}{2}\left(\frac{\kappa}{\kappa+1} + \frac{\kappa+2}{\kappa+1}\cdot\frac{r^2}{R^2} + \frac{3}{\kappa(\kappa+1)}\cdot\frac{r^2}{R^2}\cdot\left(1-\frac{r^2}{R^2}\right)\right)x \\ &+\frac{1}{2}\left(\frac{3-\kappa}{\kappa(\kappa+1)}\frac{r^2}{R^4}\left(1-\frac{r^2}{R^2}\right)\right)x^3 + \frac{3}{2\kappa}\frac{r^2}{R^4}\left(1-\frac{r^2}{R^2}\right)xy^2 + x \end{aligned} \tag{2.20}$$

and

$$\begin{aligned} B_{11} = &-\frac{1}{2}\left(\frac{\kappa+2}{\kappa+1}\cdot\frac{r^2}{R^2} + \frac{3}{\kappa(\kappa+1)}\cdot\frac{r^2}{R^2}\cdot\left(1-\frac{r^2}{R^2}\right)\right)x \\ &-\frac{1}{2}\cdot\frac{\kappa-3}{\kappa(\kappa+1)}\cdot\frac{r^2}{R^4}\left(1-\frac{r^2}{R^2}\right)x^3 + \frac{1}{2}\cdot\frac{3}{\kappa}\cdot\frac{r^2}{R^4}\left(1-\frac{r^2}{R^2}\right)xy^2 + \frac{1}{2}\cdot\frac{\kappa+2}{\kappa+1}\cdot\frac{r^2}{x^2+y^2}x \\ &+\frac{1}{2}\cdot\frac{1}{\kappa+1}\cdot\frac{r^2}{\left(x^2+y^2\right)^2}\left(x^3-3xy^2\right) - \frac{1}{2}\cdot\frac{1}{\kappa+1}\cdot\frac{r^4}{\left(x^2+y^2\right)^3}\left(x^3-3xy^2\right) \end{aligned} \tag{2.21}$$

Similar to the Eshelby's tensor mapping the eigenstrain into the disturbed strain field, the matrix form equation can be written as

$$\boldsymbol{\varepsilon}^{d}=\begin{cases}\mathbf{S}^{in}\boldsymbol{\varepsilon}^{*} & |z|<r\\ \mathbf{S}^{ex}\boldsymbol{\varepsilon}^{*} & |z|>r\end{cases} \tag{2.22}$$

where

$$\mathbf{S}^{in}=\begin{bmatrix}\dfrac{\partial}{\partial x} & 0\\ 0 & \dfrac{\partial}{\partial y}\\ \dfrac{\partial}{\partial y} & \dfrac{\partial}{\partial x}\end{bmatrix}\mathbf{A}$$

$$\mathbf{S}^{ex}=\begin{bmatrix}\dfrac{\partial}{\partial x} & 0\\ 0 & \dfrac{\partial}{\partial y}\\ \dfrac{\partial}{\partial y} & \dfrac{\partial}{\partial x}\end{bmatrix}\mathbf{B} \tag{2.23}$$

2.2.2 Neumann Boundary Conditions

Similarly, the inclusion problem with Neumann boundary conditions can also be solved alternatively in the form of disturbed displacement fields. However, the complex potentials representing the disturbed displacement fields ($\varphi=\varphi_0+\varphi_*$, $\psi=\psi_0+\psi_*$) need to meet the following requirement, which stands for the traction free boundary (Muskhelilshvili 1963).

$$\left(\varphi_0(t)+\varphi_*(t)\right)+t\left(\overline{\varphi_0'(t)}+\overline{\varphi_*'(t)}\right)+\left(\overline{\psi_0(t)}+\overline{\psi_*(t)}\right)=0,\ t\in L_0, \tag{2.24}$$

Similar to Eq. (2.14), one may find

$$\sum_{n=0}^{\infty} a_n R^n e^{in\theta} + \sum_{n=0}^{\infty} nR^n \overline{a}_n e^{-i(n-2)\theta} + \sum_{n=0}^{\infty} R^n \overline{b}_n e^{-in\theta} = -\frac{\mu}{\kappa+1}\frac{r^2}{R}\left(\varepsilon_1^* - \varepsilon_2^* + i\gamma_{12}^*\right)e^{-i\theta} + \frac{\mu}{\kappa+1}\frac{2r^2}{R}\left(\varepsilon_1^* + \varepsilon_2^*\right)e^{i\theta} - \frac{\mu}{\kappa+1}\frac{r^2}{R}\left(\frac{r^2}{R^2}-1\right)\left(\varepsilon_1^* - \varepsilon_2^* - i\gamma_{12}^*\right)e^{i3\theta} \tag{2.25}$$

Again, because of the linear independency of the basis $e^{in\theta}$, $n = 0,1,\cdots\infty$, Eq. (2.25) leads to

$$a_1 = \frac{\mu}{\kappa+1}\frac{r^2}{R^2}\left(\varepsilon_1^* + \varepsilon_2^*\right)$$

$$a_3 = -\frac{\mu}{\kappa+1}\frac{r^2}{R^4}\left(\frac{r^2}{R^2}-1\right)\left(\varepsilon_1^* - \varepsilon_2^* - i\gamma_{12}^*\right) \tag{2.26}$$

$$b_1 = \frac{3\mu}{\kappa+1}\frac{r^2}{R^2}\left(\frac{r^2}{R^2}-\frac{4}{3}\right)\left(\varepsilon_1^* - \varepsilon_2^* - i\gamma_{12}^*\right)$$

Similarly, the stress-free state needs to be added to achieve the final solution of the inclusion problem. Under the Neumann boundary conditions, the disturbance of the displacement field could also be given in the similar form of Eq. (2.19). Following Eq. (2.23), the Eshelby's tensor for Neumann boundary conditions could be found in a straightforward way.

2.3 ASYMPTOTICAL PERFORMANCE AND COMPARISON WITH FEM

Utilizing the complex potential method, the analytical solutions of elastic fields in a concentric RVE containing a circular inclusion are obtained. In the limiting case, i.e., the matrix enlarged to infinity, the newly-derived solutions must recover Eshelby's tensor for infinite domain. Since there only exists the classical Eshelby's tensor for plane strain in 2D problems, only the results corresponding to Dirichlet boundary conditions under plane strain will be discussed next.

To compare with the classic Eshelby's tensor in the limiting case, the interior and exterior tensors in Eq. (2.23) are visualized in Figure 2.3. Unlike the classical Eshelby's tensor, the interior tensor for finite domain is no longer a constant. Instead, it is a position dependent function. Based on Eqs (2.20) and (2.23), the first component of interior tensor $S_{1111}^{in}(x,y)$ can be expressed as

$$S_{1111}^{in}(x,y)=\frac{1}{2}\left(\frac{\kappa+2}{\kappa+1}\cdot\left(1-\frac{r^2}{R^2}\right)-\frac{3}{\kappa(\kappa+1)}\cdot\frac{r^2}{R^2}\cdot\left(1-\frac{r^2}{R^2}\right)-\frac{3(\kappa-3)}{\kappa(\kappa+1)}\frac{r^2}{R^4}\left(1-\frac{r^2}{R^2}\right)x^2+\frac{3}{\kappa}\frac{r^2}{R^4}\left(1-\frac{r^2}{R^2}\right)y^2\right) \tag{2.27}$$

from which it can be seen that $S_{1111}^{in}(x,y)$ is not only dependent on its position inside the inclusion, but also on the volume fraction ratio of inclusion to matrix characterized by *r* and *R*. The same characteristics can be found for other components of the interior tensor. When the matrix is enlarged to infinity, the expression of $S_{1111}^{in}(x,y)$ is transformed to as follows

$$S_{1111}^{in}(x,y)=\frac{1}{2}\left(\frac{\kappa+2}{\kappa+1}\right)=\frac{5-4\nu}{8(1-\nu)} \tag{2.28}$$

This is the same as the first component of the classical Eshelby's interior tensor. As documented in Figure 2.3a, $S_{1111}^{in}(0,0)$ gradually approaches the asymptote dictated by the classical Eshelby's tensor (dashed line) as the size of matrix goes to infinity.

Same observations can be obtained for the exterior tensor for finite domain. Similarly, based on Eqs. (2.21) and (2.23), the first component of exterior tensor can be written as

$$S_{1111}^{ex}(x,y)=\frac{1}{2}\Bigg[-\left(\frac{\kappa+2}{\kappa+1}\cdot\frac{r^2}{R^2}+\frac{3}{\kappa(\kappa+1)}\cdot\frac{r^2}{R^2}\cdot\left(1-\frac{r^2}{R^2}\right)\right)-\frac{3(\kappa-3)}{\kappa(\kappa+1)}\frac{r^2}{R^4}\left(1-\frac{r^2}{R^2}\right)x^2$$
$$+\frac{3}{\kappa}\frac{r^2}{R^4}\left(1-\frac{r^2}{R^2}\right)y^2+\frac{\kappa+2}{\kappa+1}\frac{r^2}{\left(x^2+y^2\right)^2}\left(y^2-x^2\right) \tag{2.29}$$
$$+\frac{r^2}{\kappa+1}\frac{3\left(x^4-y^4\right)-4\left(x^4-3x^2y^2\right)}{\left(x^2+y^2\right)^3}-\frac{r^4}{\kappa+1}\frac{3\left(x^4-y^4\right)-6\left(x^4-3x^2y^2\right)}{\left(x^2+y^2\right)^4}\Bigg]$$

Again, it is a function of both the volume fraction ratio and position. For the limiting case of infinitely large *R*, it is changed to

$$S_{1111}^{ex}(x,y)=\frac{1}{2}\Bigg[\frac{\kappa+2}{\kappa+1}\frac{r^2}{\left(x^2+y^2\right)^2}\left(y^2-x^2\right)+\frac{r^2}{\kappa+1}\frac{3\left(x^4-y^4\right)-4\left(x^4-3x^2y^2\right)}{\left(x^2+y^2\right)^3}$$
$$-\frac{r^4}{\kappa+1}\frac{3\left(x^4-y^4\right)-6\left(x^4-3x^2y^2\right)}{\left(x^2+y^2\right)^4}\Bigg] \tag{2.30}$$

This again recovers the classical Eshelby's exterior tensor. In Figure 2.3b, it shows $S_{1111}^{ex}(x,y)$ on the point (*r*, 0) of the interface. It can be seen as *R* increases, $S_{1111}^{ex}(x,y)$ approaches the value given by the classical Eshelby's exterior tensor. If the values of exterior tensor along positive *x* axis are plotted (Figure 2.4), a firm agreement with the classical Eshelby's tensor can be found when the size of inclusion is negligible.

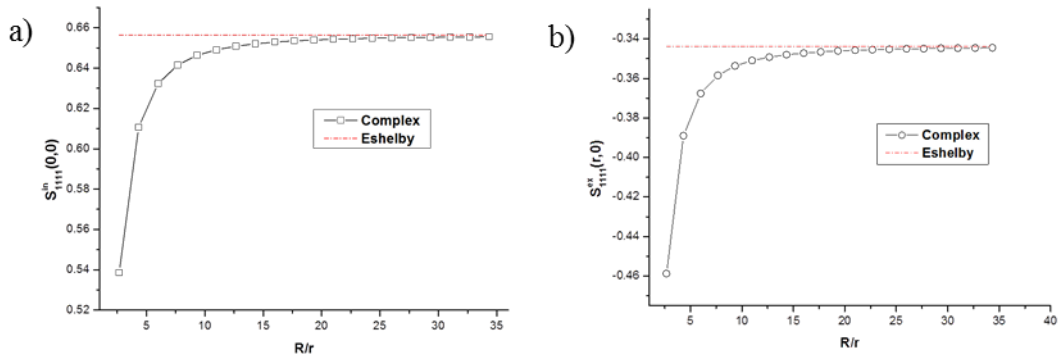

Figure 2.3. a)**.** Comparison of interior tensor; b)**.** Comparison of exterior tensor

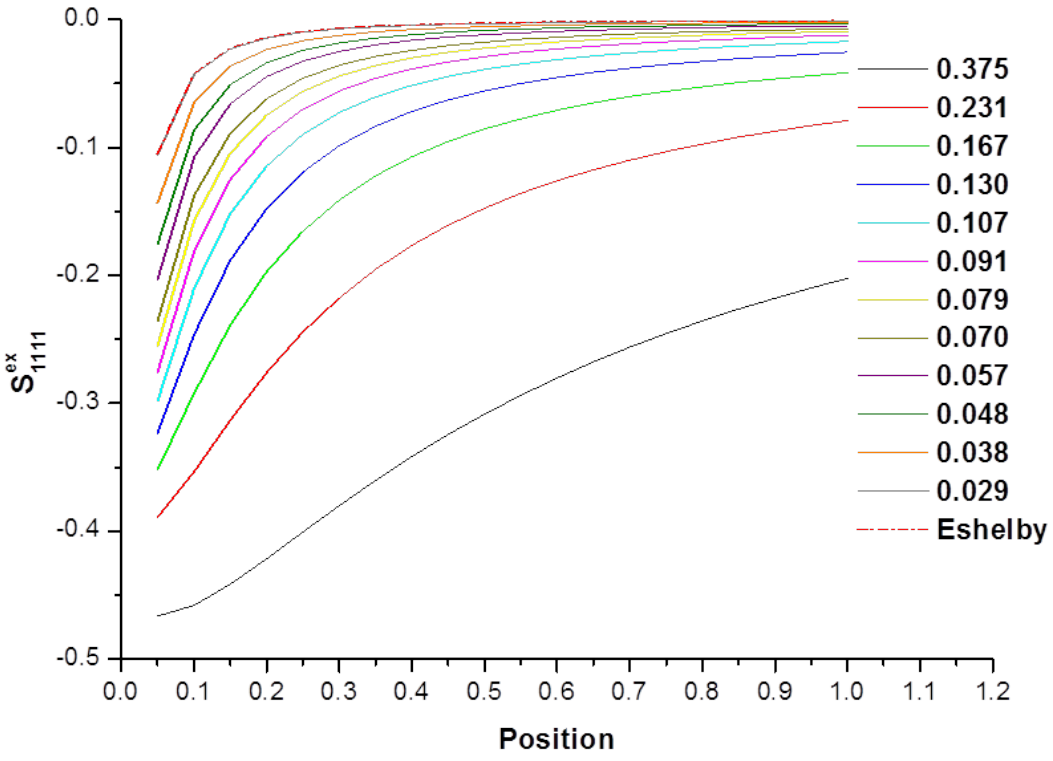

Figure 2.4. The first component of the Exterior tensor along the *x* -axis

In addition to the classical Eshelby's tensor, the solutions obtained here recover the tensors proposed by Li et al. (2005). For simplicity, only the expressions for the first terms in theinterior and exterior tensors are compared here.

According to Li et al's solution, the first terms of the Eshelby's tensor for a concentric finite RVE under Dirichelet boundary condition can be obtained as

$$\mathbf{S}_{1111}^{in}(\mathbf{x}) = \frac{1}{8(1-\nu)}\left[(5-4\nu)(1-\rho_0^2) + \frac{3\rho_0^2(\rho_0^2-1)}{(4\nu-3)}\left(4(1-\nu)t^2 - 1 + 4(2\nu-1)t^2 r_1^2\right)\right] \tag{2.31}$$

$$\begin{aligned}\mathbf{S}_{1111}^{ex}(\mathbf{x}) = \frac{\rho_0^2/t^2}{8(1-\nu)}\Bigg\{&\left[3\rho_0^2/t^2 + 4\nu + 2 - t^2(5-4\nu) + \frac{3t^2(\rho_0^2-1)\left(4t^2(1-\nu)-1\right)}{(4\nu-3)}\right] \\ &+\left[-24\rho_0^2/t^2 + 8\nu + 8 + \frac{12t^2(2\nu-1)(\rho_0^2-1)}{(4\nu-3)}\right]r_1^2 + \left[8\left(3\rho_0^2/t^2 - 2\right)\right]r_1^4\Bigg\}\end{aligned} \tag{2.32}$$

where $\mathbf{x} = (x, y)$, $\rho_0 = r/R$, $t = |\mathbf{x}|/R$ and $r_1 = x/|\mathbf{x}|$.

The corresponding terms obtained via complex potential method are listed in Eqs (2.27) and (2.29) respectively. It is not difficult to see that the two methods indeed result in the same expression. Further examination could reveal that the rest terms of the interior and exterior tensors coincide with each other too.

For complex potential method, one of the foci is the displacement field of the elastic problem. To demonstrate that the solutions accurately describe the displacement field in the RVE, comparison with FEM results are made here. In the computational model, a RVE under Dirichelet boundary condition is studied for a specified eigenstrain $\left[\varepsilon_1^* \quad \varepsilon_2^* \quad \gamma_{12}^*\right] = \left[0.01 \quad -0.02 \quad 0.03\right]^T$. In this RVE with the inclusion size $r = 0.6$ and matrix size $R = 1$, the material properties are assigned as $E = 30$ GPa and $\nu = 0.2$.

The results of the disturbed displacement fields obtained theoretically and numerically are depicted in Figure 2.5. It can be seen from Figure 2.5 that the disturbed displacement fields along 8 main orientations obtained from FEM firmly agree with the proposed theoretical

solutions. This means that the complex potential method can theoretically predict the disturbed fields in the concentric finite RVE caused by an arbitrary eigenstrain.

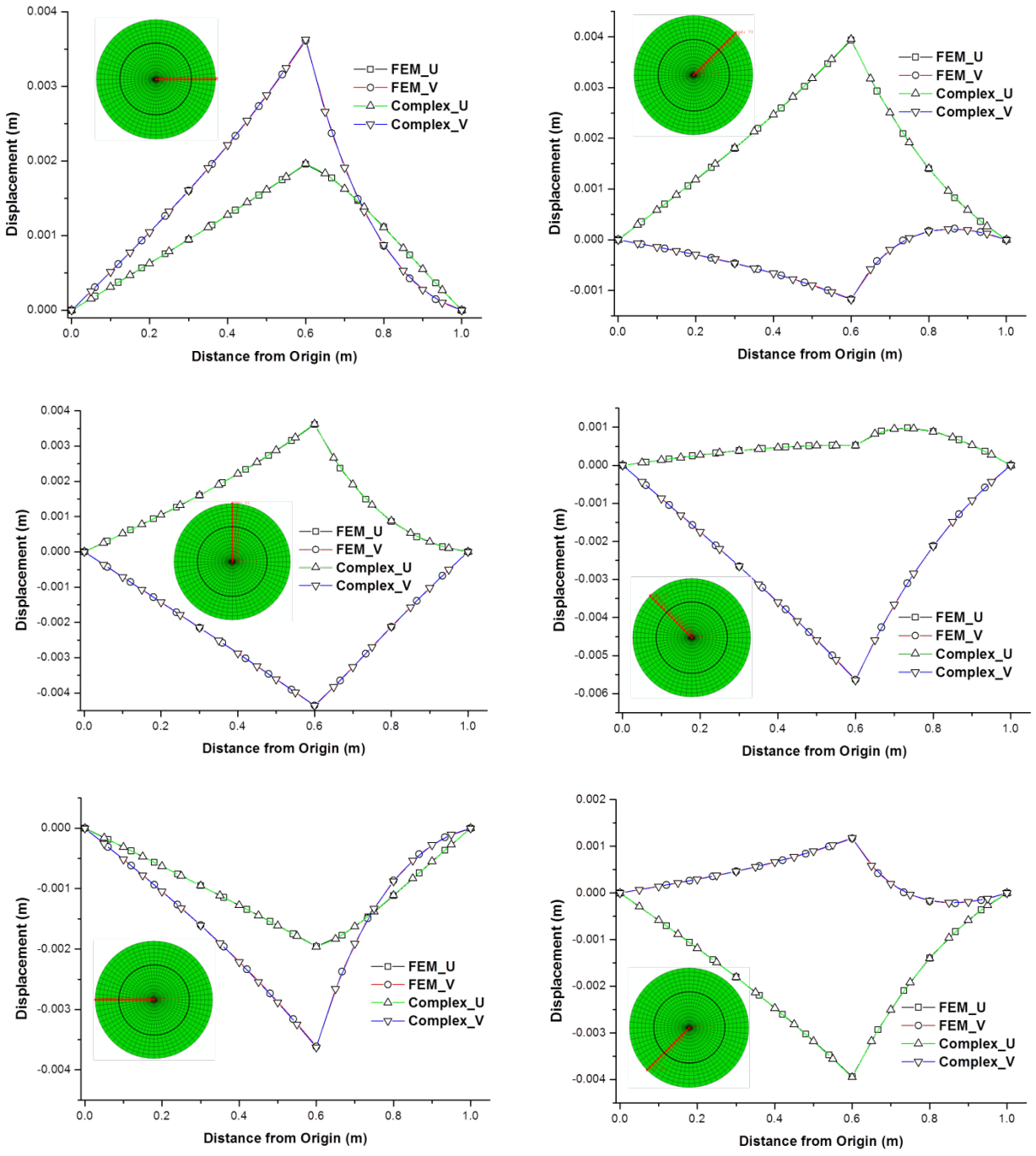

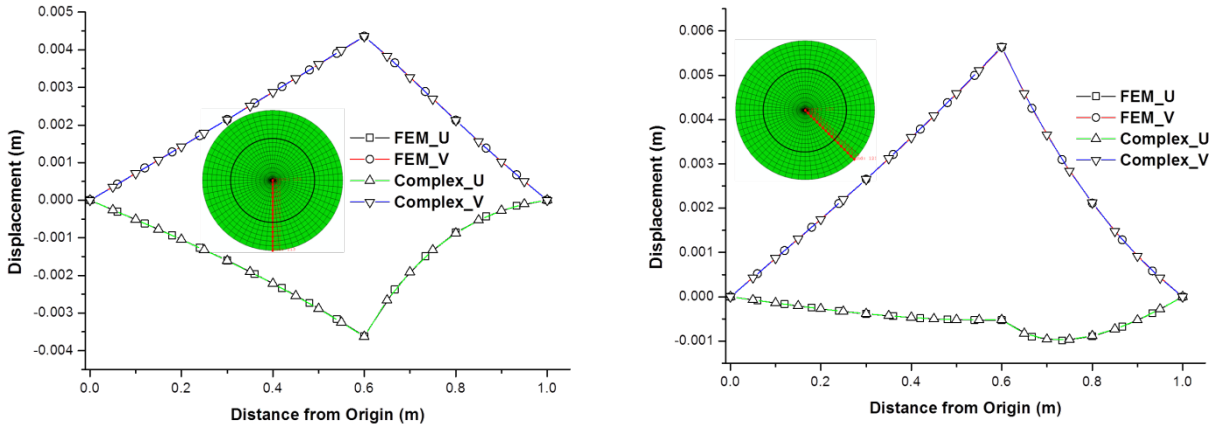

Figure 2.5. Disturbed displacement field in the finite domain inclusion problem along 8 main directions

2.4 DISCUSSION AND CONCLUSION

In this study, the complex potential method is used successfully to study the problem of a circular inclusion in a finite elastic domain of 2D plane strain. It is found that this method can theoretically predict the disturbed displacement and the strain fields of the 2D inclusion problem, without any postulation based on the special shape of the matrix. Although the solutions based on this approach coincide with those obtained by Li et al. (2005), Gao et al. (2010) and Zou et al (2012), this attempt is not a simple repeat but a starting point of solving 2D inclusion problem of more complicated shape, for which it is hard to construct the interior and exterior tensors directly based on the geometrical characteristics. And this derivation can be systematically extended to the more complicated configurations, which will be demonstrated in the following chapters.

Based on theoretical derivation and computational comparison, the following conclusions can be drawn:

1. 2D inclusion problems of a concentric finite domain can be described by complex potential method without any postulate on its geometry characteristics;

2. The interior and exterior tensors obtained for finite domain recover the classical Eshelby's tensors in the limiting case of infinite matrix;
3. The interior and exterior tensors obtained based on the complex potential method coincide with the results by Li et al., which is only effective to concentric configuration;
4. The proposed approach in this study can be further extended to describe 2D inclusion problems in a finite domain of more complicated shape.

3.0 SHAPE EFFECT OF THE MATRIX

In many engineering applications, the shape of the RVE cannot be circular because the composite solids cannot be discretized by circular RVEs. Instead, squared, hexagonal and other complicatedly shaped RVEs have to be used. Therefore, the mathematical formulations developed above have to be extended to take into account the shape effect of the matrix. A great advantage of complex potential method is that the shape effect on the complex potentials can be handled by conformal mapping (Sendeckyj 1970, Jasiuk et al 1992). Thus, solutions on a simple geometry like a unit circle, which brings simplicity in mathematical formulation, can be utilized for complex shapes. As documented by Sherman (1940) and Muskhelishvili (1953), the closed form solutions of the complex potentials for inclusion problems can be expressed by complex polynomials, which make it possible to employ the injective conformal mapping in the form of one to one polynomials to take the shape effect into account.

The objective of this chapter is to extend the solutions based on the complex potential approach developed in the previous chapter to inclusion problems in finite domains of shapes other than a circle. The focus is placed on providing a systematic approach built upon complex potential formulation coupled with conformal mapping transformation. The chapter is presented as follows. Following the description of the finite domain and its boundary condition, the key aspects of the conformal mapping to transform the complicatedly shaped matrix to a unit circle is introduced. Based on the Schwarz-Christoffel mapping (Prochazka 1983), a square can be

closely approximated by a curved polygon expressed in the form of complex polynomials. Then, the general formulations for complex potentials governing the finite domain and their expressions in the mapped domain are delineated. Subsequently, the explicit solutions for the elastic fields are obtained for bounded domains showing shape of Pascal's limaçon which can easily recover the concentric circular configuration and of a curved square which gives realistic approximation of the perfect square. In addition to the comparison with the classical Elshelby's solution and theoretical solutions for concentric circular RVEs, the solutions are compared with FEM simulations as well. At the end, discussions about the inverse of conformal mapping are presented and conclusions are reported.

3.1 RVE OF SHAPES OTHER THAN A CIRCLE

In this study, the representative volume element (RVE) is characterized by a circular inclusion embedded at the center of a bounded matrix, which has shape other than a circle. As illustrated in Figure 3.1, a circular inclusion Ωe of radius *r* is surrounded by a finite matrix Ω with the shape of Pascal's limaçon or square. Both the inclusion and the matrix are isotropic, homogeneous and share same elastic properties. A salient property of the RVEs in Figure 3.1 is that the matrix is bounded and the volume fraction of inclusion to matrix is not negligible. To focus on the theoretical formulation of complex potentials in complex geometry, the RVE is assumed to be plane strain and only Dirichlet (displacement) boundary condition is imposed on the matrix boundary $\partial\Omega$.

If a uniform eigenstrain ε_{ij}^{*} is induced in the inclusion due to certain physical activation, the inclusion problem can be characterized as

$$\varepsilon_{ij}^{*}(\mathbf{x}) = \begin{cases} \varepsilon_{ij}^{*} & \mathbf{x} \in \Omega e \\ 0 & \mathbf{x} \in \Omega / \Omega e \end{cases} \tag{3.1}$$

Here **x** represents any point within the RVE. The Dirichlet boundary condition is then described as

$$u_i^d = 0, \forall\, \mathbf{x} \in \partial\Omega \tag{3.2}$$

where u_i^d is the disturbance of the displacement field. Based on Eqs (3.1) and (3.2), the inclusion problem can be decomposed into determining 2 elastic fields: 1) uniform field of the bounded RVE under Dirichlet boundary and 2) a disturbance of the displacement field due to eigenstrain ε_{ij}^{*}. This disturbance field can alternatively be characterized by solving the problem illustrated by Figure 3.1, in which the boundary of matrix Ω is fixed and a constant eigenstrain ε_{ij}^{*} exists in the inclusion.

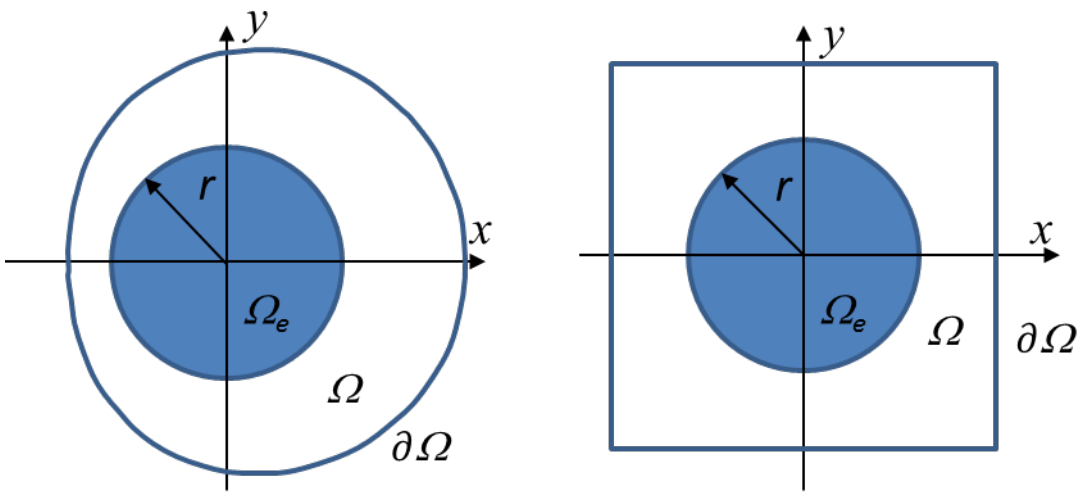

Figure 3.1. RVEs with matrix shape other than circle

Unlike the circular configuration, the direct formulation of the disturbed field is now perplexed by the noncircular shape of the matrix. To simplify the mathematical formulation, the RVE needs to be transformed to a unit circle by conformal mapping.

3.2 CONFORMAL MAPPING

Given two open sets in the complex plane, an invertible analytic function mapping one of them onto the other is called as conformal mapping if angle preservation is satisfied. The idea supporting the use of invertible conformal mapping in problems involving harmonic functions is that a give problem on an open set (e.g., a noncircular shape) can be converted to its conformal mapping (e.g., a unit circle) and the solutions on this mapped set can be inverted to the original set. Thus, it allows mathematical formulation on an open set forming simpler shape.

The complex potentials sought for 2D elastic problems are indeed sectional holomorphic (analytical) complex functions. The conformal mapping performed by an analytical function will preserve the analytical property of the complex potentials. For example, a holomorphic function can map the region bounded by a circle in the ζ plane in Figure 3.2 into a square in the z (x, y) plane, which is conventionally called Schwarz-Christoffel Mapping (Prochazka 1983). Then the problem in z plane could be transformed and solved alternatively in the 'virtual' circular ζ domain.

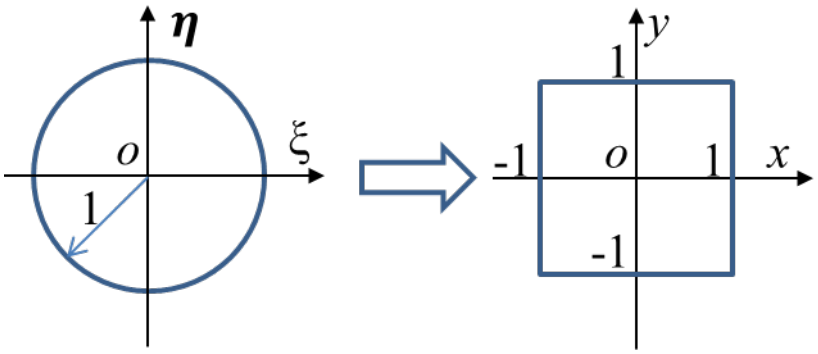

Figure 3.2. Illustration of conformal mapping for a perfect square

In general, one can define the conformal mapping function as

$$z = w(\zeta) \tag{3.3}$$

here $\zeta = \xi + i\eta$ is in the 'virtual' domain Ω' while z in the true domain Ω. The complex potential in the true domain could therefore be expressed as

$$\varphi(z) = \varphi(w(\zeta)) = \tilde{\varphi}(\zeta) \tag{3.4}$$

where $\tilde{\varphi}(\zeta)$ is holomorphic on the circular domain and therefore could be expressed in the form of power series:

$$\tilde{\varphi}(\zeta) = \sum_{n=0}^{\infty} a_n \zeta^n \tag{3.5}$$

For Figure 3.1a), the region bounded by a Pascal's limaçon could be mapped into the circular domain by

$$z = R(\zeta + m\zeta^2) \tag{3.6}$$

where R and m are real numbers and $m \le 0.5$. For square, the specified Schwarz-Christoffel mapping is given as (Prochazka, 1983)

$$z(\zeta) = \alpha_1 \int_0^{\zeta} (s^4 - 1)^{-1/2}\, ds + \alpha_2 \tag{3.7}$$

where α_1 and α_2 are arbitrary constants. In Eqs. (3.6) and (3.7), the constants R, α_1 and α_2 should be determined based on the position and size of the true domain. For example, the transformation shown in Figure 3.2 could be described by setting $\alpha_1 = 0.7627597632 \times (1-i)$ and $\alpha_2 = 0$.

Unlike the Pascal's limaçon, because of the troubles brought up by the elliptic integral in Eq. (3.7), it is not possible to express Schwarz-Christoffel mapping for a perfect square in the form of elementary functions. However, due to $|\zeta| \le 1$, it is possible to express the term $(s^4 - 1)^{-1/2}$ by Taylor's series so as to replace the conformal mapping by polynomials, which give close approximation everywhere except for the ends $|s| = 1$. Using Taylor's expansion, it follows

$$(s^4 - 1)^{-1/2} = \sum_{n=0}^{\infty} T_n s^n \tag{3.8}$$

where T_n could be found simply by carrying out the corresponding Taylor expansion. Subsequently, one obtains a curved square as an approximation:

$$z(\zeta) = \alpha_1 \sum_{n=0}^{\infty} \frac{1}{n+1} T_n \zeta^{n+1} \tag{3.9}$$

In practice, the first few terms (e.g., n = 8) in the series give a good approximation, with only slight modification needed around the corners; see Figure 3.3. The bold curve in Figure 3.3 is described by the first three non-zero terms, which will be used for the subsequent formulation.

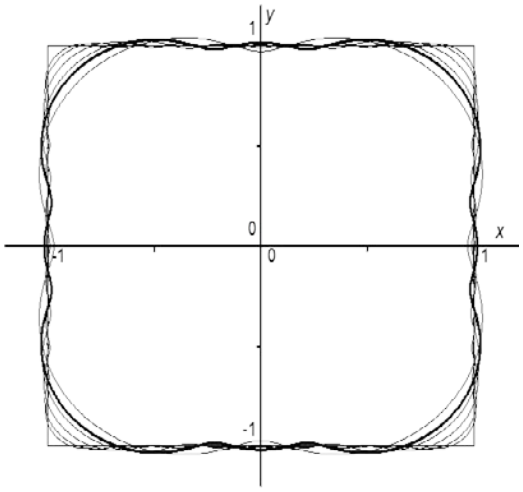

Figure 3.3. A square approximated by curved one based on complex polynomials

3.3 GENERAL FORMULATION FOR A NONCIRCULAR DOMAIN

Once the complex potentials are constructed, it is ready to find the elastic field in the RVEs and the corresponding Eshelby's tensors. So we focus on building the complex potentials here. Despite the noncircular shape of the matrix, the complex potentials in the REV are still sectionally holomorphic with a gap at interface introduced by the eigenstrain $\boldsymbol{\varepsilon}^*$ in the inclusion. Following Sherman (1940) and Muskhelishvili (1953), the complex potentials can be expressed as

$$\varphi(z)=\varphi_0(z)+\varphi_*(z);\ \psi(z)=\psi_0(z)+\psi_*(z) \tag{3.10}$$

where

$$\varphi_*(z)=\begin{cases}-\dfrac{\mu}{\kappa+1}z\left(\varepsilon_1^*+\varepsilon_2^*-2id^*\right) & z\in\Omega e\\ \dfrac{\mu}{\kappa+1}\dfrac{r^2}{z}\left(\varepsilon_1^*-\varepsilon_2^*+i\gamma_{12}^*\right) & z\in\Omega/\Omega e\end{cases} \tag{3.11}$$

and

$$\psi_*(z)=\begin{cases} \dfrac{\mu}{\kappa+1}z\left(\varepsilon_1^*-\varepsilon_2^*-i\gamma_{12}^*\right) & z\in\Omega e \\ -\dfrac{\mu}{\kappa+1}\dfrac{2r^2}{z}\left(\varepsilon_1^*+\varepsilon_2^*\right)+\dfrac{\mu}{\kappa+1}\dfrac{r^4}{z^3}\left(\varepsilon_1^*-\varepsilon_2^*+i\gamma_{12}^*\right) & z\in\Omega/\Omega e \end{cases} \tag{3.12}$$

here ε_{ij}^* denotes the components of the eigenstrain in plane strain, d^* is an arbitrary constant, r denotes radius of the circular inclusion, μ is shear modulus, κ is the Kolosov constant (Kolosov 1909) defined as $3-4\nu$ for plain strain, and $\varphi_0(z)$ and $\psi_0(z)$ are holomorphic functions constructed to meet the boundary conditions on the finite domain (true domain).

If the conformal mapping to a unit circle is expressed in the form of a finite series

$$z=w(\zeta)=\sum_{k=1}^{M}C_k\zeta^k \tag{3.13}$$

where M is a finite integer, then the boundary value problem of the complex potentials $\varphi_0(z)$ and $\psi_0(z)$ could be stated alternatively by seeking for the coefficients a_n and b_n in the following expressions

$$\varphi_1(\zeta)=\varphi_0\left(w(\zeta)\right)=\sum_{n=0}^{\infty}a_n\zeta^n \tag{3.14}$$

$$\psi_1(\zeta)=\psi_0\left(w(\zeta)\right)=\sum_{n=0}^{\infty}b_n\zeta^n \tag{3.15}$$

here n cannot be negative because the domain contains the origin (0, 0). They must satisfy the fixed boundary condition for the disturbed field, which can be listed in the following equations if $t=e^{i\theta}$ stands for the points on the unit circle boundary γ.

$$\kappa\varphi_1(t)-\frac{\omega(t)}{\overline{\omega'(t)}}\overline{\varphi_1'(t)}-\overline{\psi_1(t)}=F(t) \tag{3.16}$$

Here

$$F(t) = -\kappa\varphi_*\left(w(t)\right) + w(t)\overline{\varphi_*'\left(w(t)\right)} + \overline{\psi_*\left(w(t)\right)} \tag{3.17}$$

According to Muskhelishvili (1953), since the functions $\varphi_1(t)$ and $\psi_1(t)$ are the boundary values of $\varphi_1(\zeta)$ and $\psi_1(\zeta)$, it is necessary and sufficient to require the functions $\varphi_1(\zeta)$ and $\psi_1(\zeta)$ to meet the following equations expressed in the form of Cauchy Integral:

$$\kappa\varphi_1(\zeta) - \frac{1}{2\pi i}\int_\gamma \frac{\omega(t)}{\overline{\omega'(t)}}\frac{\overline{\varphi_1'(t)}dt}{t-\zeta} - \overline{b}_0 = \frac{1}{2\pi i}\int_\gamma \frac{F(t)\,dt}{t-\zeta} \tag{3.18}$$

$$\kappa\overline{a}_0 - \frac{1}{2\pi i}\int_\gamma \frac{\overline{\omega(t)}}{\omega'(t)}\frac{\varphi_1'(t)\,dt}{t-\zeta} - \psi_1(\zeta) = \frac{1}{2\pi i}\int_\gamma \frac{\overline{F(t)}dt}{t-\zeta} \tag{3.19}$$

here the term $\dfrac{\omega(t)}{\overline{\omega'(t)}}$ could be expressed as

$$\frac{\omega(t)}{\overline{\omega'(t)}} = c_N t^N + c_{N-1}t^{N-1} + \cdots + c_1 t + c_0 + \sum_{k=1}^{\infty} c_{-k}t^{-k} \tag{3.20}$$

where the coefficients c_0 to c_N can be obtained via elementary algebraic operation. N is the highest order of the quotient. After carrying out the contour integral according to the Cauchy Residue Theorem (Priestley 2003), the following results could be obtained:

$$\frac{1}{2\pi i}\int_\gamma \frac{\omega(t)}{\overline{\omega'(t)}}\frac{\overline{\varphi_1'(t)}dt}{t-\zeta} = K_0 + K_1\zeta + \cdots + K_N\zeta^N \tag{3.21}$$

where

$$K_l = \sum_{m=1}^{N-l+1} m\overline{a}_m c_{l+m-1}\,,\ l = 0, 1, \cdots, N \tag{3.22}$$

Besides,

$$\frac{1}{2\pi i}\int_{\gamma}\frac{F(t)\,dt}{t-\zeta}=\beta_0+\beta_1\zeta+\cdots+\beta_N\zeta^N+\cdots \tag{3.23}$$

It is worth mentioning here that this integral needs to be evaluated according to the specified $F(t)$ shown in Eq. (3.17).

If one denotes

$$\mathbf{c}=\begin{bmatrix} & c_0 & 2c_1 & 3c_2 & \cdots & (N+1)c_N \\ & & & & \ddots & \\ & c_1 & 2c_2 & & & \\ \mathbf{0}_{(N+1)\times 1} & c_2 & & \ddots & & \\ & \vdots & \ddots & & & \\ & c_N & & & & \\ 0 & & & \mathbf{0}_{1\times(N+1)} & & \end{bmatrix} \tag{3.24}$$

$$\mathbf{A}=\begin{bmatrix}\tilde{a}_0 & a_1 & a_2 & \cdots & a_{N+1}\end{bmatrix}^T \tag{3.25}$$

$$\boldsymbol{\beta}=\begin{bmatrix}\beta_0 & \beta_1 & \beta_2 & \cdots & \beta_{N+1}\end{bmatrix}^T \tag{3.26}$$

then the matrix equation for the coefficients a_n sought in Eq. (3.14) is

$$[\mathbf{K}]\begin{Bmatrix}\mathbf{A}\\ \overline{\mathbf{A}}\end{Bmatrix}=\begin{Bmatrix}\boldsymbol{\beta}\\ \overline{\boldsymbol{\beta}}\end{Bmatrix} \tag{3.27}$$

where

$$\mathbf{K}=\begin{bmatrix}\kappa\mathbf{I} & -\mathbf{c}\\ -\mathbf{c} & \kappa\mathbf{I}\end{bmatrix} \tag{3.28}$$

Here $\mathbf{I}$ stands for the identity matrix. Note that in order to express the equation in matrix form, the constant term $\overline{b}_0$ is included in the $\tilde{a}_0$ by setting

$$\tilde{a}_0=a_0-\frac{\overline{b}_0}{\kappa} \tag{3.29}$$

without change of the final solution of the displacement field.

The solution of Eq. (3.27) results in the coefficients a_n, $n = 0, 1, 2, \cdots, N+1$. For the results corresponding to terms with order greater than $N+1$, it is straightforward to write the following equation:

$$\kappa a_n = \beta_n, \quad n = N+2, \cdots \tag{3.30}$$

Once the coefficients are determined for $\varphi_1(\zeta)$, one can find the expression of $\psi_1(\zeta)$ according to Eq. (3.19). Finally, the real elastic field can be calculated based on mapping equation and the solutions for $\varphi_1(\zeta)$and $\psi_1(\zeta)$ in the virtual domain. To demonstrate the validity of the general formulation, two RVEs, one bounded by a Pascal's limaçon and the other a curved square, are studied.

3.4 SOLUTION FOR NONCIRCULAR RVES

3.4.1 RVE bounded by a Pascal's Limaçon

As shown in Eq. (3.27) and Eq. (3.28), once the components of the matrix **K** and the right hand side vector **β** are determined, the coefficients are easy to find by solving the elementary matrix equation. The sequential steps of solving this problem are listed below.

(1) Find the coefficients needed for the matrix **K**.

In this step, the conformal mapping is characterized by Eq. (3.6). According to Eq. (3.20), the coefficients needed to fill in the matrix **K**, namely c_k, $k = 0, 1, 2, \cdots, N$ could be found via some elementary algebraic manipulation. The results are listed here.

$$\frac{\omega(t)}{\omega'(t)} = mt^2 + \left(1-2m^2\right)t - 2m\left(1-2m^2\right) + \sum_{k=1}^{\infty} c_{-k} t^{-k} \tag{3.31}$$

It means that $N = 2$, $c_2 = m$, $c_1 = 1-2m^2$ and $c_0 = -2m\left(1-2m^2\right)$. Then the matrix **K** could be finalized according to Eq. (3.24) and Eq. (3.28).

(2) Determine the terms β_k, $k = 0, 1, 2, \cdots$.

According to Eq. (3.23), the coefficients β_k could be determined after the integrals have been carried out. First, the expression for $F(t)$ could be found according to equations (3.6), (3.11), (3.12) and (3.17). It is

$$\begin{aligned} F(t) = &-\kappa\frac{\mu r^2}{\kappa+1}\left(\varepsilon_1^* - \varepsilon_2^* + i\gamma_{12}^*\right)\frac{1}{R}\frac{1}{\left(t+mt^2\right)} - \frac{\mu r^2}{\kappa+1}\left(\varepsilon_1^* - \varepsilon_2^* - i\gamma_{12}^*\right)\frac{1}{R}\frac{\left(t+mt^2\right)}{\left(\frac{1}{t}+m\frac{1}{t^2}\right)^2} \\ &-\frac{2\mu r^2}{\kappa+1}\left(\varepsilon_1^* + \varepsilon_2^*\right)\frac{1}{R}\frac{1}{\left(\frac{1}{t}+m\frac{1}{t^2}\right)} + \frac{\mu r^4}{\kappa+1}\left(\varepsilon_1^* - \varepsilon_2^* - i\gamma_{12}^*\right)\frac{1}{R^3}\frac{1}{\left(\frac{1}{t}+m\frac{1}{t^2}\right)^3} \end{aligned} \tag{3.32}$$

where *r* denotes the radius of the circular inclusion as shown in Figure 3.1a. Thus, Eq. (3.23) consists of the following independent integrals.

$$\frac{1}{2\pi i}\int_\gamma \frac{d\sigma}{t-\zeta}\cdot\frac{1}{\left(t+mt^2\right)} = \sum_{p=0}^{\infty}(-m)^{p+1}\zeta^p \tag{3.33a}$$

$$\begin{aligned} \frac{1}{2\pi i}\int_\gamma \frac{dt}{t-\zeta}\cdot\frac{\left(t+mt^2\right)}{\left(\frac{1}{t}+m\frac{1}{t^2}\right)^2} = &\, m\zeta^4 + \left(1-2m^2\right)\zeta^3 - m\left(2-3m^2\right)\zeta^2 \\ &+ m^2\left(3-4m^2\right)\zeta - m^3\left(4-5m^2\right) \end{aligned} \tag{3.33b}$$

$$\frac{1}{2\pi i}\int_\gamma \frac{dt}{t-\zeta}\cdot\frac{1}{\left(\frac{1}{t}+m\frac{1}{t^2}\right)} = \zeta - m \tag{3.33c}$$

$$\frac{1}{2\pi i}\int_{\gamma}\frac{dt}{t-\zeta}\cdot\frac{1}{\left(\frac{1}{t}+m\frac{1}{t^2}\right)^3}=\zeta^3-3m\zeta^2+6m^2\zeta-10m^3 \tag{3.33d}$$

Then it is with no difficulty to write explicitly the terms β_k, $k=0,1,2,\cdots$ as

$$\begin{aligned}\beta_0=&-\kappa\frac{\mu r^2}{\kappa+1}\left(\varepsilon_1^*-\varepsilon_2^*+i\gamma_{12}^*\right)\frac{1}{R}\cdot(-m)-\frac{\mu r^2}{\kappa+1}\left(\varepsilon_1^*-\varepsilon_2^*-i\gamma_{12}^*\right)\frac{1}{R}\cdot\left(-m^3\left(4-5m^2\right)\right)\\&-\frac{2\mu r^2}{\kappa+1}\left(\varepsilon_1^*+\varepsilon_2^*\right)\frac{1}{R}\cdot(-m)+\frac{\mu r^4}{\kappa+1}\left(\varepsilon_1^*-\varepsilon_2^*-i\gamma_{12}^*\right)\frac{1}{R^3}\cdot\left(-10m^3\right)\end{aligned} \tag{3.34a}$$

$$\begin{aligned}\beta_1=&-\kappa\frac{\mu r^2}{\kappa+1}\left(\varepsilon_1^*-\varepsilon_2^*+i\gamma_{12}^*\right)\frac{1}{R}\cdot(-m)^2-\frac{\mu r^2}{\kappa+1}\left(\varepsilon_1^*-\varepsilon_2^*-i\gamma_{12}^*\right)\frac{1}{R}\cdot m^2\left(3-4m^2\right)\\&-\frac{2\mu r^2}{\kappa+1}\left(\varepsilon_1^*+\varepsilon_2^*\right)\frac{1}{R}+\frac{\mu r^4}{\kappa+1}\left(\varepsilon_1^*-\varepsilon_2^*-i\gamma_{12}^*\right)\frac{1}{R^3}\cdot\left(6m^2\right)\end{aligned} \tag{3.34b}$$

$$\begin{aligned}\beta_2=&-\kappa\frac{\mu r^2}{\kappa+1}\left(\varepsilon_1^*-\varepsilon_2^*+i\gamma_{12}^*\right)\frac{1}{R}\cdot(-m)^3-\frac{\mu r^2}{\kappa+1}\left(\varepsilon_1^*-\varepsilon_2^*-i\gamma_{12}^*\right)\frac{1}{R}\cdot\left(-m\left(2-3m^2\right)\right)\\&+\frac{\mu r^4}{\kappa+1}\left(\varepsilon_1^*-\varepsilon_2^*-i\gamma_{12}^*\right)\frac{1}{R^3}\cdot(-3m)\end{aligned} \tag{3.34c}$$

$$\begin{aligned}\beta_3=&-\kappa\frac{\mu r^2}{\kappa+1}\left(\varepsilon_1^*-\varepsilon_2^*+i\gamma_{12}^*\right)\frac{1}{R}\cdot(-m)^4-\frac{\mu r^2}{\kappa+1}\left(\varepsilon_1^*-\varepsilon_2^*-i\gamma_{12}^*\right)\frac{1}{R}\cdot\left(1-2m^2\right)\\&+\frac{\mu r^4}{\kappa+1}\left(\varepsilon_1^*-\varepsilon_2^*-i\gamma_{12}^*\right)\frac{1}{R^3}\end{aligned} \tag{3.34d}$$

$$\beta_4=-\kappa\frac{\mu r^2}{\kappa+1}\left(\varepsilon_1^*-\varepsilon_2^*+i\gamma_{12}^*\right)\frac{1}{R}\cdot(-m)^5-\frac{\mu r^2}{\kappa+1}\left(\varepsilon_1^*-\varepsilon_2^*-i\gamma_{12}^*\right)\frac{1}{R}\cdot m \tag{3.34e}$$

$$\beta_q=-\kappa\frac{\mu r^2}{\kappa+1}\left(\varepsilon_1^*-\varepsilon_2^*+i\gamma_{12}^*\right)\frac{1}{R}\cdot(-m)^{q+1},\ q=5,6,\cdots \tag{3.34f}$$

Note here that according to Eq. (3.26), only $\beta_0,\beta_1,\beta_2,\beta_3$ are placed in the right hand side vector $\boldsymbol{\beta}$, since for this case $N = 2$. The rest terms are substituted in Eq. (3.30).

(3) Determine the two complex potentials $\varphi_1(\zeta)$ and $\psi_1(\zeta)$.

Solving the elementary matrix equation (3.27), and writing the rest of the terms explicitly according to Eq. (3.30), the coefficients needed in Eq. (3.14), namely a_n, $n = 0, 1, 2, \cdots$, are determined as

$$a_n = \begin{cases} \boldsymbol{\beta}^T \mathbf{K}^{-T} \boldsymbol{\Delta}_n & n = 0, 1, \cdots, N+1 \\ \beta_n / \kappa & n \geq N+2 \end{cases} \tag{3.35}$$

where $N = 2$ and the auxiliary vector $\boldsymbol{\Delta}_n$ is defined as $\boldsymbol{\Delta}_n = \left[0, \quad \cdots \quad 0, \quad \overset{(n+1)th}{1}, \quad 0, \quad \cdots \quad 0 \right]^T_{2N+4}$.

Therefore, $\varphi_1(\zeta)$ is obtained explicitly as following:

$$\varphi_1(\zeta) = \boldsymbol{\beta}^T \mathbf{K}^{-T} \boldsymbol{\zeta}_1 + \sum_{k_1=4}^{\infty} \frac{\beta_{k_1}}{\kappa} \zeta^{k_1} \tag{3.36}$$

where $\boldsymbol{\zeta}_1 = \left[1, \quad \zeta, \quad \zeta^2, \quad \zeta^3, \quad 0, \quad 0, \quad 0, \quad 0 \right]^T$. According to Eq. (3.19), $\psi_1(\zeta)$ could be evaluated. Take the conjugate of Eq. (3.32), the explicit expression for $\overline{F(t)}$ is easy to obtain:

$$\begin{aligned} \overline{F(t)} = & -\kappa \frac{\mu r^2}{\kappa+1} \left(\varepsilon_1^* - \varepsilon_2^* - i\gamma_{12}^* \right) \frac{1}{R} \frac{1}{\left(\frac{1}{t} + m \frac{1}{t^2} \right)} - \frac{\mu r^2}{\kappa+1} \left(\varepsilon_1^* - \varepsilon_2^* + i\gamma_{12}^* \right) \frac{1}{R} \frac{\left(\frac{1}{t} + m \frac{1}{t^2} \right)}{\left(t + mt^2 \right)^2} \\ & - \frac{2\mu r^2}{\kappa+1} \left(\varepsilon_1^* + \varepsilon_2^* \right) \frac{1}{R} \frac{1}{\left(t + mt^2 \right)} + \frac{\mu r^4}{\kappa+1} \left(\varepsilon_1^* - \varepsilon_2^* + i\gamma_{12}^* \right) \frac{1}{R^3} \frac{1}{\left(t + mt^2 \right)^3} \end{aligned} \tag{3.37}$$

$\psi_1(\zeta)$ could be determined via the two contour integrals listed in Eq. (3.19), which consist of the following three independent integrals.

$$\frac{1}{2\pi i} \int_\gamma \frac{dt}{t - \xi} \cdot \frac{\left(\frac{1}{t} + m \frac{1}{t^2} \right)}{\left(t + mt^2 \right)^2} = \frac{-3m^3}{1 + m\zeta} + \frac{-m^3}{\left(1 + m\zeta \right)^2} + m \left(\frac{4m^4}{1 + m\zeta} + \frac{m^4}{\left(1 + m\zeta \right)^2} \right) \tag{3.38a}$$

$$\frac{1}{2\pi i}\int_{\gamma}\frac{dt}{t-\xi}\cdot\frac{1}{\left(t+mt^{2}\right)^{3}}=\frac{-6m^{3}}{1+m\zeta}+\frac{-3m^{3}}{\left(1+m\zeta\right)^{2}}+\frac{-m^{3}}{\left(1+m\zeta\right)^{3}} \tag{3.38b}$$

$$\begin{aligned}\frac{1}{2\pi i}\int_{\gamma}\frac{\overline{\omega(t)}}{\omega'(t)}\frac{\varphi'(t)dt}{t-\zeta}&=a_{1}\frac{2m}{1+2m\zeta}+2a_{2}\frac{1}{1+2m\zeta}+\sum_{n=3}^{\infty}na_{n}\frac{\zeta^{n-2}}{1+2m\zeta}\\&+m\left(a_{1}\frac{2m^{2}}{1+2m\zeta}+2a_{2}\frac{2m}{1+2m\zeta}+3a_{3}\frac{1}{1+2m\zeta}\right)\\&+m\sum_{n=4}^{\infty}na_{n}\frac{\zeta^{n-3}}{1+2m\zeta}\end{aligned} \tag{3.38c}$$

Finally, the analytical expression for $\psi_{1}(\zeta)$ is:

$$\begin{aligned}\psi_{1}(\zeta)&=\kappa\frac{\mu}{\kappa+1}\left(\varepsilon_{1}^{*}-\varepsilon_{2}^{*}-i\gamma_{12}^{*}\right)\frac{r^{2}}{R}\zeta\\&+\frac{\mu r^{2}}{\kappa+1}\left(\varepsilon_{1}^{*}-\varepsilon_{2}^{*}+i\gamma_{12}^{*}\right)\frac{1}{R}\left(\left(-3m^{3}+4m^{5}\right)\left(\frac{1}{1+m\zeta}-1\right)+\left(-m^{3}+m^{5}\right)\left(\frac{1}{\left(1+m\zeta\right)^{2}}-1\right)\right)\\&+\frac{2\mu}{\kappa+1}\left(\varepsilon_{1}^{*}+\varepsilon_{2}^{*}\right)\frac{r^{2}}{R}\left(-m\left(\frac{1}{1+m\xi}-1\right)\right)\\&-\frac{\mu}{\kappa+1}\left(\varepsilon_{1}^{*}-\varepsilon_{2}^{*}+i\gamma_{12}^{*}\right)\frac{r^{4}}{R^{3}}\left(-6m^{3}\left(\frac{1}{1+m\zeta}-1\right)-3m^{3}\left(\frac{1}{\left(1+m\zeta\right)^{2}}-1\right)-m^{3}\left(\frac{1}{\left(1+m\zeta\right)^{3}}-1\right)\right)\\&-\left(a_{1}\frac{\left(-2m\right)^{2}\zeta}{1+2m\zeta}+2a_{2}\frac{\left(-2m\right)\zeta}{1+2m\zeta}+\sum_{n=3}^{\infty}na_{n}\frac{\zeta^{n-2}}{1+2m\zeta}\right)\\&-\left(m\left(a_{1}\frac{\left(-2m\right)^{3}\zeta}{1+2m\zeta}+2a_{2}\frac{\left(-2m\right)^{2}\zeta}{1+2m\zeta}+3a_{3}\frac{\left(-2m\right)^{1}\zeta}{1+2m\zeta}\right)+m\sum_{n=4}^{\infty}na_{n}\frac{\zeta^{n-3}}{1+2m\zeta}\right)\end{aligned} \tag{3.39}$$

Note here this analytical expression agrees with Eq. (3.15) because $|\zeta|\le 1$ ensures it could be written as an infinite series.

Finally, once the $\varphi_{1}(\zeta)$ and $\psi_{1}(\zeta)$ are determined, they can be substituted back to Eq. (3.10) to obtain the final potentials sought for this RVE. For easy application, the inverse

mapping of the Eq. (3.6) is needed to complete the explicit expression for the elastic fields, which will be discussed later.

3.4.2 RVE bounded by a Curved Square.

Similar to the Pascal's limaçon, the RVE bounded by a curved square which approximates a perfect square could be solved following the same steps, since the mapping in Eq. (3.9) is able to be expressed in the form of polynomials shown in Eq. (3.13). Here for simplicity, only the first three terms of the mapping function are employed which will be shown later to be accurate enough for engineering application. The following mapping function is employed,

$$z = C_1\zeta + C_5\zeta^5 + C_9\zeta^9 \tag{3.40}$$

where the coefficients are determined according to Eq. (3.9), namely $C_1 = -i\alpha_1$, $C_5 = -\dfrac{i\alpha_1}{10}$ and $C_9 = -\dfrac{i\alpha_1}{24}$.

(1) Find the coefficients needed for the matrix **K**.

According to Eq. (3.20), the coefficients needed to fill in the matrix **K**, namely c_k, $k = 0, 1, 2, \cdots, n_0$ could be found similarly. The results are:

$$\begin{aligned}\frac{\omega(t)}{\overline{\omega'(t)}} = &\left(\frac{C_9}{\overline{C}_1}\right)t^9 + \left(\frac{C_5}{\overline{C}_1} - 5\frac{\overline{C}_5}{\overline{C}_1^2}C_9\right)t^5 \\ &+ \left(\frac{C_1}{\overline{C}_1} - 9\frac{\overline{C}_9}{\overline{C}_1^2}C_9 - 5\frac{\overline{C}_5}{\overline{C}_1^2}C_5 + 25\frac{\overline{C}_5^2}{\overline{C}_1^3}C_9\right)t + \sum_{k=1}^{\infty} c_{-k}t^{-k}\end{aligned} \tag{3.41}$$

It means $N = 9$, $c_9 = \dfrac{C_9}{\overline{C}_1}$, $c_5 = \dfrac{C_5}{\overline{C}_1} - 5\dfrac{\overline{C}_5}{\overline{C}_1^2}C_9$ and $c_1 = \dfrac{C_1}{\overline{C}_1} - 9\dfrac{\overline{C}_9}{\overline{C}_1^2}C_9 - 5\dfrac{\overline{C}_5}{\overline{C}_1^2}C_5 + 25\dfrac{\overline{C}_5^2}{\overline{C}_1^3}C_9$. Then the matrix **K** could be finalized according to Eq. (3.24) and Eq. (3.28).

(2) Determine the terms β_k, $k = 0, 1, 2, \cdots$.

First, the expression for $F(t)$ in Eq. (3.23) could be found according to equations (3.11), (3.12), (3.17) and (3.40). It is

$$F(t) = -\kappa\frac{\mu r^2}{\kappa+1}\left(\varepsilon_1^* - \varepsilon_2^* + i\gamma_{12}^*\right)\frac{1}{C_1 t + C_5 t^5 + C_9 t^9} - \frac{\mu r^2}{\kappa+1}\left(\varepsilon_1^* - \varepsilon_2^* - i\gamma_{12}^*\right)\frac{t^{18}\left(C_1 t + C_5 t^5 + C_9 t^9\right)}{\left(\bar{C}_1 t^8 + \bar{C}_5 t^4 + \bar{C}_9\right)^2}$$
$$-\frac{2\mu r^2}{\kappa+1}\left(\varepsilon_1^* + \varepsilon_2^*\right)\frac{1}{\bar{C}_1\frac{1}{t} + \bar{C}_5\frac{1}{t^5} + \bar{C}_9\frac{1}{t^9}} + \frac{\mu r^4}{\kappa+1}\left(\varepsilon_1^* - \varepsilon_2^* - i\gamma_{12}^*\right)\frac{1}{\left(\bar{C}_1\frac{1}{t} + \bar{C}_5\frac{1}{t^5} + \bar{C}_9\frac{1}{t^9}\right)^3} \tag{3.42}$$

Thus, the evaluation of Eq. (3.23) consists of the following independent integrals.

$$\frac{1}{2\pi i}\int_\gamma \frac{dt}{t-\zeta}\cdot\frac{1}{C_1 t + C_5 t^5 + C_9 t^9} = -\frac{C_5\zeta^3 + C_9\zeta^7}{C_1^2 + C_1 C_5\zeta^4 + C_1 C_9\zeta^8} = \sum_{p=0}^{\infty}\theta_p\zeta^p \tag{3.43a}$$

$$\frac{1}{2\pi i}\int_\gamma \frac{dt}{t-\xi}\cdot\frac{t^{18}\left(C_1 t + C_5 t^5 + C_9 t^9\right)}{\left(\bar{C}_1 t^8 + \bar{C}_5 t^4 + \bar{C}_9\right)^2} = \left(\frac{C_1}{\bar{C}_1^2} - \frac{2\bar{C}_5 C_5}{\bar{C}_1^3} + \frac{3\bar{C}_5^2 C_9}{\bar{C}_1^4} - \frac{2\bar{C}_9 C_9}{\bar{C}_1^3}\right)\zeta^3$$
$$+\left(\frac{C_5}{\bar{C}_1^2} - \frac{2\bar{C}_5 C_9}{\bar{C}_1^3}\right)\zeta^7 + \frac{C_9}{\bar{C}_1^2}\zeta^{11} \tag{3.43b}$$

$$\frac{1}{2\pi i}\int_\gamma \frac{dt}{t-\zeta}\cdot\frac{1}{\bar{C}_1\frac{1}{t} + \bar{C}_5\frac{1}{t^5} + \bar{C}_9\frac{1}{t^9}} = \frac{\zeta}{\bar{C}_1} \tag{3.43c}$$

$$\frac{1}{2\pi i}\cdot\int_\gamma \frac{dt}{t-\zeta}\cdot\frac{1}{\left(\bar{C}_1\frac{1}{t} + \bar{C}_5\frac{1}{t^5} + \bar{C}_9\frac{1}{t^9}\right)^3} = \frac{\zeta^3}{\bar{C}_1^3} \tag{3.43d}$$

Note here the integral in Eq. (3.43a) is explicitly expanded as the power series of the rational fraction, and the coefficients θ_p could be found without theoretical difficulties. For example:

$$\theta_3=-\frac{C_5}{C_1^{\,2}},\ \theta_7=-\left(-\frac{C_5^{\,2}}{C_1^{\,3}}+\frac{C_9}{C_1^{\,2}}\right),\ \theta_{11}=-\left(\frac{C_5^{\,3}}{C_1^{\,4}}-\frac{2C_5C_9}{C_1^{\,3}}\right),$$
$$\theta_{15}=-\left(-\frac{C_5^{\,4}}{C_1^{\,5}}+\frac{3C_5^{\,2}C_9}{C_1^{\,4}}-\frac{C_9^{\,2}}{C_1^{\,3}}\right),\ \theta_{19}=-\left(\frac{C_5^{\,5}}{C_1^{\,6}}-\frac{4C_5^{\,3}C_9}{C_1^{\,5}}+\frac{3C_5C_9^{\,2}}{C_1^{\,4}}\right),\cdots \tag{3.44}$$

Then the terms $\beta_k,\ k=0,1,2,\cdots$ could be written out similarly as Eq. (3.34),

$$\beta_1=-\frac{2\mu r^2}{\kappa+1}\left(\varepsilon_1^*+\varepsilon_2^*\right)\frac{1}{\overline{C}_1} \tag{3.45a}$$

$$\begin{aligned}\beta_3=&\kappa\frac{\mu r^2}{\kappa+1}\left(\varepsilon_1^*-\varepsilon_2^*+i\gamma_{12}^*\right)\frac{C_5}{C_1^{\,2}}\\&-\frac{\mu r^2}{\kappa+1}\left(\varepsilon_1^*-\varepsilon_2^*-i\gamma_{12}^*\right)\left(\frac{C_1}{\overline{C}_1^{\,2}}-\frac{2\overline{C}_5C_5}{\overline{C}_1^{\,3}}+\frac{3\overline{C}_5^{\,2}C_9}{\overline{C}_1^{\,4}}-\frac{2\overline{C}_9C_9}{\overline{C}_1^{\,3}}\right)\\&+\frac{\mu r^4}{\kappa+1}\left(\varepsilon_1^*-\varepsilon_2^*-i\gamma_{12}^*\right)\frac{1}{\overline{C}_1^{\,3}}\end{aligned} \tag{3.45b}$$

$$\beta_7=\kappa\frac{\mu r^2}{\kappa+1}\left(\varepsilon_1^*-\varepsilon_2^*+i\gamma_{12}^*\right)\left(-\frac{C_5^{\,2}}{C_1^{\,3}}+\frac{C_9}{C_1^{\,2}}\right)-\frac{\mu r^2}{\kappa+1}\left(\varepsilon_1^*-\varepsilon_2^*-i\gamma_{12}^*\right)\left(\frac{C_5}{\overline{C}_1^{\,2}}-\frac{2\overline{C}_5C_9}{\overline{C}_1^{\,3}}\right) \tag{3.45c}$$

$$\beta_{11}=\kappa\frac{\mu r^2}{\kappa+1}\left(\varepsilon_1^*-\varepsilon_2^*+i\gamma_{12}^*\right)\left(\frac{C_5^{\,3}}{C_1^{\,4}}-\frac{2C_5C_9}{C_1^{\,3}}\right)-\frac{\mu r^2}{\kappa+1}\left(\varepsilon_1^*-\varepsilon_2^*-i\gamma_{12}^*\right)\frac{C_9}{\overline{C}_1^{\,2}} \tag{3.45d}$$

$$\beta_{15}=\kappa\frac{\mu r^2}{\kappa+1}\left(\varepsilon_1^*-\varepsilon_2^*+i\gamma_{12}^*\right)\left(-\frac{C_5^{\,4}}{C_1^{\,5}}+\frac{3C_5^{\,2}C_9}{C_1^{\,4}}-\frac{C_9^{\,2}}{C_1^{\,3}}\right) \tag{3.45e}$$

$$\beta_k=\begin{cases}0 & k=2,4,5,6,8,9,10,12,13,14\\ -\kappa\dfrac{\mu r^2}{\kappa+1}\left(\varepsilon_1^*-\varepsilon_2^*+i\gamma_{12}^*\right)\theta_k & k\geq 15\end{cases} \tag{3.45f}$$

(3) Determine the two complex potentials $\varphi_1(\zeta)$ and $\psi_1(\zeta)$.

As shown above, the matrix **K** and the right hand side terms $\beta_k,\ k=0,1,2,\cdots$ have been obtained. Solving the elementary matrix equation (3.27) and writing the rest of the terms

explicitly according to Eq. (3.30), the coefficients a_n needed in Eq. (3.14) and the corresponding potential $\varphi_1(\zeta)$ could be obtained via updating Eq. (3.35) and Eq. (3.36). Once all the coefficients in Eq. (3.14) are determined, the other complex potential $\psi_1(\zeta)$ could be found via evaluation of two contour integrals, which are documented in the appendix for simplicity.

The obtained $\varphi_1(\zeta)$ and $\psi_1(\zeta)$ are substituted back to Eq. (3.10) to construct the final potentials sought for this RVE, where the inverse of the mapping Eq. (3.40) is needed to obtain the explicit expression as a function of *z* for easy application.

3.5 COMPARISON WITH FEM SIMULATION

First the analytical solutions obtained via complex potential method are compared with the numerical results from the FEM model for the same problem, which shows in details that the solutions accurately describe the displacement field in the RVE.

Here, a RVE bounded by Pascal's Limacon (*R*=1, *m*=0.2) and the other one by a curved square described by Eq. (3.40) are studied numerically by FEM. The model are shown in Figure 3.4. In both cases, Dirichelet boundary condition is applied for a specified eigenstrain $\left[\varepsilon_1^*,\ \ \varepsilon_2^*,\ \ \gamma_{12}^*\right] = \left[0.01,\ \ -0.02,\ \ 0.03\right]^T$. The inclusion size is described by $r = 0.6$ and the material properties are assigned as $E = 30$ GPa and $\nu = 0.2$.

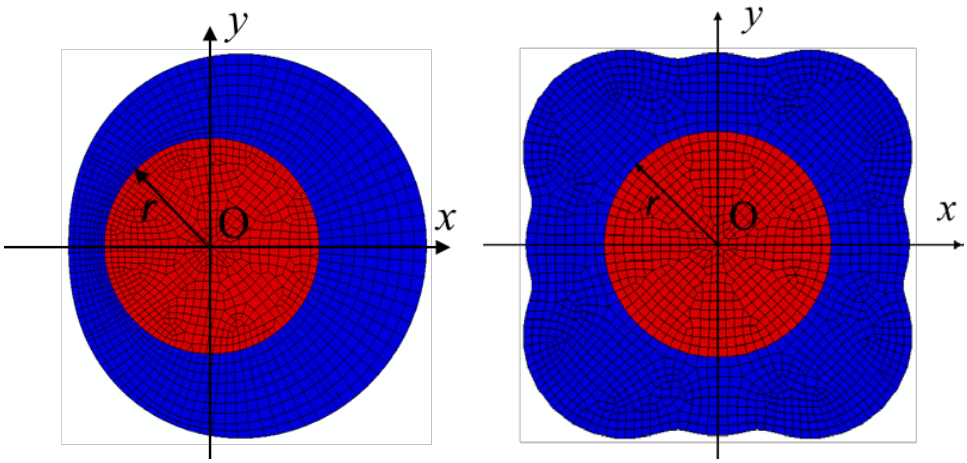

Figure 3.4. The FEM models for the RVEs

Here the disturbance of displacement along five main directions obtained theoretically and numerically are depicted in Figure 3.5. It can be seen that the FEM solutions firmly agree with the proposed theoretical solutions. This means that the complex potential method can theoretically predict the disturbed fields caused by an arbitrary eigenstrain in RVEs with noncircular shape.

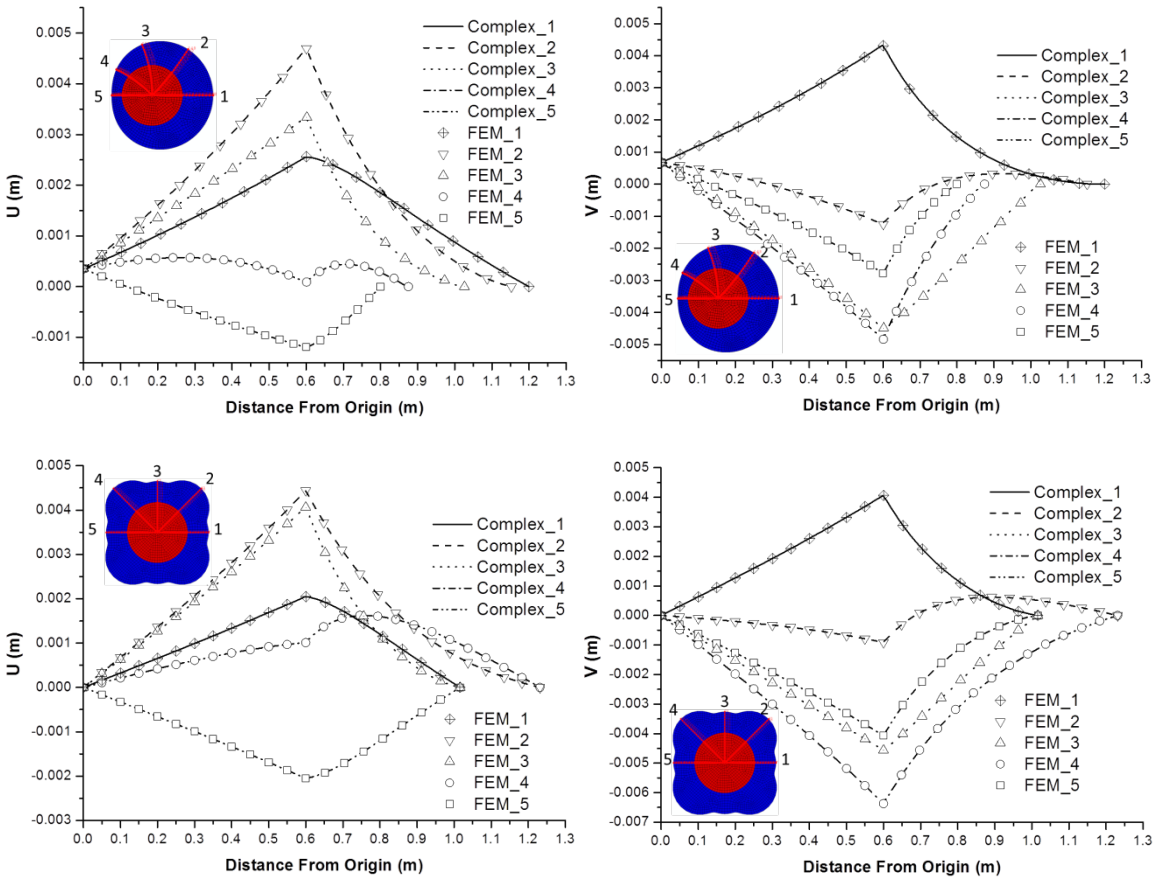

Figure 3.5. Disturbance of displacement field in the finite domain RVEs

In addition, it is shown here that the curved square is indeed a good approximation of the RVE bounded by a perfect square. The comparison of the disturbance of displacement along direction 1 and 2 inside the pefect square RVE and the curved one is documented in Figure 3.6.

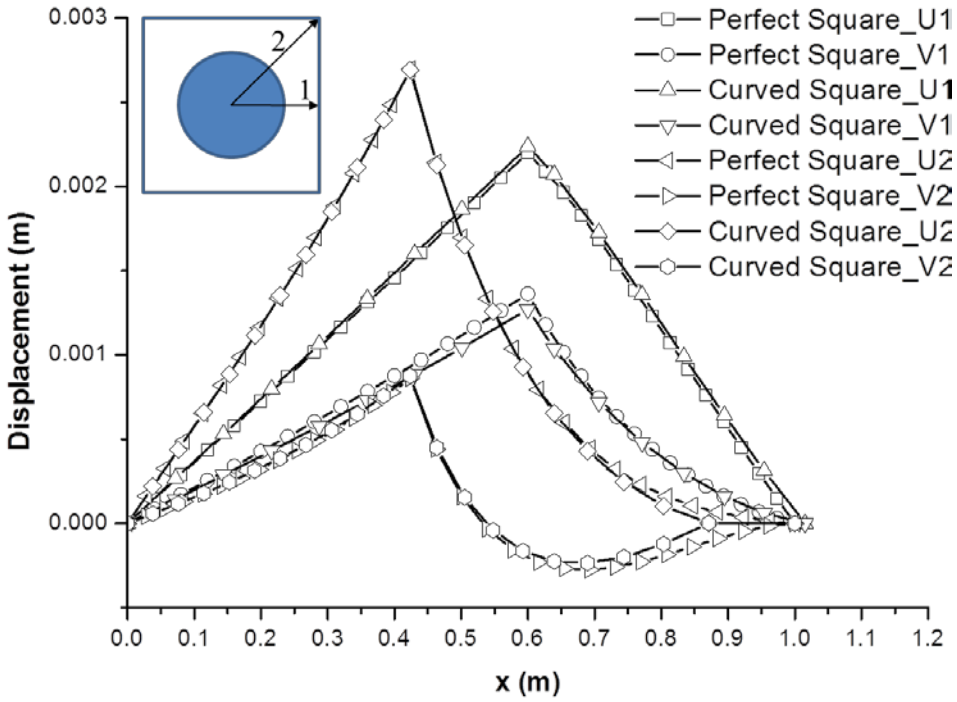

Figure 3.6. Comparison of disturbance of displacement in curved square and perfect square

It could be seen that the disturbance of displacement in the curved square is slightly different from the perfect one. The difference is less than 2%, which means this curved square RVE is a good approximation. Besides, it is rational to conclude that more accurate results could be obtained if more terms in the conformal mapping in Eq. (3.9) are used.

3.6 RELATION TO ESHELBY'S SOLUTION AND INVERSE CONFORMAL MAPPING

As discussed above, the RVEs are in a finite domain, which is different from the classic Eshelby's inclusion problem. However, if the volume fraction of the inclusion is set infinitesimal, the solution must recover the classic Esbelby's solution. For the RVE bounded by

Pascal's limacon, the volume fraction of the inclusion could be described by the ratio $|r/R|$, while for the one bounded by square by $|r/\alpha_1|$. It is not difficult to find that asymptotes of $|r/R| \to 0$ and $|r/\alpha_1| \to 0$ imply that $\beta_k = 0,\ k = 0, 1, 2, \cdots$ in Eqs. (3.27) and (3.30). This means that a_n and $b_n = 0,\ n = 0, 1, 2, \cdots$ in Eqs (3.14) and (3.15), and consequently the two potentials φ_0 and ψ_0 in Eq. (3.10) vanish. Therefore, the complex potentials for the inclusion problem in infinite domain are in fact φ_* and ψ_*, which recovers the classic Eshelby's solution in 2D plane strain problem; see Pan and Yu (2013).

The obtained results for the disturbance of displacement field could be easily used if expressed as a function of *z*. In order to transform the complex potentials defined in the ζ plane back to the *z* plane, the inverse conformal mapping of (3.6) and (3.9) are needed. Fortunately, guaranteed by Lagrange inversion theorem, the inverse could be given in the form of an infinite power series. The theorem states that at certain point ζ_0 where the first derivative of the analytic function $z = \omega(\zeta)$ is nonzero, the inverse function of it could be expressed as a Taylor series, which is named Lagrange-Burmann formula (Stenlund 2010). Accordingly, the inverse mapping could be expressed alternatively as infinite series, and thus enable the explicit expression of the disturbance of the displacement field in the form of *z*.

For example, if $\zeta = \zeta(z)$ is assumed to be the inverse of $z = R\left(\zeta + m\zeta^2\right)$ in Eq. (3.6), it could be expressed explicitly as the following infinite series.

$$\zeta = \sum_{n=0}^{\infty} \lambda_n z^n \tag{3.46}$$

where $\lambda_n = \frac{1}{n!}\frac{\partial^n \zeta}{\partial z^n}\bigg|_{z=0}$. Observing that $z = 0$ is corresponding to $\zeta = 0$, there exists no theoretical difficulty to find the coefficients via some basic calculations. Here $\lambda_0 = 0$, $\lambda_1 = R^{-1}$ and $\lambda_n = \frac{1}{n!}(-1)(-3)\cdots(3-2n)R^{-n}(2m)^{n-1}$, $n = 2, 3, \cdots$.

It is worth mentioning that one needs to pay attention to the radius of convergence each time for the obtained Lagrange series. For example, the interval of convergence for the power series in Eq. (3.46) is $|z| \le \left|\frac{R}{4m}\right|$, which is not able to cover the whole domain of interests for $m \ge 0.3$. In order to get the converging inverse series for the uncovered domain, the power series could be obtained via Taylor expansion at certain points other than the origin. According to Lagrange's inverse theorem, it is guaranteed at least sectional expression for the converging inverse series could be found for the inverse mapping. In fact, some celebrated math software, e.g. Mathmatica, provides the tool to calculate the infinite series to an arbitrary order as needed, which is very convenient for application.

3.7 DISCUSSION AND CONCLUSION

The complex potential method is developed to solve the finite domain inclusion problems where the matrices could be in different shape. To build the potentials troubled by the difficulties brought up by the shape effect of the matrices, the conformal mapping is employed to enable the construction in a much simpler virtual domain, and then the inverse of the mapping gives in an infinite series to map the potentials back to the origin domain. The solutions of the RVEs

bounded by the Pascal's Limacon and a curved square are shown theoretically predicted the displacement field. In addition, the curved square is proved to be a good approximation of the perfect one, which means the solution provided here is ready for application. Furthermore, the obtained expressions recover the classical Eshelby's solution in asymptotical cases.

Based on the theoretical derivation and computational results, it is rational to conclude that the Eshelby's tensor for finite domain inclusion problem is able to be obtained via the complex potential method combined with conformal mapping strategy. Obviously the shape effect of the matrices results in different expressions of the tensors.

4.0 SHAPE EFFECT OF THE INCLUSION

In this chapter, the shape effect of the inclusion is considered. The focus is particularly placed on constructing a general methodology to seek for the analytical solutions of the disturbed elastic field within a two-dimensional (2D) finite domain containing an arbitrarily shaped inclusion. In the theoretical derivation, the complex potential method is adopted and Laurent series expansion is employed to express the governing potential functions within the finite elastic domain. To overcome the mathematical challenges imposed by the complex geometries of inclusion-matrix interface and matrix boundary, the inclusion is replaced with an arbitrarily-sided polygon, which enables 1) the shape of inclusion to be closely approximated and 2) the gap function on the inclusion-matrix interface to be evaluated by Cauchy integrals performed on the straight edges. Then conformal mapping is utilized to map the real domain to a virtual unit circle. It is found that after the boundary condition is enforced, the coefficient of every term in the Laurent series expansion for the potential functions can be explicitly determined by evaluating the Fourier transform of the boundary effect and its conjugate on the exterior boundary. To further delineate the mathematical framework, several examples are presented, and the obtained results are verified by numerical analysis and some analytical benchmarks available in the literature.

4.1 MOTIVATION AND BACKGROUND

As documented in the previous chapters, compared with the vast body of analytical solutions obtained for the inclusions embedded in unbounded domains, explicit expressions of the disturbed fields in finite domains are very limited in the literature. This scarcity can be attributed to the disturbance bounced back from the boundary of matrix. For any analytical derivations anchored at the Green's function-based approaches, it is a formidable challenge to mathematically evaluate this type of boundary value problem. Thus, numerical approaches (Theocaris and Ioakimidis 1977, Andreev and O'Reilly 2000, Franciosi and Lormand 2004) have to be frequently used to handle the inclusion problems in a variety of engineering applications, where the elastic matrix is bounded and the volume fraction of inclusion cannot be considered negligible.

To investigate the effect of matrix boundary, a framework based on complex potential method is constructed in this study. Residing on the complex potential method and conformal mapping, one can obtain the analytical solutions for a finite matrix shaped as a curved square or a Pascal's Limaçon. However, in the last chapter, we did not consider inclusions of noncircular shapes, which are widely used in many engineering applications (Maranganti and Sharma, 2001). Recently, Zuo et al. (2012) proposed a general approach based on the complex potential method and boundary integrals to analyze the disturbance in a finite 2D domain. Although they gave the examples of a squared inclusion and an eccentric circular inclusion embedded in a circular 2D domain respectively, their solutions contain complex integral forms that are difficult to evaluate for arbitrarily shaped inclusions. Furthermore, the role of conformal mapping in tackling the complicatedly shaped matrix boundary is not considered in their derivation. More importantly, in their solutions for the governing potential functions, there exist terms containing $1/z$, where z is a

complex number representing a point in the 2D domain. The existence of these terms means that singular displacement and singular stress will appear at the origin with $z = 0$. This contradicts with the general perception that except for the locations of geometrical discontinuities (e.g., corners), a finite eigenstrain should not induce singular displacement and stress fields in an elastic body (Markenscoff and Dundurs 2014).

To eliminate this suspicious singularity, as well as to meet the demands for the solutions of complicatedly shaped inclusions and matrixes, a general approach is constructed in this study. In view of the difficulties associated with the evaluation of boundary integral along the inclusion-matrix interface, the inclusion is replaced with an arbitrarily-sided polygon in this study. An advantage of this replacement is that the Cauchy integral on the interface can be decomposed into piecewise integrals along the straight edges of polygon. This study is organized as follows. In Section 4.2, the general formulation of Eshelby's first problem in a finite 2D domain containing an arbitrarily shaped inclusion is presented. The replacement of original inclusion with a polygon and the conformal mapping of matrix boundary are described. Then, the process to determine the explicit expressions of governing potential functions is detailed in Section 4.3 for a given mapping function. In the evaluation of piecewise integrals along the polygon edges, the mathematical operation on the logarithmic functions must be limited within the single-valued branch $[-\pi, \pi]$. After the general framework is established, three examples are presented in Section 4.4, where the obtained analytical solutions are compared with the numerical results and some theoretical benchmarks available in the literature. In Section 4.5, the stress singularity caused by the vertices of polygon and the accuracy of this solution are discussed, followed by the illustration of the approach to identify Eshelby’s tensor in section 4.6. Finally, some conclusions are drawn in Section 4.7.

4.2 GENERAL FORMULATION

In Figure 4.1a, a complicatedly shaped inclusion, which is enclosed by a singly connected curve, is arbitrarily placed in a 2D elastic matrix. Here both the inclusion and the matrix are assumed to be isotropic, homogeneous, and share same elastic property. Due to a certain physical activation (e.g., thermal expansion or plastic flow), a uniform eigenstrain ε^* is induced within the inclusion, which can be expressed as

$$\varepsilon_{ij}^{*}(z)=\begin{cases}\varepsilon_{ij}^{*} & z\in\omega\\ 0 & z\in\Omega/\omega\end{cases} \tag{4.1}$$

here Ω represents the elastic body; ω is the embedded inclusion; and $z = x + iy$ is a complex number representing an arbitrary point (x, y) within Ω.

If the 2D matrix is unbounded, an approach widely used in the formulation of Eshelby's first problem is to map the real inclusion to a virtual unit circle, and then identify the governing potential functions in this virtual domain (Ru 2001, Gao 2011). However, if the matrix is bounded, the evaluation of the imposed boundary conditions in the virtual domain will be a difficult task. This is due to the fact that the conformal mapping, which turns the inclusion into a virtual unit circle, usually maps the matrix to a virtual domain of complex shape, and thus leads to a more challenging boundary value problem. Here a more efficient approach is demonstrated after the description of the problem below.

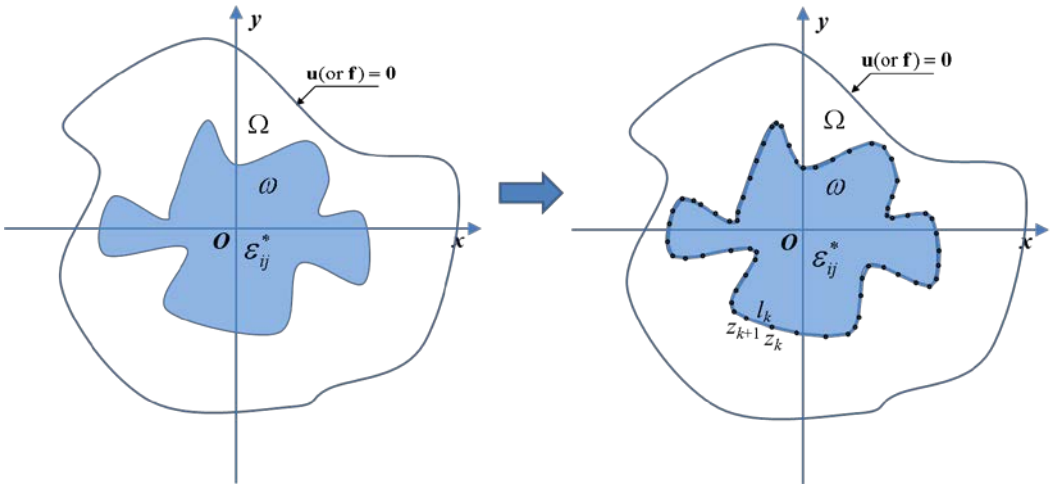

Figure 4.1. A finite domain containing an arbitrarily shaped inclusion, and the replacement of inclusion with an arbitrarily-sided polygon

Due to the uniform eigenstrain within the inclusion, there is a gap in the displacement field along the inclusion-matrix interface. This displacement gap can be treated mathematically as a simplified Riemann-Hilbert Problem as follows (Sherman 1940, Muskelishivili 1953)

$$\begin{aligned} \varphi^+ - \varphi^- &= -\left(C_1 t - \overline{C}_2 \overline{t}\right) \\ \psi^+ - \psi^- &= 2C_1 \overline{t} - C_2 t - \overline{C}_2 \overline{t} \frac{d\overline{t}}{dt} \end{aligned} \tag{4.5}$$

where φ^+ and ψ^+ are the potentials inside the inclusion while φ^- and ψ^- inside the matrix. If the eigenstrain is $\varepsilon^* = \begin{bmatrix} \varepsilon_1^* & \varepsilon_2^* & \gamma_{12}^* \end{bmatrix}$ within the inclusions, the coefficients C_1 and C_2 can be defined as

$$\begin{aligned} C_1 &= \frac{\mu}{\kappa + 1}\left(\varepsilon_1^* + \varepsilon_2^*\right) \\ C_2 &= -\frac{\mu}{\kappa + 1}\left(\varepsilon_1^* - \varepsilon_2^* - i\gamma_{12}^*\right) \end{aligned} \tag{4.6}$$

According to the Sokhotski-Plemelj Theorem (Sherman 1940, Musklishivili 1953), the solutions of the governing potential functions within this finite domain are composed of two parts:

$$\begin{aligned} \varphi(z) &= \varphi_1(z) + \varphi_*(z) \\ \psi(z) &= \psi_1(z) + \psi_*(z) \end{aligned} \tag{4.7}$$

where φ_1 and ψ_1 are potentials within the whole domain, and φ_* and ψ_*, which are related to the gap function, are expressed as

$$\begin{aligned} \varphi_* &= -\frac{1}{2\pi i}\oint_{\partial\omega} \frac{C_1 t - \bar{C}_2 \bar{t}}{t - z}\, dt \\ \psi_* &= \frac{1}{2\pi i}\oint_{\partial\omega} \frac{2C_1 \bar{t} dt - C_2 t dt - \bar{C}_2 \bar{t} d\bar{t}}{t - z} \end{aligned} \tag{4.8}$$

In Eq. (4.8), it shows that the determination of φ_* and ψ_* requires the evaluation of the Cauchy integrals along the interface $\partial\omega$. For a complicatedly shaped inclusion as shown in Figure 4.1, the evaluation of the Cauchy integrals along the singly connected curve is challenging. In light of this difficulty, here the singly connected curve is replaced with a multisided polygon with L vertices (see black dots in Figure 4.1). To closely approximate the shape of inclusion, the vertices of polygon can be arbitrarily increased. Here the vertices are denoted as z_k, k = 1, 2, …, L. Thus, the kth edge of the L-sided polygon connects vertices z_k and z_{k+1}, except for the last one, which links z_N and z_1. Note that after the inclusion is replaced, the term $d\bar{t}/dt$ in Eq. (4.5) has discontinuity of first kind at the vertices z_k. Fortunately, this discontinuity does not ruin the integrability of Eq. (4.8) and piecewise integrals can still be used for evaluation.

To find out the explicit expressions of the potential functions φ_1 and ψ_1, one may need to write the potentials in their Laurent series expansion so as to connect the coefficient in each term with the boundary condition. However, for an arbitrarily shaped matrix as shown in Figure 4.1, φ_1 and ψ_1 cannot be expressed in their Laurent series expansion, which requires that the domain to be bounded by a circle (Priestley 2003). To overcome this obstacle, conformal mapping is employed to convert the real domain to a virtual unit circle. Note that since φ_1 and ψ_1 are holomorphic in the real domain, they should be holomorphic in the virtual domain after conformal mapping. If the holomorphic mapping function is $z = w(\zeta)$, the Laurent series expansion of the potential functions in the virtual unit circle is

$$\begin{aligned} \varphi_1(z) &= \varphi_1\left(w(\zeta)\right) = \sum_{n=0}^{\infty} a_n \zeta^n \\ \psi_1(z) &= \psi_1\left(w(\zeta)\right) = \sum_{n=0}^{\infty} b_n \zeta^n \end{aligned} \tag{4.9}$$

To identify the coefficients a_n and b_n in the expansion, the Dirichlet boundary is enforced in the virtual unit circle, which leads to

$$\kappa\varphi_1\left(w(\zeta)\right) - \frac{w}{\overline{w}'}\overline{\varphi_1'\left(w(\zeta)\right)} - \overline{\psi_1\left(w(\zeta)\right)} = F(\zeta),\ |\zeta| = 1, \tag{4.10}$$

Here the boundary effect function $F(\zeta)$ is determined by the Cauchy integrals in Eq. (4.8) along the interface as follows

$$F(\zeta) = -\kappa\varphi_*\left(w(\zeta)\right) + \frac{w}{\overline{w}'}\overline{\varphi_*'\left(w(\zeta)\right)} + \overline{\psi_*\left(w(\zeta)\right)} \tag{4.11}$$

According to Eqs. (4.9) to (4.11) in the general formulation, the explicit expressions of the potential functions can be determined if the mapping function is found and the evaluation of Cauchy integral along the interface is successful. Here the singly connected curve enclosing the

inclusion is replaced with an arbitrarily-sided polygon, which significantly simplifies the evaluation of Cauchy integral.

4.3 EXPLICIT EXPRESSIONS OF POTENTIAL FUNCTIONS

After the inclusion is replaced with an *L*-sided polygon, the evaluation of Cauchy integral along the singly connected curve is decomposed into the evaluation of piecewise integrals along the straight edges of a polygon. For the *k*th edge linking vertices z_k and z_{k+1}, any point on this segment must satisfy

$$\overline{z} = \theta_k z + \delta_k \tag{4.12}$$

where $\theta_k = \dfrac{\overline{z}_{k+1} - \overline{z}_k}{z_{k+1} - z_k}$ and $\delta_k = \dfrac{z_{k+1}\overline{z}_k - z_k\overline{z}_{k+1}}{z_{k+1} - z_k}$. Residing on this relation, one may simplify the integral on the *k*th edge as follows

$$\begin{aligned} \int_{l_k} \frac{\overline{t}}{t-z}\,dt &= \int_{l_k} \frac{\theta_k t + \delta_k}{t-z}\,dt = \left(\theta_k \left(z_{k+1} - z_k \right) + \left(\theta_k z + \delta_k \right) \log \frac{z_{k+1} - z}{z_k - z} \right) \\ \int_{l_k} \frac{\overline{t}}{t-z}\,d\overline{t} &= \int_{l_k} \frac{\left(\theta_k t + \delta_k \right)\theta_k}{t-z}\,dt = \theta_k \left(\theta_k \left(z_{k+1} - z_k \right) + \left(\theta_k z + \delta_k \right) \log \frac{z_{k+1} - z}{z_k - z} \right) \end{aligned} \tag{4.13}$$

here l_k refers to the path of *k*th edge.

According to Eq. (4.8), φ_* and ψ_* are the sums of the integrals on the polygon edges. Hinging on the fact that $\sum_{k=1}^{L} \theta_k \left(z_{k+1} - z_k \right) = 0$, one can express φ_* and ψ_* as follows

$$\varphi_* = -\frac{1}{2\pi i}\oint_{\partial\omega}\frac{C_1 t-\bar{C}_2\bar{t}}{t-z}dt$$
$$= -\frac{1}{2\pi i}\left(-\bar{C}_2\sum_{k=1}^{L}\left(\left(\theta_k z+\delta_k\right)\log\frac{z_{k+1}-z}{z_k-z}\right)\right)-C_1\chi^{\omega}z$$

$$\psi_* = \frac{1}{2\pi i}\oint_{\partial\omega}\frac{2\bar{C}_1\bar{t}dt-C_2 tdt-\bar{C}_2\bar{t}d\bar{t}}{t-z} \tag{4.14}$$
$$= \frac{\bar{C}_1}{\pi i}\sum_{k=1}^{L}\left(\left(\theta_k z+\delta_k\right)\log\frac{z_{k+1}-z}{z_k-z}\right)$$
$$-\frac{\bar{C}_2}{2\pi i}\sum_{k=1}^{L}\theta_k\left(\theta_k\left(z_{k+1}-z_k\right)+\left(\theta_k z+\delta_k\right)\log\frac{z_{k+1}-z}{z_k-z}\right)-C_2\chi^{\omega}z$$

here χ^{ω} is the characteristic function of ω, which is equal to 1 if *z* falls within ω and equal to zero otherwise. Here it should be noted that the logarithm terms in Eq. (4.14) cannot be combined or decomposed freely. This is due to the fact that for complex valued functions α and β, the relation $\log(\alpha\beta)=\log\alpha+\log\beta$ is no longer effective for evaluation. The complex logarithm function $\log(\alpha\beta)$ must be evaluated in the single-valued branch $[-\pi, \pi]$, which cannot be guaranteed by the separate evaluation of $\log(\alpha)$ and $\log(\beta)$.

The expressions of φ_* and ψ_* obtained in Eqs. (4.14) are then substituted into Eqs. (4.10) and (4.11) to determine φ_1 and ψ_1. To demonstrate the use of conformal mapping for a noncircular matrix, the elastic domain is assumed to be bounded by a Pascal's Limaçon here. Thus, the function to map the real domain to a virtual unit circle is

$$z = w(\zeta) = R\left(\zeta + m\zeta^2\right),\ \ \zeta\in\tilde{\Omega}\left(|\zeta|\le 1\right) \tag{4.15}$$

here $m<0.5$, and $\tilde{\Omega}$ stands for the image of the original domain in the virtual ζ plane, which is a unit circle. When *m* = 0, this function maps a circle with radius *R* to a unit one.

If one multiples both sides of Eq. (4.10) with the term $\frac{1}{2\pi i}\frac{d\zeta}{\zeta-\zeta_1}$ ($|\zeta|=1$, $|\zeta_1|<1$), and then evaluates the integral along the positive direction of the unit virtual circle, Eq. (4.10) is transformed to

$$\frac{1}{2\pi i}\int_{\partial\tilde{\Omega}}\frac{1}{\zeta-\zeta_1}\left(\kappa\varphi_1(\zeta)-\frac{w}{\overline{w}'}\overline{\varphi_1'(\zeta)}-\overline{\psi_1(\zeta)}\right)d\zeta=\frac{1}{2\pi i}\int_{\partial\tilde{\Omega}}\frac{1}{\zeta-\zeta_1}F(\zeta)\,d\zeta \tag{4.16}$$

According to Cauchy's Residue Theorem and with the help of Eq. (4.9), it can be further simplified as

$$\begin{aligned}\kappa\varphi_1(\zeta_1)=&\frac{1}{2\pi i}\int_{\partial\tilde{\Omega}}\frac{F(\zeta)}{\zeta-\zeta_1}d\zeta+(\overline{a}_1 m)\zeta_1^2+\left(2\overline{a}_2 m+\overline{a}_1\left(1-2m^2\right)\right)\zeta_1\\&+3\overline{a}_3 m+2\overline{a}_2\left(1-2m^2\right)-\overline{a}_1 2m\left(1-2m^2\right)+\overline{b}_0\end{aligned} \tag{4.17}$$

By performing similar operations on the conjugate of Eq. (4.10), one may obtain the expression of ψ_1 as follows

$$\begin{aligned}\psi_1(\zeta_1)=&-\frac{1}{2\pi i}\int_{\partial\tilde{\Omega}}\frac{\overline{F(\zeta)}}{\zeta-\zeta_1}d\zeta\\&-\left(\sum_{n=3}^{\infty}\frac{1}{2m}na_n\zeta_1^{\,n-3}+\sum_{n=4}^{\infty}\sum_{n_1=1}^{n-3}(-1)^{n_1+1}\left(m-\frac{1}{2m}\right)\left(\frac{1}{2m}\right)^{n_1}na_n\zeta_1^{\,n-3-n_1}\right)+\kappa\overline{a}_0\end{aligned} \tag{4.18}$$

Since φ_1 and ψ_1 governs the entire finite domain, Eqs. (4.17) and (4.18) must be effective for every point within the virtual unit circle. Therefore, if one differentiates Eqs. (4.17) and (4.18) with respect to ζ_1 = 0 up to the *k*th order (*k* = 0, 1, 2, …), all the coefficients in Eqs. (4.17) and (4.18) can be explicitly identified as

$$a_1 = \frac{\overline{\left(1-2m^2\right)}}{\kappa}\Bigg/\left(\left(\frac{2m^2}{\kappa^2}-1\right)^2-\left(\frac{1-2m^2}{\kappa}\right)^2\right)\left(\frac{1}{\kappa}\overline{\frac{1}{2\pi i}\int_{\partial\tilde{\Omega}}\frac{F(\zeta)}{\zeta^2}d\zeta}+\frac{2m}{\kappa^2}\frac{1}{2\pi i}\int_{\partial\tilde{\Omega}}\frac{F(\zeta)}{\zeta^3}d\zeta\right)$$
$$+\frac{\left(1-\frac{2m^2}{\kappa^2}\right)}{\left(\left(\frac{2m^2}{\kappa^2}-1\right)^2-\left(\frac{1-2m^2}{\kappa}\right)^2\right)}\left(\frac{1}{\kappa}\frac{1}{2\pi i}\int_{\partial\tilde{\Omega}}\frac{F(\zeta)}{\zeta^2}d\zeta+\frac{2m}{\kappa^2}\overline{\frac{1}{2\pi i}\int_{\partial\tilde{\Omega}}\frac{F(\zeta)}{\zeta^3}d\zeta}\right) \tag{4.19}$$

$$a_2 = \frac{1}{\kappa}\frac{1}{2\pi i}\int_{\partial\tilde{\Omega}}\frac{F(\zeta)}{\zeta^3}d\zeta+\frac{m}{\kappa}\overline{a}_1 \tag{4.20}$$

$$a_k = \frac{1}{\kappa}\frac{1}{2\pi i}\int_{\partial\tilde{\Omega}}\frac{F(\zeta)}{\zeta^{k+1}}d\zeta \quad \text{for } k>2 \tag{4.21}$$

$$\begin{aligned} b_k = &-\frac{1}{2\pi i}\int_{\partial\tilde{\Omega}}\frac{\overline{F(\zeta)}}{\zeta^{k+1}}d\zeta-\frac{1}{2m}(k+3)a_{k+3} \\ &-(-1)^{-k}(2m)^k\left(3a_3\left(m-\frac{1}{2m}\right)+2a_2\left(1-2m^2\right)-a_1 2m\left(1-2m^2\right)\right) \\ &-(-1)^{-k}(2m)^k\left(+\overline{\frac{1}{2\pi i}\int_{\partial\tilde{\Omega}}\frac{1}{\zeta}F(\zeta)d\zeta}-\frac{1}{2\pi i}\int_{\partial\tilde{\Omega}}\frac{\overline{F(\zeta)}}{\zeta}d\zeta\right) \\ &-(-1)^{-k}(2m)^k\left(-\sum_{n=4}^{k+3}(-1)^{n-2}\left(m-\frac{1}{2m}\right)\left(\frac{1}{2m}\right)^{n-3}na_n\right) \end{aligned} \tag{4.22}$$

Here the coefficients corresponding to the constant terms can be simplified as follows,

$$\tilde{a}_0 = a_0-\frac{1}{\kappa}\overline{b}_0 = \frac{1}{\kappa}\frac{1}{2\pi i}\int_{\partial\tilde{\Omega}}\frac{1}{\zeta}F(\zeta)d\zeta+\frac{1}{\kappa}\left(3\overline{a}_3 m+2\overline{a}_2\left(1-2m^2\right)-\overline{a}_1 2m\left(1-2m^2\right)\right)$$
$$\tilde{b}_0 = 0 \tag{4.23}$$

and replace a_0, b_0 by $\tilde{a}_0, \tilde{b}_0$ in Eq. (4.9). As a result, the unknown a_0 and b_0 which are always combined in the expression of displacement fields do not have to be considered separately since they are now replaced by one nonzero term $\tilde{a}_0$.

In Eqs. (4.19) to (4.23), the definite integrals $I_n^F = \frac{1}{2\pi i}\int_{\partial\tilde{\Omega}} \frac{F(\zeta)d\zeta}{\zeta^n}$ and $I_n^{Fc} = \frac{1}{2\pi i}\int_{\partial\tilde{\Omega}} \frac{\overline{F(\zeta)}d\zeta}{\zeta^n}$ are in fact the Fourier Transform of the function $F(\zeta)$ and its conjugate on the boundary, which can be directly evaluated. Here the results of I_n^F and I_n^{Fc} for a circular domain (i.e., m = 0) are listed in the Appendix. It can be seen after the coefficients a_k and b_k in the Laurent series expansion are determined, the explicit expressions of governing potential functions are obtained by this general formulation.

4.4 NUMERICAL EXAMPLES

To validate the general formulation described in the preceding sections, the analytical solution presented above is compared with three typical cases: 1) a circular domain containing a triangular inclusion; 2) a V-shaped Quantum Wire; and 3) a Pascal's Limaçon containing a square inclusion.

In Figure 4.2a, it shows a triangular inclusion is placed in a circular matrix with radius R = 2. The three vertices of inclusion are located at (-1.5, 0), (1, 1.5) and (1, -1.5) respectively. The material properties of the elastic medium are Young's modulus E = 30 GPa and υ = 0.2. The uniform eigenstrain within the inclusion is selected to be $\left[\varepsilon_1^* \quad \varepsilon_2^* \quad \gamma_{12}^*\right] = \left[0.10 \quad 0.20 \quad 0.30\right]^T$. Note that in order to validate the generality of the proposed formulation, all geometrical

parameters, material properties and eigenstrain components are arbitrarily selected. Since the matrix is circular and the inclusion is triangular, the mapping function is $z = R\zeta$, and there is no need to replace the inclusion with a multiple-sided polygon. The piecewise boundary integrals can be directly evaluated along the straight edges of inclusion.

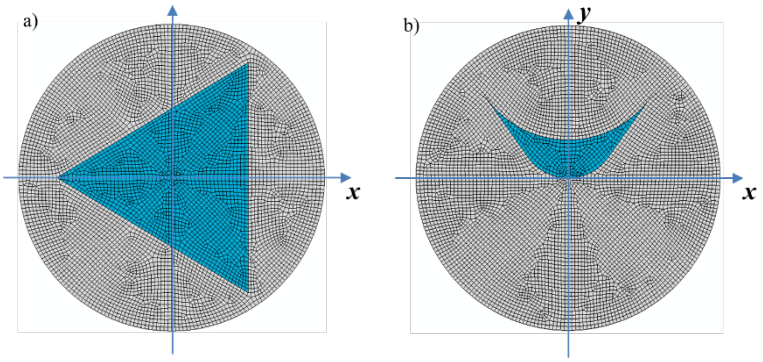

Figure 4.2. a) FEM model of a circular finite domain containing a triangle inclusion and b) a crescent-shaped inclusion.

Figure 4.3 shows the displacement obtained by the analytical solutions based on the general formulation. In Figure 4.3a, the horizontal displacement u along 8 different orientations is plotted. Since theoretical solutions are unavailable for this finite domain in the literature, the comparison has to be made with the numerical analysis. In Figure 4.3a, it can be seen that the FEM results, which are represented by the symbols, coincide with the analytical solutions for all the orientations. Similarly, firm agreement is achieved for the vertical displacement v, which is shown in Figure 4.3b.

Additionally, if simply set $L = 4$ and pick the four vertices as (1,1), (-1, 1), (-1, -1) and (1, -1), and let R go to infinity, the matrix will be unbounded and the disturbance is induced by a square inclusion embedded in an infinite domain which is exactly the case studied by List and

Silberstein (1966). The theoretical benchmark solution obtained by List and Silberstein (1966) was later validated by the results of Rodin (1996), who investigated the disturbance caused by simple polygonal inclusions embedded in infinite domains. For this problem, in the general formulation obtained in this research, the coefficients a_k and b_k vanish as R is extended to infinity; see the evaluation of of I_n^F and I_n^{Fc} in the appendix. Thus, the elastic field is entirely dictated by the potential functions φ_* and ψ_*, which are evaluated in Eq. (4.14). The terms shown in Eq. (4.14) are exactly the same as those given by List and Silberstein (1966). This means the general formulation presented in this study is able to recover the theoretical benchmarks for unbounded domains.

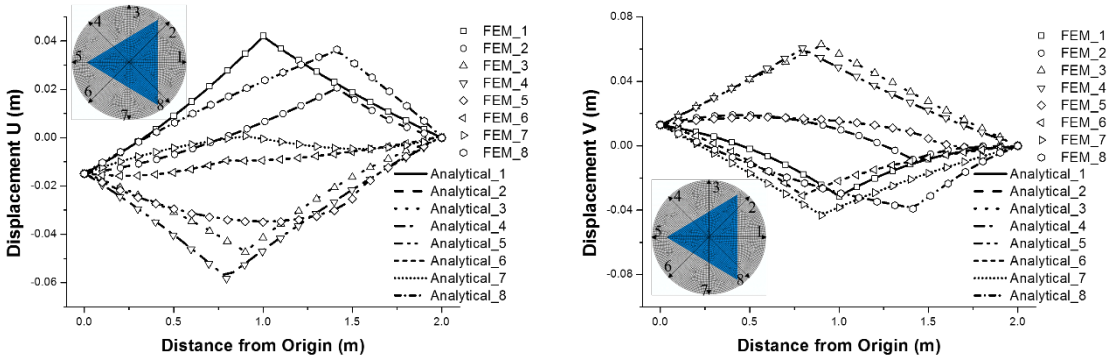

Figure 4.3. Comparison of the displacement field based on the analytical solution (lines) with FEM (symbols) for a circular domain containing a triangular inclusion

In Figure 4.2b, it shows a circular matrix containing a crescent-shaped inclusion, similar to a Quantum Wire (QWR). With the advance in materials science and nano-technology, it has been found that QWRs are able to significantly enhance the properties of semiconductor devices (Freund and Johnson 2001, Johnson and Freund 2001, Davies 2003). Due to the fabrication technique, QWRs are usually shaped like a crescent, which causes severe disturbance in the

matrix, and thus significantly affects the performance of semiconductor devices (Faux et al 1997). Therefore, the elastic field disturbed by a crescent-shaped inclusion is garnering increasing attentions in engineering applications.

To avoid the complexity induced by the surface force, which is strong for nano-sized inclusions (Sharma and Ganti 2004), the configuration is scaled up in this study to focus on the inclusion shape. The radius of matrix is set to be R = 40 mm (Figure 4.2b). The crescent-shaped inclusion is 10 mm thick, and is enclosed by a singly connected curve consisting of two arcs and two straight lines. The radius of curvature is 13 mm for the bottom arc and 26.66 mm for the upper one (Figure 4.2b). The two line segments are inclined at angles of ±57.74° respectively. The elastic properties are set to be E = 160 GPa and υ = 0.31, typical for QWRs (Maranganti and Sharma 2001). The eigenstrain is arbitrarily selected to be $\left[\varepsilon_1^* \quad \varepsilon_2^* \quad \gamma_{12}^*\right] = \left[0.05 \quad 0.10 \quad -0.12\right]^T$.

Since the inclusion is complicatedly shaped, it is replaced with a polygon in the analysis. Here each arc is approximated by 20 line segments of equal length, while the two line segments remain unchanged. Thus, the original inclusion is replaced with a polygonal inclusion of 42 edges. Based on the analytical solutions presented in this study, the horizontal displacement u along eight different orientations is plotted in Figure 4.4a. In the same Figure, the results obtained by FEM are illustrated by the symbols. To ensure the accuracy of the numerical analysis, fine mesh is used in FEM and the whole domain is discretized by 6139 linear plain strain elements. It can be seen that the difference between the analytical solutions and numerical results is almost negligible. Similarly, good agreement is achieved for the vertical displacement v along the 8 different orientations. This shows that the general formulation presented in this study is capable of identifying the disturbance induced by an arbitrarily shaped inclusion.

In Figure 4.5, it shows a noncircular matrix containing a squared inclusion. The matrix is enclosed by a Pascal's Limaçon, which is described by Eq. (4.15) with m = 0.3 and R = 1. The elastic properties are arbitrarily selected to be E = 30 GPa and υ = 0.3. The Dirichelet boundary condition $\mathbf{u}$ = 0 is enforced on the matrix boundary and the eigenstrain is set to be $\left[\varepsilon_1^* \quad \varepsilon_2^* \quad \gamma_{12}^*\right] = \left[0.05 \quad 0.10 \quad -0.12\right]^T$.

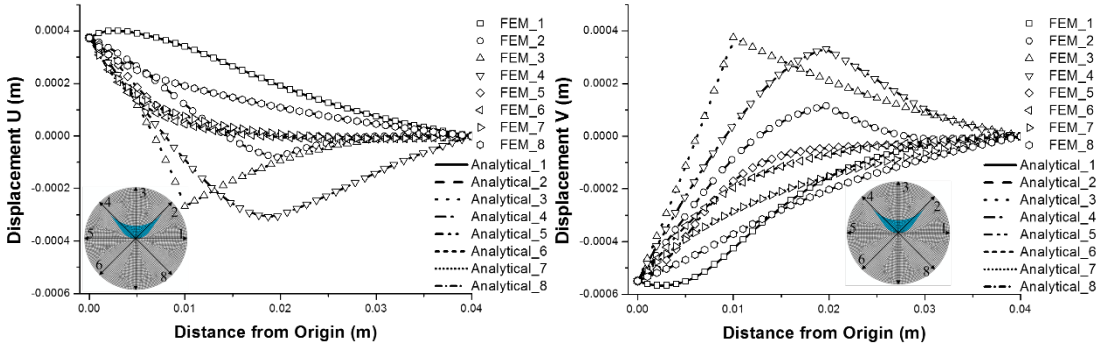

Figure 4.4. Comparison of the displacement field based on the polygonal inclusion approximation with 42 sides (lines) with FEM fine mesh simulation (symbols) for a circular domain containing a QWR inclusion

According to the general formulation, the matrix will be mapped to a virtual unit cell based on Eq. (4.15). Since the inclusion is a square, there is no need to replace it with a polygon. In Figure 4.6, the displacement along eight different curves, which respectively correspond to eight orientations in the virtual domain, is predicted by the analytical solutions. In FEM analysis, the domain is meshed with 6114 linear plane strain elements and the obtained displacement along these eight curves is demonstrated by the symbols. In Figure 4.6, it can be seen that the analytical solutions agree perfectly with the FEM results. This means the disturbance bounced back from a complicatedly shaped exterior boundary is captured by the general formulation.

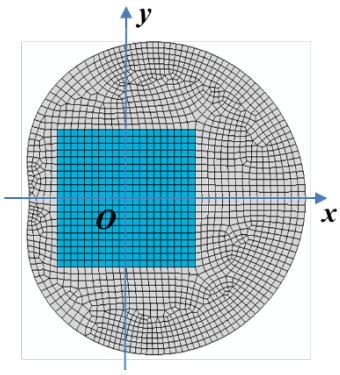

Figure 4.5. FEM model of a finite domain bounded by a Pascal's Limaçon containing squared inclusion

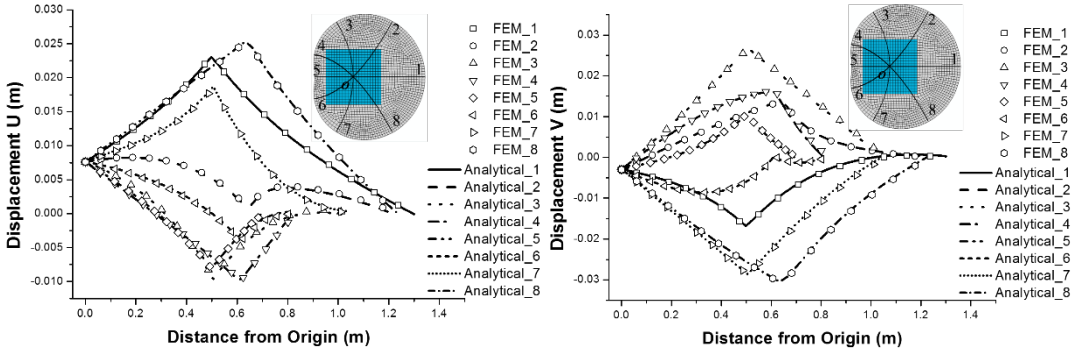

Figure 4.6. Comparison of the displacement field based on the analytical solution (lines) with FEM (symbols) for a finite domain bounded by a Pascal's Limaçon containing a squared inclusion

4.5 DISCUSSION OF THE ASYMPTOTIC BEHAVIOR

In the general formulation, the inclusion is replaced with an *L*-sided polygon to simplify the evaluation of Cauchy integral along the interface. However, the appearance of vertices usually changes the original curvature of the interface and generates the discontinuity of first kind, which does not ruin the integrability but leads to singularity in the stress field. Here the stress singularity triggered by the vertices and its effect on solution accuracy are investigated.

In the analytical solution, the elastic fields of the 2D domain are described by the superposition of the potential pairs φ_1 and ψ_1, and φ_* and ψ_*; see Eq. (4.7). Since φ_1 and ψ_1 can be expressed by the Laurent series expansion in Eq. (4.9) after conformal mapping, they will not be the source of any singularity. Therefore, the focus must be placed on the pair φ_* and ψ_*.

Before the discussion of the stress field inside the RVE, it is worthwhile to spend some time here to demonstrate that the expression of displacement fields possesses no singularity inside the RVE. The displacement fields corresponding to φ_* and ψ_* are

$$u + iv = \frac{1}{2\mu}\left(\kappa\varphi_*(z) - z\overline{\varphi_*'(z)} - \overline{\psi_*(z)}\right) \tag{4.25}$$

Without loss of generality, one may assume the two edges of the polygon, namely l_{m-1} and l_m, joins at the vertex z_m; see Fig 7. The angles between the edges and horizontal axis are α_{m-1} and α_m, respectively. The displacement fields at the vertex z_m is obtained as following after some simple operations:

$$
\begin{aligned}
\left(u+iv\right)\Big|_{z=z_m} &= \frac{\bar{C}_2}{2\pi i}\left(\sum_{\substack{k=1\\k\neq m\\k\neq m-1}}^{L}\left(\left(\theta_k z_m+\delta_k\right)\log\frac{z_{k+1}-z_m}{z_k-z_m}\right)+\bar{z}_m\lim_{z\to z_m}\left(\log\frac{z_m-z}{z_{m-1}-z}+\log\frac{z_{m+1}-z}{z_m-z}\right)\right)\\
&\quad -C_1\chi^{\omega}z_m\\
&\quad +conj\left[\frac{\bar{C}_2}{2\pi i}\left(\sum_{\substack{k=1\\k\neq m\\k\neq m-1}}^{L}\left(\bar{z}_m\theta_k\log\frac{z_{k+1}-z_m}{z_k-z_m}+\bar{z}_m\left(\theta_k z_m+\delta_k\right)\left(-\frac{1}{z_{k+1}-z_m}+\frac{1}{z_k-z_m}\right)\right)\right)-C_1\chi^{\omega}\bar{z}_m\right]\\
&\quad +conj\left[\frac{\bar{C}_2}{2\pi i}\left(+\bar{z}_m{}^2\left(-\frac{1}{z_{m+1}-z_m}+\frac{1}{z_{m-1}-z_m}\right)\right)\right]\\
&\quad +conj\left[\frac{\bar{C}_1}{\pi i}\left(\sum_{\substack{k=1\\k\neq m\\k\neq m-1}}^{L}\left(\left(\theta_k z_m+\delta_k\right)\log\frac{z_{k+1}-z_m}{z_k-z_m}\right)+\bar{z}_m\lim_{z\to z_m}\left(\log\frac{z_m-z}{z_{m-1}-z}+\log\frac{z_{m+1}-z}{z_m-z}\right)\right)\right]\\
&\quad -conj\left[\frac{\bar{C}_2}{2\pi i}\left(\sum_{k=1}^{L}\theta_k{}^2\left(z_{k+1}-z_k\right)+\sum_{\substack{k=1\\k\neq m\\k\neq m-1}}^{L}\theta_k\left(\theta_k z_m+\delta_k\right)\log\frac{z_{k+1}-z_m}{z_k-z_m}\right)-C_2\chi^{\omega}z_m\right]
\end{aligned}
\tag{4.26}
$$

Observing the fact that

$$
\log\frac{z_m-z}{z_{m-1}-z}+\log\frac{z_{m+1}-z}{z_m-z}=\log\frac{z_{m+1}-z}{z_{m-1}-z}+H_1 \tag{4.27}
$$

where H_1 is a constant representing the geometric configuration at the point *z*, it is clear that the expression of the displacement fields produce no singularity at z_m.

Similarly, the stress components described by φ_* and ψ_* can be expressed as

$$
\sigma_1+\sigma_2=4\,\mathrm{Re}\left(\varphi_*'\left(z\right)\right) \tag{4.28}
$$

$$
\sigma_2-\sigma_1+2i\sigma_{12}=2\left(\bar{z}\varphi_*''\left(z\right)+\psi_*''\left(z\right)\right) \tag{4.29}
$$

Substituting φ_* and ψ_* along these two edges into Eqs. (4.28) and (4.29), one can quantify the stress concentration at z_m. Here only the singular terms in Eq. (4.28) are analyzed because those

in Eq. (4.29) are similar, differing only in the constant coefficients. When a point z is approaching the vertex z_m, the volumetric stress at this point is

$$\lim_{z\to z_m}\left(\sigma_{11}+\sigma_{22}\right)=4\,\mathrm{Re}\left(\frac{\bar{C}_2}{2\pi i}\left(\lim_{z\to z_m}\left(\theta_m\log\frac{z_{m+1}-z}{z_m-z}+\theta_{m-1}\log\frac{z_m-z}{z_{m-1}-z}\right)\right)\right)$$
$$+4\,\mathrm{Re}\left(\frac{\bar{C}_2}{2\pi i}\left(\sum_{\substack{k=1\\k\neq m-1,m}}^{L}\theta_k\log\frac{z_{k+1}-z_m}{z_k-z_m}+\sum_{\substack{k=1\\k\neq m-1,m}}^{L}\left(\theta_k z+\delta_k\right)\left(-\frac{1}{z_{k+1}-z_m}+\frac{1}{z_k-z_m}\right)\right)-C_1\chi^{\omega}\right) \tag{4.30}$$

It can be observed that the terms that control the stress singularity are always in the form of

$$f_s\left(z_m\right)=Ce^{-2i\alpha_m}\lim_{z\to z_m}\log\left(z_m-z\right)^{\left(e^{-2i\Delta_m}-1\right)}+H_2 \tag{4.31}$$

where C and H_2 are constants related to the material properties and geometric configuration, and $\Delta_m=\alpha_{m-1}-\alpha_m$.

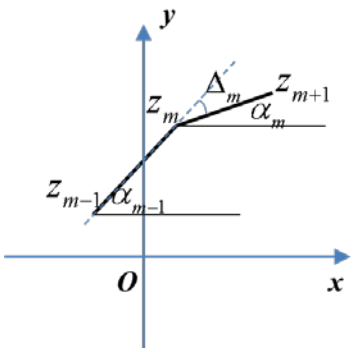

Figure 4.7. The vicinity of the *m*th vertex in the polygonal approximation

Eq. (4.31) shows that with the decrease of the angle difference Δ_m, the intensity of stress concentration decreases. When $\Delta_m=0$, the stress singularity disappears based on the following relation

$$e^{-2i\Delta_m} - 1 = \sum_{n=1}^{\infty} \frac{(-2i)^n}{n!} (\Delta_m)^n = O(\Delta_m) \tag{4.32}$$

Observing the fact that when $r \to 0$

$$\left| \log r^{(\alpha_{m-1} - \alpha_m)} \right| \ll \left| \left(\frac{1}{r} \right)^{(\alpha_{m-1} - \alpha_m)} \right| \tag{4.33}$$

the singular term in Eq. (4.31) can be examined with the help of its superior bound, which is a typical indicator of stress concentration in fracture mechanics. First, according to (4.33), the stress concentration at the vertices of the polygonal inclusion is far less significant than the one encountered in fracture mechanics. Second and more importantly, as we can see, when Δ_m decrease, the bound of the singularity can be expected to converge to a constant in the power law. This means that if more vertices are used to approximate the curved interface, the stress concentration at the vertices will be mitigated with the value of Δ_m approaching zero. This is similar to the stress concentration at corners. For a sharp crack, the stress singularity is the most severe; while for a re-entrant corner, the stress concentration is less important. If the corner transforms to a smooth surface, which is the asymptotic case, the stress singularity totally disappears.

In addition to mitigating the stress concentration in the vicinity of the vertices, inserting more edges in the polygon will improve the accuracy of the analytical solutions. To demonstrate this, the crescent-shaped inclusion in Figure 4.4 is approximated by polygons of 42, 22, 14 and 10 sides respectively. The corresponding horizontal displacement along the 45^o orientation is plotted in Figure 4.8 based on the analytical solutions. When compared with the benchmark values (the symbols) predicted by the FEM analysis, it can be seen that with the increase of vertices, a better agreement is achieved between the numerical results and analytical solutions. It

is also worth mentioning that the difference between the analytical solutions of the 22-sided and 42-sided polygons is negligible. This means that even for such a complicatedly shaped inclusion, acceptable accuracy can be attained by a polygon of a manageable number of vertices.

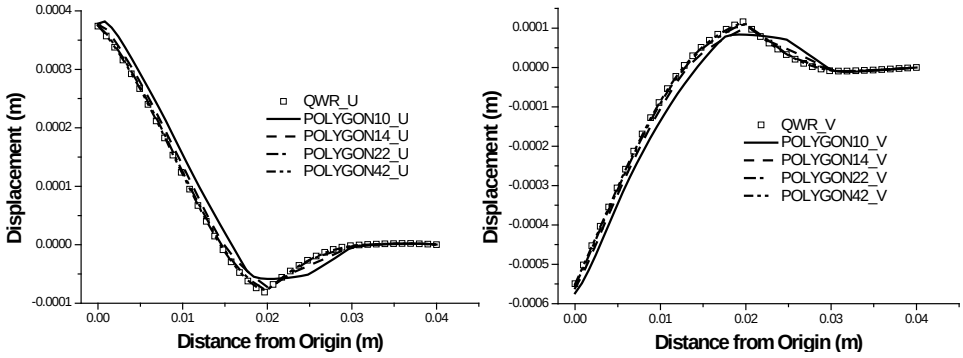

Figure 4.8. Comparison of the displacement field along the 45^o direction based on 10, 14, 22 and 42 sides polygonal approximation with FEM fine mesh solution (symbols) for a circular domain containing a QWR inclusion

4.6 THE GENERAL ESHELBY'S TENSOR

In this section, it is discussed on how to get the expression of the Eshelby's tensor corresponding to the obtained complex potential functions. For Eshelby's first problem, it is conventional to find out the Eshelby tensor for the geometrical configuration of interest. For a 2D finite elastic body, the Eshelby tensor can be written in a Voigt form as follow:

$$\begin{Bmatrix} \varepsilon_1 \\ \varepsilon_2 \\ \gamma_{12} \end{Bmatrix} = \begin{pmatrix} S_{1111} & S_{1122} & S_{1112} \\ S_{2211} & S_{2222} & S_{2212} \\ S_{1211} & S_{1222} & S_{1212} \end{pmatrix} \begin{Bmatrix} \varepsilon_1^* \\ \varepsilon_2^* \\ \gamma_{12}^* \end{Bmatrix} \tag{4.34}$$

This means that each component S_{ijkl} of the Eshelby tensor can be determined based on the given eigenstrain ε^* and the disturbed strain field ε, which can be obtained by the analytical solutions. For example, if one sets $\varepsilon_2^* = \gamma_{12}^* = 0$, the components S_{1111}, S_{1122} and S_{1112} can be determined.

For a given geometrical configuration, the disturbed strain field ε is described by the governing potential functions, which are explicitly expressed by the analytical solutions. If differentiation with respect to x and y is performed respectively on both sides of Eq. (4.4), the following equations are obtained

$$\begin{aligned} 2\mu\left(\frac{\partial u}{\partial x}+i\frac{\partial v}{\partial x}\right) &= \frac{\partial f}{\partial z}+\frac{\partial f}{\partial \overline{z}} \\ 2\mu\left(\frac{\partial u}{\partial y}+i\frac{\partial v}{\partial y}\right) &= i\left(\frac{\partial f}{\partial z}-\frac{\partial f}{\partial \overline{z}}\right) \end{aligned} \tag{4.35}$$

where $f\left(z,\overline{z}\right)=\kappa\varphi\left(z\right)-z\overline{\varphi'\left(z\right)}-\overline{\psi\left(z\right)}$. Then the disturbed strain field ε can be evaluated as

$$\begin{aligned} \varepsilon_1 &= \frac{1}{2\mu}\mathrm{Re}\left(\frac{\partial f}{\partial z}+\frac{\partial f}{\partial \overline{z}}\right) \\ \varepsilon_2 &= \frac{1}{2\mu}\mathrm{Re}\left(\frac{\partial f}{\partial z}-\frac{\partial f}{\partial \overline{z}}\right) \\ \gamma_{12} &= \frac{1}{\mu}\mathrm{Im}\left(\frac{\partial f}{\partial \overline{z}}\right) \end{aligned} \tag{4.36}$$

Here Re and Im stand for the real and image parts of the complex expression, respectively. Thus, one can insert φ and ψ given in the analytical solutions into Eq. (4.36) to attain the disturbed strain field, and then determine the Elshelby tensor listed in Eq. (4.34).

4.7 DISCUSSION AND CONCLUSION

In this study, Eshelby's first problem in a finite 2D domain is investigated. A general formulation is constructed to determine the disturbance, induced by an arbitrarily shaped inclusion, and its reflection from the exterior boundary of matrix. To evaluate the boundary effect of the bounded matrix, conformal mapping is employed to transform the elastic domain to a virtual unit circle, which enable the use of Laurent expansion series to express the governing complex potentials. To simplify the evaluation of Cauchy integral along the interface, which is described by a singly connected curve, an *L*-sided polygon is employed to replace the complicatedly shaped inclusion. Thus, the evaluation of Cauchy integral is decomposed into piecewise boundary integrals performed on the straight edges, and the conformal mapping on the matrix does not complicate this evaluation.

The formulation shows that if the boundary condition is enforced, the coefficient of every term in the Laurent series expansion for the potential functions is related to the Fourier transform of the boundary effect function and its conjugate on the exterior boundary. The terms in the Laurent series expansion can be explicitly determined by differentiation with respect to $\zeta = 0$ to the corresponding orders in the virtual domain. Thus, there are no any integral forms in the analytical solutions, which brings great convenience in application.

The general formulation and analytical solutions are validated by three typical examples, which include complicatedly shaped inclusions and a noncircular matrix. The comparison between the analytical solutions and numerical results shows that the general formulation is capable of determining the disturbed elastic fields within a finite 2D domain of a complex inclusion-matrix interface and exterior boundary. The first example also shows that the general formulation recovers the theoretical benchmarks when the matrix is extended to infinity. The

analysis about the stress singularity at vertices and its effect on accuracy indicates that with a manageable number of vertices, the general formulation is able to achieve acceptable accuracy and mitigate the stress concentration.

5.0 INHOMOGENEOUS INCLUSION PROBLEM IN A CONCENTRIC CIRCULAR DOMAIN

Identification of the elastic disturbance induced by an inhomogeneity in a finite Representative Volumetric Element (RVE) is one of the essential problems in the contemporary composite mechanics and micromechanics, and thus attracts increasing interests in a wide range of engineering applications. The classical Equivalent Inclusion Method (EIM) proposed by Eshelby, which is effective only for an infinite domain containing an ellipsoidal inhomogeneous inclusion, fails here due to the fact that uniform equivalent eigenstrain may not exist in the inclusion for a finite RVE. To identify the disturbance in a finite RVE in a systematic manner, this chapter is focused on seeking for analytical solutions by using the complex potential method. The 2D inhomogeneous inclusion problem is decomposed into 2 parts: the first one is without eigenstrain and subject to the prescribed boundary condition; and the second one is with eigenstrain while the boundary is fixed. Based on Sokhotski-Plemelj Theorem, an auxiliary function is introduced in the second part to enable the construction of the complex potentials via Cauchy Integrals to describe the displacement gap induced by the eigenstrain. Following the corresponding boundary conditions and displacement continuity and traction equilibrium on the inclusion-matrix interface, the coefficients of potential functions in the form of Laurent series can be identified. The analytical solution is shown to accurately predict the elastic disturbance induced by an inhomogeneous inclusion in a 2D concentric finite RVE when compared with

FEM results. In addition, the obtained analytical solution agrees with the theoretical solutions available for some special cases in which the matrix goes to infinity, material mismatch disappears, or eigenstrain is caused by dilation.

5.1 BACKGROUND AND MOTIVATION

Disturbance induced by inhomogeneous inclusion is one of the essential problems in contemporary composite mechanics and micromechanics and its identification plays a significant role in developing advanced engineering materials widely used in aerospace, marine, automotive, civil, energy, biomedicine and many other engineering applications. For these advanced composite solids, their performance is strongly influenced by the geometry and size of their representative volume element (RVE) where the inhomogeneous inclusion is embedded. For example, the mechanical, electronic and optical properties of nanocomposites are significantly influenced by the geometrical configuration of their RVEs.

Following Mura's nomenclature (Mura 1987), if an inclusion has elastic property different from its hosting matrix, it is referred as an inhomogeneity. The sources of inhomogeneity include material mismatch, cavity, defects, crack, and so forth. If eignestrains resulting from physical changes such as thermal expansion, plastic strain, magnetomechanical and optical excitation, to name a few, are allowed to happen within the inhomogeneity, then the problem is conventionally referred as inhomogeneous inclusion problem.

Taking advantage of the position-independence of the interior Eshelby tensor mapping the eigenstrain into the disturbance, Eshelby (1957) introduced the elegant Equivalent Inclusion Method (EIM) to determine the elastic field in an unbounded RVE disturbed by an ellipsoidal

inhomogeneous inclusion. In this method, the inhomogeneity is treated as an equivalent eigenstrain, which can be superposed with other eigenstrains induced by physical changes (if exist). The EIM allows the composite RVE to be converted to a homogeneous one with eigenstrains in the inclusion, and thus makes it possible to take advantage of the results available in solving homogeneous inclusion problem in unbounded domains. Detailed descriptions of the application of EIM can be found in the classical work by Christensen (1979), Mura (1982) and Nemat-Nasser and Hori (1999).

However, the effectiveness of EIM is limited to inhomogeneous inclusions of ellipsoidal shape and the surrounding matrix must be unbounded (Eshelby 1957, Mura 1987). The prerequisite for the application of EIM is that the interior Eshelby tensor mapping the eigenstrain into the corresponding disturbance field must be independent of the position. As pointed out by Rodin (1996, 1998) as well as Nemat-Nasser and Hori (1999), even in 2D space this condition cannot be satisfied if the inclusions are of shapes other than ellipse or have a significant volume fraction compared to the matrix.

If the inhomogeneity size is approaching nano-scale, the effectiveness of EIM will be further narrowed to inclusions with a constant curvature (e.g., sphere in 3D and cylinder in 2D) because of the surface-interface stress (Sharma and Ganti 2004). For ellipsoidal inclusions without constant curvature in unbounded domains, only approximate solutions are available (Sharma and Wheeler 2007). Therefore, for inhomogeneity of complex shape, EIM is generally not effective even for unbounded domain because uniform equivalent eigenstrain and stress are not available (Waldvogel 1979, Rodin 1996, 1998, Nozaki and Taya, 2001). Therefore, more complicated methods based on Green's function combined with surface/volume integral evaluation of harmonic and bi-harmonic potentials (Kuvshinov 2008) or dislocation loop (Li and

Anderson 2001) have to be employed. If the RVE is bounded, the Eshelby's conjecture of uniform interior eigenstrain may not hold even for ellipsoidal inclusions due to the influence of RVE boundary. In this case, the size and shape of the RVE must be taken into account in formulating the boundary value problem of the RVE, which is a formidable challenge for analytical approaches residing on Green's function and integral evaluation.

In real applications, there is no infinite RVE, and in many cases including the nanocomposites, the volume ratio of the inclusion to the RVE is not negligible. As a result of the finite volume fraction ratio of the inhomogeneous inclusion to matrix, the solutions derived from EIM cannot realistically capture the disturbance induced by the inhomogeneous inclusion and correspondingly, the elastic field determined is no longer accurate. This limitation obstructs calculation of mechanical strength, determination of local response and prediction of damage initiation. Furthermore, the important homogenization schemes including the Mori-Tanaka method (Mori and Tanaka 1973, Weng 1990) and the self-consistent method (Hill 1965, Huang et al. 1994) can no longer be used to estimate the global properties and responses of the composite solids. Therefore, FEM and other numerical approaches are frequently employed to handle inhomogeneous inclusion problem in finite domains. However, numerical approach, effective for individual analysis, is not capable of providing the basic physical insights of the fundamentals governing the local and global property and response of the composite solids, which is essential for developing innovative composites.

To circumvent this obstacle, analytical solutions of the inhomogeneous inclusion problem in a finite domain are indispensible. Compared to the recent advance in formulating the disturbed elastic field in a finite domain containing homogeneous inclusion (Li et al. 2005, 2007, Wang et al. 2005, Gao and Ma 2010, Mao and Gao 2011, Zou et al. 2012), limited progress has been

made for inhomogeneous inclusion problem in a finite domain. Sherman (1959) proposed the equations based on complex potentials for 2D inhomogeneous inclusion problem, but did not give any analytical solutions. Then Theocaris and Ikakimidis (1977) presented the complex Cauchy-type singular integral equation and a numerical scheme to solve it. Using stress function, Luo and Weng (1987, 1989) formulated the elastic fields for 3-phase 2D and 3D inhomogeneous inclusion problems with the third phase (i.e., the exterior matrix) being unbounded. This implicitly provides analytical solutions for inhomogeneity problem in a finite domain of the 2 interior phases forming a concentric configuration in 2 limiting cases when eigenstrain happens in the interior inclusion: 1) free boundary if the third phase is infinitely soft and 2) fixed boundary if the third phase is perfectly rigid. Recently, Markenscoff and Dunders (2013) proposed a solution for the 3-phase inclusion problem in an infinite domain with eigenstrain in the intermediate phase, which might also provide the solution for the limiting cases with eigenstrain in the matrix.

Except for some extremely special cases, e.g., a concentric configuration under hydrostatic eigenstrain or loading, analytical solutions for inhomogeneous inclusion problem in bounded domain are still very limited. This work is aimed at formulating the disturbed elastic field in a 2D finite domain containing an inhomogeneity in a systematic manner. To simplify the formulation, the inhomogeneous inclusion problem is decomposed into 2 parts: one without eigenstrain but subject to the given boundary conditions and the other with eigenstrain while the boundary being fixed. The solution of each part is formulated separately and their superposition gives the analytical solution for the disturbed elastic field being sought for. The solution is first compared with FEM results for an arbitrary eigenstrain and arbitrary material mismatch. Then comparison with analytical solutions available for some special cases will be made. At the end,

discussion of the effect of size and material mismatch on disturbance is reported and conclusions are drawn.

5.2 GENERAL FORMULATION

In what follows, the 2D finite RVE is characterized by a circular inhomogeneous inclusion embedded at the center of a bounded circular matrix. Both the inclusion and the matrix are isotropic, homogeneous but with different elastic properties. The problem is illustrated in Figure 5.1a) where the far-field strain is imposed in the form of initial displacement u^0 on L_1, the exterior boundary of the RVE. The eigenstrain is assumed to be

$$\varepsilon_{ij}^*(\mathbf{x}) = \begin{cases} \varepsilon_{ij}^* & \mathbf{x} \in \Omega e \\ 0 & \mathbf{x} \in \Omega / \Omega e \end{cases} \tag{5.1}$$

here $\mathbf{x} = (x, y)$. Based on the far field strain $\begin{bmatrix} \varepsilon_1^0 & \varepsilon_2^0 & \gamma_{12}^0 \end{bmatrix}^T$, the corresponding boundary condition on L_1 could be generally expressed as:

$$\left\{u_x^0, \quad u_y^0\right\}^T = \left\{\varepsilon_1^0 x + \gamma_{12}^0 y, \quad \varepsilon_2^0 y\right\}^T + \left\{\tilde{a} + \tilde{b}y, \quad \tilde{c} - \tilde{b}x\right\}^T, \ (x, y) \in L_1 \tag{5.2}$$

where the last term represents rigid body movement (Timoshenko and Goodier 1970). Since it has no effect on the elastic deformation, it will be ignored in the subsequent analysis and therefore the boundary condition is simplified to $\left\{u_x^0, \quad u_y^0\right\}^T = \left\{\varepsilon_1^0 x + \gamma_{12}^0 y, \quad \varepsilon_2^0 y\right\}^T$, $(x, y) \in L_1$.

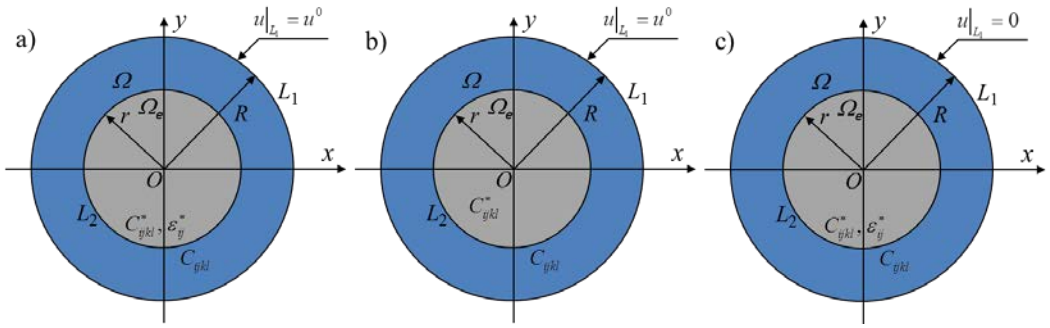

Figure 5.1. a) Inhomogeneous inclusion problem of a 2D concentric RVE; b) under far-field displacement condition without eigenstrain; and c) fixed boundary with eigenstrain

To simplify the analysis, the problem described in Figure 5.1a can be further decomposed into two parts characterized by Figure 5.1b) and c) respectively. In the formulation of complex potentials for the 2D elastic problem, the displacements and tractions along the boundary can be written in terms of two complex potential functions of complex variable $z = x + iy$ as

$$u + iv = \frac{1}{2\mu}\left(\kappa\varphi(z) - z\overline{\varphi'(z)} - \overline{\psi(z)}\right)$$
$$\sigma_x + i\sigma_y = \varphi(z) + z\overline{\varphi'(z)} + \overline{\psi(z)} \tag{5.3}$$

where u and v as well as σ_x and σ_y are displacements and tractions in x and y direction, respectively; μ is shear modulus and κ is the Kolosov constant. Here μ_1 and κ_1 are assigned to the material properties of matrix while μ_2 and κ_2 the inclusion. Next, the complex potentials will be constructed separately for the 2 cases.

5.2.1 Disturbance induced by inhomogeneity alone.

Four complex potentials are constructed to describe the elastic fields for the first part illustrated in Figure 5.1b). They are denoted as $\varphi_{11}(z)$ and $\psi_{11}(z)$ for the matrix as well as $\varphi_{21}(z)$ and $\psi_{21}(z)$ for the inclusion. Note that on the interface L_2, the continuity of displacement and equilibrium of traction must be guaranteed, while on the exterior boundary L_1 the displacement u^0 is enforced. Thus the complex potentials must satisfy the following equations:

$$\varphi_{11}(t)+t\overline{\varphi'_{11}(t)}+\overline{\psi_{11}(t)}=\varphi_{21}(t)+t\overline{\varphi'_{21}(t)}+\overline{\psi_{21}(t)},\ t\in L_2 \tag{5.4-a}$$

$$\kappa_1\varphi_{11}(t)-t\overline{\varphi'_{11}(t)}-\overline{\psi_{11}(t)}=\Gamma\left(\kappa_2\varphi_{21}(t)-t\overline{\varphi'_{21}(t)}-\overline{\psi_{21}(t)}\right),\ t\in L_2 \tag{5.4-b}$$

$$\kappa_1\varphi_{11}(t)-t\overline{\varphi'_{11}(t)}-\overline{\psi_{11}(t)}=f_0(t),\quad t\in L_1 \tag{5.4-c}$$

where $\Gamma=\mu_1/\mu_2$ and according to Eq. (5.2), $f_0(t)$ describing the boundary condition u^0 imposed on L_1 can be expressed as

$$f_0(t)=\left(\varepsilon_1^0+\varepsilon_2^0-i\gamma_{12}^0\right)\frac{t}{2}+\left(\varepsilon_1^0-\varepsilon_2^0+i\gamma_{12}^0\right)\frac{\overline{t}}{2} \tag{5.5}$$

Based on the fact that the complex potentials must be holomorphic functions in each material phase and the solution of an elastic problem is unique, $\varphi_{21}(z)$ and $\psi_{21}(z)$ can be expressed in the form of the Laurent series

$$\varphi_{21}(z)=\sum_{n=0}^{\infty}a_n z^n,\ \psi_{21}(z)=\sum_{n=0}^{\infty}b_n z^n \tag{5.6}$$

where n is non-negative because origin z = 0 is inside the inclusion. Then $\varphi_{11}(z)$ and $\psi_{11}(z)$ could be expressed explicitly by utilizing Eq. (5.4-a) and Eq. (5.4-b)

$$\varphi_{11}(z)=\frac{(1+\Gamma\kappa_2)}{(\kappa_1+1)}\sum_{n=0}^{\infty}a_n z^n+\frac{(1-\Gamma)}{(\kappa_1+1)}\left(\sum_{n=0}^{\infty}nr^{2(n-1)}\overline{a}_n z^{2-n}+\sum_{n=0}^{\infty}r^{2n}\overline{b}_n z^{-n}\right)$$

$$\begin{aligned}\psi_{11}(z)=&\left(1-\frac{(1-\Gamma)}{(\kappa_1+1)}\right)\sum_{n=0}^{\infty}b_n z^n+\sum_{n=0}^{\infty}\left(\left(1-\frac{(1+\Gamma\kappa_2)}{(\kappa_1+1)}\right)-\frac{(1-\Gamma)}{(\kappa_1+1)}n(2-n)\right)r^{2n}\overline{a}_n z^{-n}\\&+\left(1-\frac{(1+\Gamma\kappa_2)}{(\kappa_1+1)}-\frac{(1-\Gamma)}{(\kappa_1+1)}\right)\sum_{n=0}^{\infty}nr^2a_n z^{n-2}-\frac{(1-\Gamma)}{(\kappa_1+1)}\sum_{n=0}^{\infty}(-n)r^{2(n+1)}\overline{b}_n z^{-n-2}\end{aligned}\tag{5.7}$$

Substituting Eq. (5.7) into Eq. (5.4-c), the following equation could be obtained:

$$\begin{aligned}&\kappa_1\frac{(1+\Gamma\kappa_2)}{(\kappa_1+1)}\sum_{n=0}^{\infty}R^n a_n e^{in\theta}+\left(\frac{(1+\Gamma\kappa_2)}{(\kappa_1+1)}-1\right)\sum_{n=0}^{\infty}r^{2n}R^{-n}a_n e^{in\theta}\\&+\frac{(1-\Gamma)}{(\kappa_1+1)}\sum_{n=0}^{\infty}n(2-n)r^{2n}R^{-n}a_n e^{in\theta}-\frac{(1-\Gamma)}{(\kappa_1+1)}\sum_{n=0}^{\infty}n(2-n)r^{2(n-1)}R^{2-n}a_n e^{in\theta}\\&+\kappa_1\frac{(1-\Gamma)}{(\kappa_1+1)}\sum_{n=0}^{\infty}r^{2n}R^{-n}\overline{b}_n e^{-in\theta}-\sum_{n=0}^{\infty}R^n b_n e^{-in\theta}+\frac{(1-\Gamma)}{(\kappa_1+1)}\sum_{n=0}^{\infty}R^n\overline{b}_n e^{-in\theta}\\&+\kappa_1\frac{(1-\Gamma)}{(\kappa_1+1)}\sum_{n=0}^{\infty}nr^{2(n-1)}R^{2-n}\overline{a}_n e^{-i(n-2)\theta}-\frac{(1+\Gamma\kappa_2)}{(\kappa_1+1)}\sum_{n=0}^{\infty}nR^n\overline{a}_n e^{-i(n-2)\theta}\\&-\sum_{n=0}^{\infty}nr^2R^{n-2}\overline{a}_n e^{-i(n-2)\theta}+\frac{(1-\Gamma)}{(\kappa_1+1)}\sum_{n=0}^{\infty}nr^2R^{n-2}\overline{a}_n e^{-i(n-2)\theta}+\frac{(1+\Gamma\kappa_2)}{(\kappa_1+1)}\sum_{n=0}^{\infty}nr^2R^{n-2}\overline{a}_n e^{-i(n-2)\theta}\\&-\frac{(1-\Gamma)}{(\kappa_1+1)}\sum_{n=0}^{\infty}(-n)r^{2n}R^{(-n)}b_n e^{i(n+2)\theta}+\frac{(1-\Gamma)}{(\kappa_1+1)}\sum_{n=0}^{\infty}(-n)r^{2(n+1)}R^{-n-2}b_n e^{i(n+2)\theta}\\&=\mu_1\left(\left(\varepsilon_x+\varepsilon_y-i\gamma_{xy}\right)Re^{i\theta}+\left(\varepsilon_x-\varepsilon_y+i\gamma_{xy}\right)Re^{-i\theta}\right)\end{aligned}\tag{5.8}$$

Based on the linear independency of the basis $e^{in\theta}$, $n=-\infty\cdots\infty$, Eq. (5.8) leads to the following conclusions: $a_n=0$, and $b_n=0$ except that

$$a_1 = \frac{\mu_1\left(\varepsilon_{11}^0 + \varepsilon_{22}^0\right)}{C_0} - i\frac{\mu_1\gamma_{12}^0}{\Gamma\left(\left(\kappa_2+1\right)\right)}$$

$$a_3 = -\frac{C_3\mu_1\left(\varepsilon_{11}^0 - \varepsilon_{22}^0\right)}{C_1C_4 - C_2C_3} + i\frac{C_3\mu_1\gamma_{12}^0}{C_1C_4 - C_2C_3} \tag{5.9}$$

$$b_1 = \frac{C_4\mu_1\left(\varepsilon_{11}^0 - \varepsilon_{22}^0\right)}{C_1C_4 - C_2C_3} - i\frac{C_4\mu_1\gamma_{12}^0}{C_1C_4 - C_2C_3}$$

where

$$C_0 = \left(\kappa_1 - 1\right)\left(\frac{\left(1+\Gamma\kappa_2\right)}{\left(\kappa_1+1\right)} + \frac{\left(1-\Gamma\right)}{\left(\kappa_1+1\right)}\right) + 2\left(\frac{\left(1+\Gamma\kappa_2\right)}{\left(\kappa_1+1\right)} + \frac{\left(1-\Gamma\right)}{\left(\kappa_1+1\right)} - 1\right)r^2R^{-2}$$

$$C_1 = \kappa_1\frac{\left(1-\Gamma\right)}{\left(\kappa_1+1\right)}r^2R^{-2} + \frac{\left(1-\Gamma\right)}{\left(\kappa_1+1\right)} - 1,$$

$$C_2 = \kappa_1\frac{\left(1-\Gamma\right)}{\left(\kappa_1+1\right)}3r^4R^{-2} - \frac{\left(1+\Gamma\kappa_2\right)}{\left(\kappa_1+1\right)}3R^2 + \left(\frac{\left(1+\Gamma\kappa_2\right)}{\left(\kappa_1+1\right)} + \frac{\left(1-\Gamma\right)}{\left(\kappa_1+1\right)} - 1\right)3r^2 \tag{5.10}$$

$$C_3 = \frac{\left(1-\Gamma\right)}{\left(\kappa_1+1\right)}r^2R^{-2} - \frac{\left(1-\Gamma\right)}{\left(\kappa_1+1\right)}r^4R^{-4}$$

$$C_4 = \kappa_1\frac{\left(1+\Gamma\kappa_2\right)}{\left(\kappa_1+1\right)}R^2 + \left(\frac{\left(1+\Gamma\kappa_2\right)}{\left(\kappa_1+1\right)} - 1\right)r^6R^{-4} - \frac{\left(1-\Gamma\right)}{\left(\kappa_1+1\right)}3r^6R^{-4} + \frac{\left(1-\Gamma\right)}{\left(\kappa_1+1\right)}3r^4R^{-2}$$

Thus, according to Eqs (5.6), (5.7) and (5.9), the complex potentials for matrix and inhomogeneity can be obtained:

$$\varphi_{11}\left(z\right) = \left(\frac{\left(1+\Gamma\kappa_2\right)}{\left(\kappa_1+1\right)}a_1 + \frac{\left(1-\Gamma\right)}{\left(\kappa_1+1\right)}\overline{a}_1\right)z + \frac{\left(1+\Gamma\kappa_2\right)}{\left(\kappa_1+1\right)}a_3z^3 + \frac{\left(1-\Gamma\right)}{\left(\kappa_1+1\right)}\left(3r^4\overline{a}_3 + a^2\overline{b}_1\right)\frac{1}{z} \tag{5.11}$$

$$\psi_{11}(z)=\left(\left(1-\frac{(1-\Gamma)}{(\kappa_1+1)}\right)b_1+\left(1-\frac{(1+\Gamma\kappa_2)}{(\kappa_1+1)}-\frac{(1-\Gamma)}{(\kappa_1+1)}\right)3r^2a_3\right)z$$
$$+\left(1-\frac{(1+\Gamma\kappa_2)}{(\kappa_1+1)}-\frac{(1-\Gamma)}{(\kappa_1+1)}\right)r^2(\overline{a}_1+a_1)\frac{1}{z}$$
$$+\left(\left(\left(1-\frac{(1+\Gamma\kappa_2)}{(\kappa_1+1)}\right)+3\frac{(1-\Gamma)}{(\kappa_1+1)}\right)r^6\overline{a}_3+\frac{(1-\Gamma)}{(\kappa_1+1)}r^4\overline{b}_1\right)\frac{1}{z^3}$$

$$\varphi_{21}(z)=a_1z+a_3z^3$$

$$\psi_{21}(z)=b_1z$$

5.2.2 Disturbance induced by Eigenstrain.

According to Figure 5.1c), in order to find the complex potentials, this problem can be further decomposed into three sequential simpler steps. First the inclusion undergoes stress-free deformation according to the given eigenstrain $\left[\varepsilon_1^* \quad \varepsilon_2^* \quad \gamma_{12}^*\right]^T$, generally expressed as

$$u_*=\varepsilon_1^*x+\left(\frac{\gamma_{12}^*}{2}+d^*\right)y;\ v_*=\left(\frac{\gamma_{12}^*}{2}-d^*\right)x+\varepsilon_2^*y \tag{5.12}$$

where d^* is an arbitrary constant and rigid body translations are ignored here. At this stage, no constraints are applied on the inclusion boundary L_2. Then surface traction is applied to bring the inclusion back to its original shape (strain-free state). The step 3 is critical. The inclusion and the matrix are welded together and undergo deformation under the prescribed constraints on matrix boundary L_1 as well as a surface traction on L_2, which is equal to what is applied in the second step but in an opposite direction. Similarly, four other complex potentials are constructed to

describe the elastic fields in the step 3. Here, they are denoted as $\varphi_{12}(z)$ and $\psi_{12}(z)$ for the matrix and $\varphi_{22}(z)$ and $\psi_{22}(z)$ for the inclusion.

Now, the governing equations of the step 3 on exterior boundary and interface can be written as

$$\varphi_{12}(t)+t\overline{\varphi'_{12}(t)}+\overline{\psi_{12}(t)}=\varphi_{22}(t)+t\overline{\varphi'_{22}(t)}+\overline{\psi_{22}(t)},\ t\in L_2 \tag{5.13-a}$$

$$\kappa_1\varphi_{12}(t)-t\overline{\varphi'_{12}(t)}-\overline{\psi_{12}(t)}=\Gamma\left(\kappa_2\varphi_{22}(t)-t\overline{\varphi'_{22}(t)}-\overline{\psi_{22}(t)}\right)-2\mu_1 g(t),\ t\in L_2 \tag{5.13-b}$$

$$\kappa_1\varphi_{11}(t)-t\overline{\varphi'_{11}(t)}-\overline{\psi_{11}(t)}=0,\quad t\in L_1 \tag{5.13-c}$$

where $g(t)$ denotes the displacement gap at the interface which would happen if the inclusion were not confined by the surrounding matrix:

$$g(t)=-\frac{t}{2}\left(\varepsilon_1^*+\varepsilon_2^*-2id^*\right)-\frac{r^2}{2t}\left(\varepsilon_1^*-\varepsilon_2^*+i\gamma_{12}^*\right) \tag{5.14}$$

Due to the material mismatch and the appearance of the displacement gap function $g(t)$ in Eq. (5.13-b), it is challenging to construct the complex potentials in the same way as the homogeneous inclusion problem. To bypass this obstacle, here an auxiliary complex function is introduced in order to take advantage of Sokhotski-Plemelj Theorem (Muskhelishvili and Radok 1953, Sherman 1959) in which the solution of the Hilbert Problem is explicitly built based on Cauchy Integrals. This auxiliary function $w(t)$ is designed as:

$$\varphi_{12}(t)-t\overline{\varphi'_{12}(t)}-\overline{\psi_{12}(t)}=\varphi_{22}(t)-t\overline{\varphi'_{22}(t)}-\overline{\psi_{22}(t)}-2w(t),\ t\in L_2 \tag{5.15}$$

Since the four complex potentials in the Eq. (5.15) are holomorphic, and $\overline{t}$ could always be replaced by a holomorphic function r^2t^{-1} when $t\in L_2$, their combinations on both sides of Eq.

(5.15) are obviously holomorphic. Therefore it enables the following expression for the auxiliary function:

$$w(t)=\sum_{m=-\infty}^{\infty} c_m t^m,\ t\in L_2 \tag{5.16}$$

After a straightforward algebraic operation, Eq. (5.13-a) and Eq. (5.15) will lead to

$$\varphi_{22}(t)-\varphi_{12}(t)=w(t);\ \psi_{22}(t)-\psi_{12}(t)=-\left(\overline{w(t)}+\overline{t}\left(w'(t)\right)\right),\ t\in L_2 \tag{5.17}$$

According to Sokhotski-Plemelj Theorem,

$$\begin{aligned}
&\frac{1}{2\pi i}\int_{L_2}\frac{w(t)}{t-z}dt+\varphi_{02}(z)=\begin{cases}\varphi_{22}(z) & z\in\Omega_e\\ \varphi_{12}(z) & z\in\Omega/\Omega_e\end{cases}\\
&\frac{1}{2\pi i}\int_{L_2}\frac{-\left(\overline{w(t)}+\overline{t}\left(w(t)\right)\right)}{t-z}dt+\psi_{02}(z)=\begin{cases}\psi_{22}(z) & z\in\Omega_e\\ \psi_{12}(z) & z\in\Omega/\Omega_e\end{cases}
\end{aligned} \tag{5.18}$$

where the holomorphic function $\varphi_{02}(z)$ and $\psi_{02}(z)$ are defined on the entire domain $z\in\Omega$, and can be expressed as

$$\begin{aligned}
\varphi_{02}(z)&=\sum_{n=0}^{+\infty}\alpha_n z^n\\
\psi_{02}(z)&=\sum_{n=0}^{+\infty}\beta_n z^n
\end{aligned} \tag{5.19}$$

Based on the evaluation of the Cauchy Integrals in Eq. (5.18), the complex potentials can be expressed as

$$\begin{aligned}
\varphi_{12}(z)&=-\sum_{m=-\infty}^{-1}c_m z^m+\varphi_{02}(z)\\
\psi_{12}(z)&=\left(\sum_{m=1}^{+\infty}r^{2m}\overline{c}_m z^{-m}+\sum_{m=-\infty}^{1}m r^2 c_m z^{m-2}\right)+\psi_{02}(z)
\end{aligned} \tag{5.20}$$

$$\varphi_{22}(z)=\sum_{m=0}^{\infty}c_m z^m+\varphi_{02}(z)$$

$$\psi_{22}(z)=-\left(\sum_{m=-\infty}^{0}r^{2m}\overline{c}_m z^{-m}+\sum_{m=2}^{\infty}mr^2c_m z^{m-2}\right)+\psi_{02}(z)$$

Substituting Eq. (5.19) and Eq. (5.20) into Eq. (5.13-b, c) and Eq. (5.14), the following equations could be obtained:

$$\begin{aligned}
&\sum_{n=1}^{+\infty}-\kappa_1R^{-n}c_{-n}e^{-in\theta}-\sum_{n=3}^{+\infty}\left(R^{-n}r^{2n}c_n+(n-2)R^{-(n-2)}\left(1-\frac{r^2}{R^2}\right)\overline{c}_{-(n-2)}\right)e^{in\theta}\\
&-\left(R^{-1}r^2(c_1+\overline{c}_1)e^{i\theta}+R^{-2}r^4c_2e^{i2\theta}\right)+\kappa_1\left(\alpha_0+R\alpha_1e^{i\theta}+R^2\alpha_2e^{i2\theta}\right)-R\overline{\alpha}_1e^{i\theta}-\left(2R^2\overline{\alpha}_2+\overline{\beta}_0\right)\\
&=-\kappa_1\sum_{n=3}^{+\infty}R^n\alpha_ne^{in\theta}+\sum_{n=1}^{+\infty}\left((n+2)R^{n+2}\overline{\alpha}_{n+2}+R^n\overline{\beta}_n\right)e^{-in\theta}
\end{aligned}\tag{5.21}$$

and

$$\begin{aligned}
&\kappa_1\left(-\sum_{n=-\infty}^{-1}c_nr^ne^{in\theta}\right)+\sum_{n=-\infty}^{-1}nr^n\overline{c}_ne^{-i(n-2)\theta}-\left(\sum_{n=1}^{+\infty}r^nc_ne^{in\theta}+\sum_{n=-\infty}^{1}nr^n\overline{c}_ne^{-i(n-2)\theta}\right)\\
&-\Gamma\left(\kappa_2\left(\sum_{n=0}^{\infty}c_nr^ne^{in\theta}\right)-\sum_{n=0}^{\infty}nr^n\overline{c}_ne^{-i(n-2)\theta}+\left(\sum_{n=-\infty}^{0}r^nc_ne^{in\theta}+\sum_{n=2}^{\infty}nr^n\overline{c}_ne^{-i(n-2)\theta}\right)\right)\\
&+\left(\kappa_1\sum_{n=0}^{+\infty}\alpha_nr^ne^{in\theta}-\sum_{n=0}^{+\infty}nr^n\overline{\alpha}_ne^{-i(n-2)\theta}-\sum_{n=0}^{+\infty}r^n\overline{\beta}_ne^{-in\theta}\right)\\
&-\Gamma\left(\kappa_2\sum_{n=0}^{+\infty}\alpha_nr^ne^{in\theta}-\sum_{n=0}^{+\infty}nr^n\overline{\alpha}_ne^{-i(n-2)\theta}-\sum_{n=0}^{+\infty}r^n\overline{\beta}_ne^{-in\theta}\right)\\
&=-\mu_1\left(-re^{i\theta}\left(\varepsilon_1^*+\varepsilon_2^*-2id^*\right)-re^{-i\theta}\left(\varepsilon_1^*-\varepsilon_2^*+i\gamma_{12}^*\right)\right)
\end{aligned}\tag{5.22}$$

Similarly, according to the linear independency of the basis $e^{in\theta}, n=-\infty,\cdots,\infty$, Eq. (5.21) and Eq. (5.22) together lead to the following conclusions: $\alpha_n=0$ and $\beta_n=0,\ n=0,\cdots\infty$ as well as $c_m=0,\ m=-\infty,\cdots,\infty$ except that

$$\alpha_1 = \frac{1}{(\kappa_1 - 1)}\left(\frac{r}{R}\right)^2 \frac{2\mu_1\left(\varepsilon_1^* + \varepsilon_2^*\right)}{M_5 + M_6}$$

$$\alpha_3 = \mu_1 r^2\left(\varepsilon_1^* - \varepsilon_2^* - i\gamma_{12}^*\right)\frac{M_4}{M_1 M_4 - M_2 M_3}$$

$$\beta_1 = -\mu_1 r^2\left(\varepsilon_1^* - \varepsilon_2^* - i\gamma_{12}^*\right)\frac{M_3}{M_1 M_4 - M_2 M_3}$$

$$c_{-1} = -\mu_1 r^2\left(\varepsilon_1^* - \varepsilon_2^* + i\gamma_{12}^*\right)\frac{1}{-\kappa_1}\frac{-3M_4 R^4 + M_3 R^2}{M_1 M_4 - M_2 M_3} \tag{5.23}$$

$$c_1 = \mu_1\left(\frac{\varepsilon_1^* + \varepsilon_2^*}{M_5 + M_6} - \frac{2id^*}{M_5 - M_6}\right)$$

$$c_3 = \mu_1 r^2\left(\varepsilon_1^* - \varepsilon_2^* - i\gamma_{12}^*\right)\cdot\frac{(\kappa_1 - \Gamma\kappa_2)}{(1 + \Gamma\kappa_2)}\cdot\frac{M_4}{M_1 M_4 - M_2 M_3}$$

$$\alpha_0 = \frac{\kappa_2 + 1}{\kappa_1 - \kappa_2}c_0$$

$$\kappa_1\alpha_0 - \overline{\beta}_0 = 0$$

where

$$M_1 = \frac{\kappa_1 + \Gamma}{\kappa_1}3R^4 + 3(\Gamma - 1)r^4$$

$$M_2 = \frac{\kappa_1 + \Gamma}{\kappa_1}R^2 + (\Gamma - 1)r^2$$

$$M_3 = \kappa_1 R^6 - r^6\frac{(\kappa_1 - \Gamma\kappa_2)}{(1 + \Gamma\kappa_2)} + 3R^6\left(1 - \frac{r^2}{R^2}\right)\frac{1}{\kappa_1} \tag{5.24}$$

$$M_4 = \left(1 - \frac{r^2}{R^2}\right)\frac{1}{\kappa_1}R^4$$

$$M_5 = \left(1-\Gamma\frac{\kappa_2-1}{\kappa_1-1}\right)\left(\frac{r}{R}\right)^2 - 1 - \Gamma\kappa_2$$

$$M_6 = \left(1-\Gamma\frac{\kappa_2-1}{\kappa_1-1}\right)\left(\frac{r}{R}\right)^2 - 1 + \Gamma$$

Subsquently, based on Eqs (5.19), (5.20) and (5.23), the complex potentials for inclusion and matrix are obtained:

$$\begin{aligned}
\varphi_{12}(z) &= -c_{-1}z^{-1} + \alpha_1 z + \alpha_3 z^3 \\
\psi_{12}(z) &= r^2\overline{c}_1 z^{-1} + r^6\overline{c}_3 z^{-3} + r^2 c_1 z^{-1} - r^2 c_{-1} z^{-3} + \beta_1 z \\
\varphi_{22}(z) &= c_1 z + c_3 z^3 + \alpha_1 z + \alpha_3 z^3 \\
\psi_{22}(z) &= -\left(r^{-2}\overline{c}_{-1} z + 3r^2 c_3 z\right) + \beta_1 z
\end{aligned} \tag{5.25}$$

It is worth mentioning here that the coefficients α_0, β_0 and c_0 disappear in the Eq. (5.25) since in fact they will cancel each other when the obtained complex potentials are combined together to give the analytical solution for the displacement field. Note here the four potentials are constructed for the step 3 only, and therefore the corresponding displacement field should be combined with the stress-free deformation in step 1, namely Eq. (5.12), to give the disturbance of displacement field induced by the eigenstrain inside the inhomogeneity.

Now, the complex potential functions have been built separately based on the decomposition of the original problem. Their superposition provides a closed form solution for the disturbance introduced by the inhomogeneous inclusion in a 2D concentric finite domain. The final explicit expression for the displacement field inside the RVE is expressed as follows

$$u+iv=\begin{cases}\dfrac{1}{2\mu_2}\left(\kappa_2\left(\varphi_{21}+\varphi_{22}\right)-z\left(\overline{\varphi'_{21}}+\overline{\varphi'_{22}}\right)-\left(\overline{\psi_{21}}+\overline{\psi_{22}}\right)\right)+u_*+iv_* & z\in\Omega_e \\ \dfrac{1}{2\mu_1}\left(\kappa_1\left(\varphi_{11}+\varphi_{12}\right)-z\left(\overline{\varphi'_{11}}+\overline{\varphi'_{12}}\right)-\left(\overline{\psi_{11}}+\overline{\psi_{12}}\right)\right) & z\in\Omega/\Omega_e\end{cases} \tag{5.26}$$

Consequently, the strain field could be determined according to the gradient of the displacement field. The explicit expression for the elastic fields are documented in the appendix.

5.3 COMPARISON WITH NUMERICAL RESULTS

To validate the obtained analytical solution, comparison is first made with the numerical results based on FEM. Here the disturbed displacement field in a concentric RVE is captured numerically via FEM, and then compared with the theoretical prediction from the analytical solution. In the comparison, the Young's Modulus and Poisson's ratio of the matrix are assigned as $E_1=30\,\text{GPa}$ and $\nu_1=0.2$ while for inclusion $E_2=100\,\text{GPa}$ and $\nu_2=0.15$. The size of the RVE is set as $r=0.6\,\text{m}$ for inclusion and $R=1\,\text{m}$ for RVE. The eigenstrain in the inclusion is given as $\left[\varepsilon_1^*\quad\varepsilon_2^*\quad\gamma_{12}^*\right]^T=\left[0.01\quad-0.01\quad0.05\right]^T$ while the boundary condition $\left[\varepsilon_1^0\quad\varepsilon_2^0\quad\gamma_{12}^0\right]^T=\left[-0.01\quad0.01\quad-0.05\right]^T$. The comparison is shown in Figure 5.2.

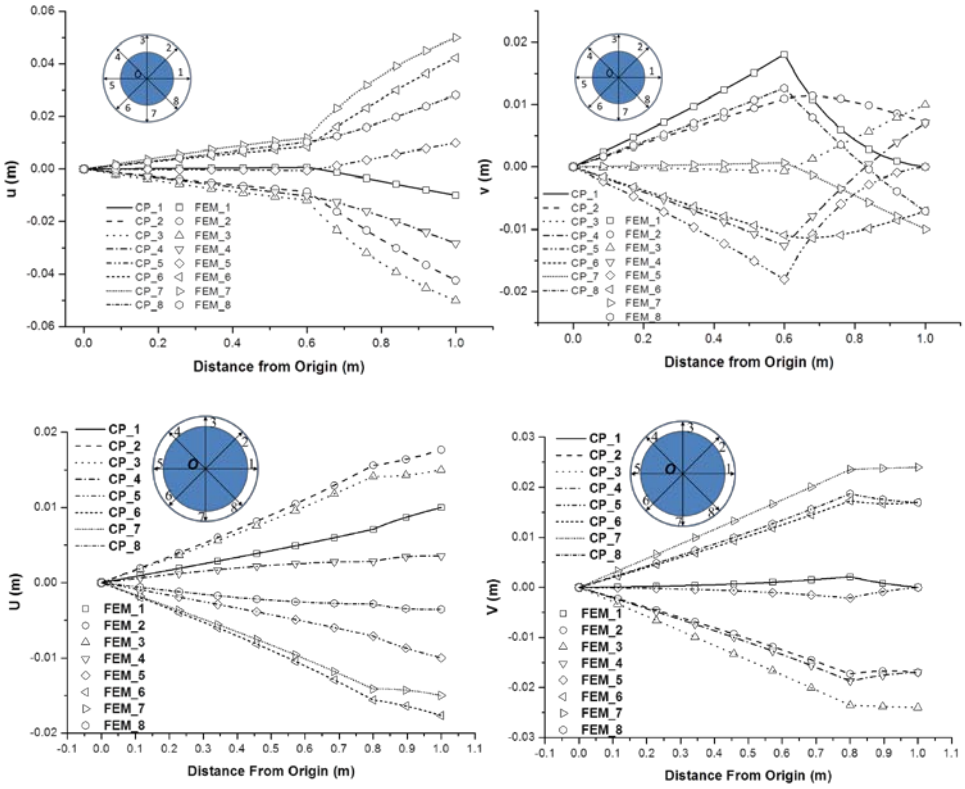

Figure 5.2. Comparison of the analytical solutions of displacement fields based on complex potential method with FEM for the concentric RVEs containing an inhomogeneous inclusion

In Figure 5.2, the firm agreement between the analytical solution and the numerical simulation along eight main directions in the RVE clearly shows that the obtained analytical solution based on complex potential method can accurately predict the disturbance induced by the inhomogeneous inclusion with an eigenstrain.

5.4 DISCUSSION AND CONCLUSION

This general analytical solution obtained for the concentric configuration can be further validated by comparing with the analytical solutions available in the literature for some special cases. First, the solution obtained for the inhomogeneous inclusion with eigenstrain under fixed boundary condition (Figure 5.1c) can be compared with the same configuration for the homogeneous inclusion problem (Zou et al 2012). The difference induced by the material mismatch must vanish if $\Gamma = \mu_1 / \mu_2 = 1$ and $\kappa_2 = \kappa_1$. In fact, according to Eqs (5.23) and (5.24), when material mismatch disappears, the coefficients for the obtained complex potentials are simplified as follows

$$\alpha_1 = -\frac{\mu_1}{\kappa_1^{\,2}-1}\frac{2r^2}{R^2}\left(\varepsilon_1^* + \varepsilon_2^*\right)$$

$$\alpha_3 = \frac{\mu_1}{\kappa_1\left(\kappa_1+1\right)}\frac{r^2}{R^4}\left(\frac{r^2}{R^2}-1\right)\left(\varepsilon_1^* - \varepsilon_2^* - i\gamma_{12}^*\right)$$

$$\beta_1 = \frac{\kappa_1\mu_1}{\kappa_1+1}\frac{r^2}{R^2}\left(\varepsilon_1^* - \varepsilon_2^* - i\gamma_{12}^*\right) - \frac{3\mu_1}{\kappa_1\left(\kappa_1+1\right)}\frac{r^2}{R^2}\left(\frac{r^2}{R^2}-1\right)\left(\varepsilon_1^* - \varepsilon_2^* - i\gamma_{12}^*\right) \tag{5.27}$$

$$c_1 = -\mu_1\frac{\varepsilon_1^* + \varepsilon_2^*}{1+\kappa_1}$$

$$c_{-1} = -\frac{\mu_1 r^2}{\kappa_1+1}\left(\varepsilon_1^* - \varepsilon_2^* + i\gamma_{12}^*\right)$$

$$c_3 = 0$$

which gives the same the results as listed in the corresponding solution for homogeneous inclusion problem in a finite concentric domain (after adding the uniform far field strain).

Second, for a special case the disturbance are induced by a dilational eigenstrain, namely $\left[\varepsilon_1^* \quad \varepsilon_2^* \quad \gamma_{12}^*\right]^T = \left[\varepsilon^* \quad \varepsilon^* \quad 0\right]^T$, the analytical solution could also be obtained via Airy-Stress function (Timoshenko and Goodier 1970) based on the symmetric property of the configuration. The radial displacement fields are listed as follows:

$$u^r = \begin{cases} \dfrac{(1-2\nu_2)(1+\nu_2)}{E_2} p_2 |z| & z \in \Omega_e \\ \dfrac{(1+\nu_1)}{E_1} \cdot \dfrac{r^2 R^2 (1-\nu_1)}{(1+\nu_1) r^2 + (1-\nu_1) R^2} \dfrac{p_1}{|z|} - \dfrac{(1+\nu_1)(1-2\nu_1)}{E_1} \cdot \dfrac{(1+\nu_1) r^2 p_1}{(1+\nu_1) r^2 + (1-\nu_1) R^2} |z| & z \in \Omega / \Omega_e \end{cases} \tag{5.28}$$

where $p_1 = \dfrac{1}{1+k} \cdot \dfrac{E_2}{(1+\nu_2)(1-2\nu_2)} \varepsilon^*$ and $p_2 = \dfrac{k}{1+k} \cdot \dfrac{E_2}{(1+\nu_2)(1-2\nu_2)} \varepsilon^*$, and

$$k = \frac{E_2}{1+\nu_2} \cdot \frac{1+\nu_1}{E_1} \cdot \frac{1-2\nu_1}{(1-2\nu_2)} \cdot \frac{R^2 - r^2}{r^2 + (1-2\nu_1) R^2} \tag{5.29}$$

Alternatively, this solution could be achieved by assigning Eq. (5.25) the same specified eigenstrain. It results in

$$u + iv = \begin{cases} \dfrac{2\left(\left(\dfrac{r}{R}\right)^2 - 1\right)}{2\left(1 - \Gamma \dfrac{\kappa_2 - 1}{\kappa_1 - 1}\right)\left(\dfrac{r}{R}\right)^2 - 2 - \Gamma(\kappa_2 - 1)} \varepsilon^* z & z \in \Omega_e \\ \dfrac{1}{2\mu_1}\left(\left(\dfrac{r}{R}\right)^2 4\mu_1 z - r^2 4\mu_1 \dfrac{1}{z}\right)\left(\dfrac{\varepsilon^*}{2\left(1 - \Gamma \dfrac{\kappa_2 - 1}{\kappa_1 - 1}\right)\left(\dfrac{r}{R}\right)^2 - 2 - \Gamma(\kappa_2 - 1)}\right) & z \in \Omega / \Omega_e \end{cases} \tag{5.30}$$

which could be shown as an identical expression to Eq. (5.28).

Third, the analytical solution obtained for disturbance induced by inhomogeneity alone (Figure 5.1b), is compared with a circular inhomogeneity embedded in an infinite domain, which

can be solved via EIM. Note here the eigenstrain is not concerned. Explicitly, the displacement fields inside the inhomogeneity are documented as

$$\begin{aligned} u_2 = \frac{\Gamma}{2}\Bigg\{ & \left(\frac{\left(\kappa_2 - 1\right)\left(\varepsilon_1^0 + \varepsilon_2^0\right)}{C_0} - \frac{C_4\left(\varepsilon_1^0 - \varepsilon_2^0\right)}{C_1C_4 - C_2C_3} \right) x + \left(\frac{\gamma_{12}^0}{\Gamma} - \frac{C_4\gamma_{12}^0}{C_1C_4 - C_2C_3} \right) y \\ & + \frac{\left(3 - \kappa_2\right)C_3\left(\varepsilon_1^0 - \varepsilon_2^0\right)}{C_1C_4 - C_2C_3} x^3 + \frac{3\left(\kappa_2 + 1\right)C_3\left(\varepsilon_1^0 - \varepsilon_2^0\right)}{C_1C_4 - C_2C_3} xy^2 \\ & - \frac{3\left(\kappa_2 - 1\right)C_3\gamma_{12}^0}{C_1C_4 - C_2C_3} x^2 y + \frac{\left(\kappa_2 + 3\right)C_3\gamma_{12}^0}{C_1C_4 - C_2C_3} y^3 \Bigg\} \\ v_2 = \frac{\Gamma}{2}\Bigg\{ & \left(\frac{\left(\kappa_2 - 1\right)\left(\varepsilon_1^0 + \varepsilon_2^0\right)}{C_0} + \frac{C_4\left(\varepsilon_1^0 - \varepsilon_2^0\right)}{C_1C_4 - C_2C_3} \right) y - \left(\frac{\gamma_{12}^0}{\Gamma} + \frac{C_4\gamma_{12}^0}{C_1C_4 - C_2C_3} \right) x \\ & + \frac{\left(\kappa_2 - 3\right)C_3\left(\varepsilon_1^0 - \varepsilon_2^0\right)}{C_1C_4 - C_2C_3} y^3 + \frac{\left(\kappa_2 + 3\right)C_3\gamma_{12}^0}{C_1C_4 - C_2C_3} x^3 \\ & - \frac{3\left(\kappa_2 + 1\right)C_3\left(\varepsilon_1^0 - \varepsilon_y\right)}{C_1C_4 - C_2C_3} x^2 y - \frac{3\left(\kappa_2 - 1\right)C_3\gamma_{12}^0}{C_1C_4 - C_2C_3} xy^2 \Bigg\} \end{aligned} \tag{5.31}$$

here the terms $C_0, C_1 ..., C_4$ are defined in Eq. (5.10). Based on their combination in Eq. (5.31), the governing parameters will be:

$$\theta_1 = \frac{1}{C_0}$$

$$\theta_2 = \frac{C_4}{C_1C_4 - C_2C_3} \tag{5.32}$$

$$\theta_3 = \frac{C_3}{C_1C_4 - C_2C_3}$$

It is observed that the nonlinear terms generating position-dependent strain field inside the inhomogeneity are governed by a common factor θ_3. The contribution of the nonlinear terms

can be characterized by the ratio θ_3 / θ_2. Similarly, given $E_1 = 30\,\text{GPa}$, $\nu_2 = \nu_1 = 0.2$ and r = 0.6 m the absolute values of θ_3 and θ_3 / θ_2 according to different E_2 and R are plotted In Figure 5.3 and Figure 5.4. It shows that with the decrease of volume fraction of the inhomogeneity characterized by r / R, θ_3 vanishes quickly as well as θ_3 / θ_2, which means that the strain field in the inhomogeneity is asymptotically position-independent, just as Eshelby (1957) predicted for the infinite domain problem.

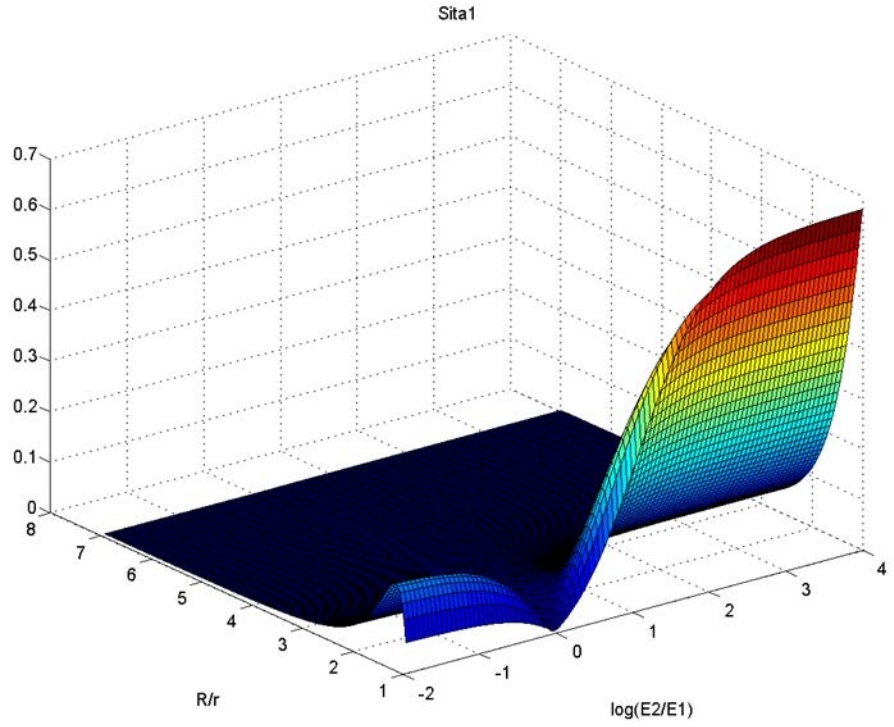

Figure 5.3. Absolute value of θ_1 for different material mismatch and volume fractions

In addition, as shown in Figure 5.4, the contribution of nonlinear terms, which stands for the position-dependent elastic field, grows with the increase of the material mismatch. Both Figure 5.3 and Figure 5.4 demonstrate that the peak value of the position-dependent part could

be achieved when the ratio of radius R/r falls in to a specified range, and for this case it is $1.1< R/r < 1.3$.

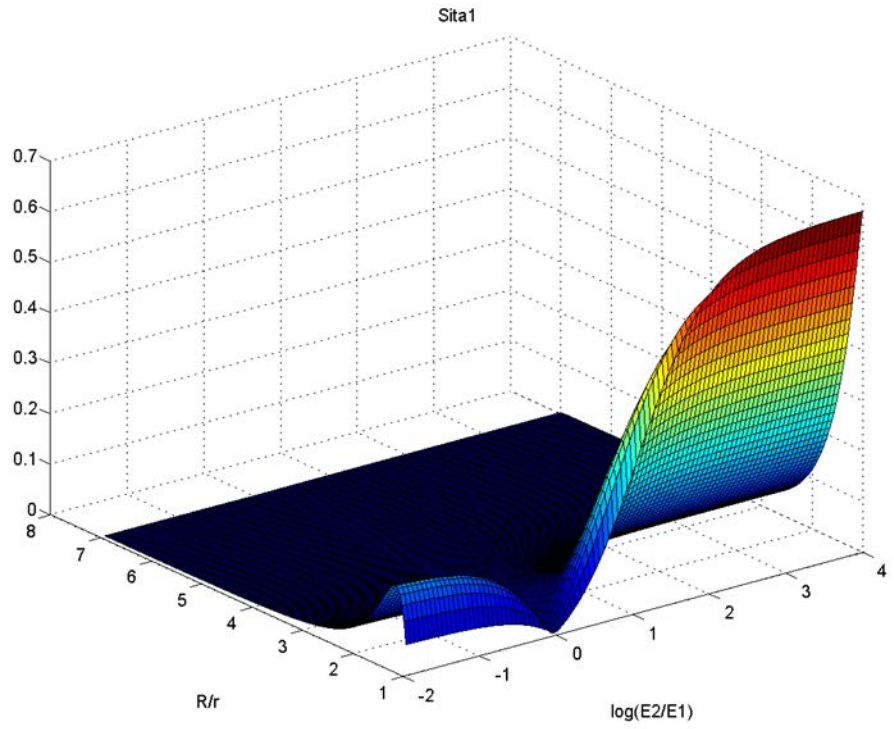

Figure 5.4. Absolute value of θ_2 for different material mismatch and volume fractions

In addition, according to Figure 5.5, the material mismatch has a significant effect on the contribution of the nonlinear terms. For different volume factions, the absolute values of θ_3 / θ_2 have similar trend with the increase of E_2 / E_1 if the inclusion is stronger than the matrix. The same trend could be observed for the decrease of E_2 / E_1 if the inclusion is weaker than the matrix. For the special case that $E_2 / E_1 = 1$, which means this RVE is indeed homogeneous, it is shown that $\theta_3 / \theta_2 = 0$ which results in a uniform strain field same as the far field strain in the inclusion. Besides, the absolute vale of θ_3 / θ_2 could be as high as 25%, which means that the

assumption of the position independency of the interior Eshelby tensor might bring a significant error for applying EIM to solve the inhomogeneous inclusion problem in a finite domain.

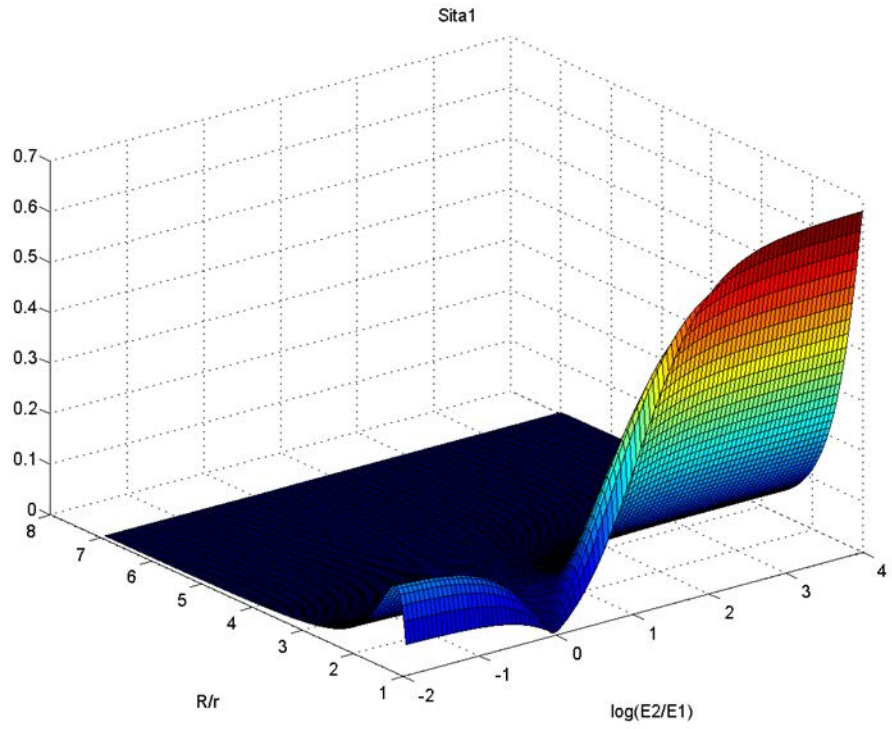

Figure 5.5. Absolute value of θ_3 for different material mismatch and volume fractions

In fact, the analytical solution recovers the corresponding one obtained via EIM for infinite domain once the volume fraction of the inhomogeneity is negligible. For simplicity, the shear strain in the inhomogeneity is taken as an example here. According to Mura (1987) and Jin et al (2011), the shear strain in an unbounded domain containing a circular inhomogeneity is

$$\gamma_{12} = \left(\frac{\kappa_1 (\Gamma - 1)}{\kappa_1 + \Gamma} + 1 \right) \gamma_{12}^0 \tag{5.33}$$

On the other hand, according to Eq. (5.27), when $r / R \to 0$, the solution for shear strain via complex potential formulation is

$$\gamma_{12} = \frac{\partial u_2}{\partial y} + \frac{\partial v_2}{\partial x} = \left(\frac{\kappa_1 (\Gamma - 1)}{\kappa_1 + \Gamma} + 1 \right) \gamma_{12}^0 \tag{5.34}$$

which is the same as Eq. (5.33).

The closed form solution for inhomogeneous inclusion problem in a 2D finite domain is obtained via complex potential method for a concentric configuration. The solution is shown to exactly predict the disturbed elastic field due to the existence of inhomogeneity and eigenstrain. The validity of the obtained analytical solution is verified by FEM and comparison with the classical solutions available for special cases. It is found the existence of nonlinear terms in the displacement field makes the Eshelby conjecture ineffective even for a circular inclusion. The contribution of the nonlinear terms increases with the material mismatch. A great advantage of the proposed formulation is that no postulate based on geometrical characteristics is needed for the complex potential method. Thus it is of potential to be extended to more complex geometry with the aid of conformal mapping.

6.0 A CIRCULAR INHOMOGENEITY SURROUNDED BY A FINITE INTERFACIAL ZONE

In order to take into account the effect of a finite interfacial zone between the inhomogeneity and matrix in an inhomogeneous representative volume element (RVE), analytical solutions for a 3-phase inclusion problem are needed. In this study, the primary focus is placed on a 3-phase concentric configuration for a 2D RVE, for which the exterior matrix is bounded and different elastic properties are assigned to the interior inclusion, interfacial zone, and exterior matrix. In addition to the inhomogeneity induced by material mismatch, arbitrary uniform eigenstrains $\varepsilon_{ij}^{(1*)}$ and $\varepsilon_{ij}^{(2*)}$ are allowed to independently happen within the inclusion and interfacial zone, respectively. In this study the analytical solution is pursued via the complex potential method with the aid of 2 auxiliary potential functions. Based on the Sokhotski-Plemelj theorem, the complex potentials in each phase are constructed to account for the eigenstrains existing in the inclusion and the interfacial zone, as well as the imposed boundary conditions on the exterior matrix. The identification of the coefficients in the complex potential functions gives the analytical expressions for the disturbance induced by the inhomogeneity and eigenstraions. When compared with FEM simulations, a firm agreement is achieved for 3-phase concentric 2D finite domains. Furthermore, if the exterior matrix is extended to infinity, the obtained analytical solution reproduces the results given by Luo and Weng (1987) for uniform eigenstrain within the inclusion and Markenscoff and Dundurs (2013) for uniform eigenstrain in the interfacial zone.

6.1 BACKGROUND AND MOTIVATION

Investigation of the disturbed elastic fields in an inhomogeneous representative volume element (RVE) is of fundamental importance in contemporary composite mechanics and micromechanics, and thus attracting increasing attentions in a wide range of engineering applications. In many engineering applications, a finite interfacial zone exists between the inclusion and matrix. This extra phase leads to a 3-phase inhomogeneous RVE. In some composite solids, the interfacial phase appears during the synthesis of composites. For example, in cementitious materials, the aggregates are surrounded by a weak interfacial layer, which is called interfacial transitional zone (Scrivener 1989, Sun et al. 2006). In some composite solids, the interfacial phase is a result of phase change in matrix or inclusion during service. For example, the growth of Li-rich phase during lithiation/delithiation in rechargeable lithium ion battery (Ryu et al. 2011, Kim et al. 2008). Obviously, to realistically estimate their performance, the effect of interfacial zone must be taken into account.

For an unbound matrix, if the embedded inhomogeneity and its surrounding interfacial zone form a concentric configuration, Luo and Weng (1987, 1989) gave the analytical solutions for an arbitrary uniform eigenstrain within the inclusion for both 2D and 3D domains. In their investigation, stress function formulation proposed by Christenson and Lo (1979) is employed and the eigenstrain within the inclusion is decomposed into dilatational and deviatoric components. Following the same methodology, Li et al (1999) extended the analytical solutions to unbounded 4-phase concentric RVEs for cementitious materials. Recently, Markenscoff and Dunders (2014) studied the disturbance induced by a uniform eigenstrain within the interfacial zone. In their work, the interfacial zone is represented by an annulus (3D) or a ring (2D), which is embedded in an unbounded homogeneous media. Thus, same elastic properties are shared by

the inclusion and the exterior matrix. Similarly, using stress function proposed by Christenson and Lo (1979) and dilatational and deviatoric decomposition, they gave analytical solutions for an unbounded 3-phase concentric RVE with an arbitrary uniform eigenstrain in the interfacial zone.

However, in real applications, there is no infinite RVE, and in many cases the volume ratio of the inhomogeneity to the RVE is finite. If the volume fractions of the inhomogeneity and interfacial zone in the composite solids are not negligible, the solutions for unbounded 3-phase RVEs obtained by Luo and Weng (1987, 1989) and Markenscoff and Dunders (2014) cannot be directly applied. In order to capture the size (volume) effect induced by inclusion and interfacial zone, this research is focused on a concentric 2D finite RVE. In this study, displacement (Dirichlet) boundary condition is imposed on the exterior matrix and arbitrary uniform eigenstrains $\varepsilon_{ij}^{(1*)}$ and $\varepsilon_{ij}^{(2*)}$ are allowed to independently happen within the inclusion and interfacial zone, respectively. Based on Sokhotski-Plemelj theorem, the complex potentials in each phase are constructed with the help of Laurent Series and Cauchy-integrals along the interfaces. The coefficients of the potential functions are identified by the imposed boundary conditions. The analytical solutions are shown to be able to reproduce the results obtained by Luo and Weng (1989) as well as Makenscoff and Dunders (2014) if the exterior matrix is set to be unbounded. In addition, firm agreements are achieved with FEM results for concentric 2D finite domains.

6.2 THEORETICAL FORMULATION OF A 3-PHASE CONCENTRIC RVE

The inhomogeneous inclusion problem is now characterized by a 3-phase RVE of a concentric configuration in 2D domain; see Figure 6.1. The circular inclusion is embedded at the center, surrounded by the intermediate phase in the shape of a ring, which is further surrounded by a bounded matrix. The intermediate phase is enclosed by interfaces L_2 and L_1 with radii r_2 and r_1 respectively. The exterior boundary of the RVE is denoted by L_0 with the radius R. Every phase in the RVE is homogeneous and isotropic, although different material properties are assigned independently to each phase with upper indices 2, 1 and 0 referring to inclusion, interfacial zone and matrix respectively. The eigenstrains are assumed to be

$$\varepsilon_{ij}^{*}\left(\mathbf{x}\right)=\begin{cases}\varepsilon_{ij}^{(2*)} & \mathbf{x}\in\Omega_2\\ \varepsilon_{ij}^{(1*)} & \mathbf{x}\in\Omega_1\\ 0 & \mathbf{x}\in\Omega_0\end{cases} \tag{6.1}$$

here $\mathbf{x}=\left(x,y\right)$ is any point within the RVE. Based on the far field strain $\left[\begin{array}{ccc}\varepsilon_1^{(0)} & \varepsilon_2^{(0)} & \gamma_{12}^{(0)}\end{array}\right]^T$, the corresponding boundary condition on L_0 could be generally expressed as:

$$\left\{u_x^{(0)},\quad u_y^{(0)}\right\}^T=\left\{\varepsilon_1^{(0)}x+\gamma_{12}^{(0)}y,\quad \varepsilon_2^{(0)}y\right\}^T,\ \left(x,y\right)\in L_0 \tag{6.2}$$

which is simplified from the general form $\left\{u_x^{(0)},\quad u_y^{(0)}\right\}^T=\left\{\varepsilon_1^{(0)}x+\gamma_{12}^{(0)}y,\quad \varepsilon_2^{(0)}y\right\}^T+\left\{\tilde{a}+\tilde{b}y,\quad \tilde{c}-\tilde{b}x\right\}^T$, $\left(x,y\right)\in L_0$ where the last part represents rigid body movement (Timoshenko and Goodier 1970) and therefore is ignored in the subsequent analysis as it has no effect on the elastic deformation.

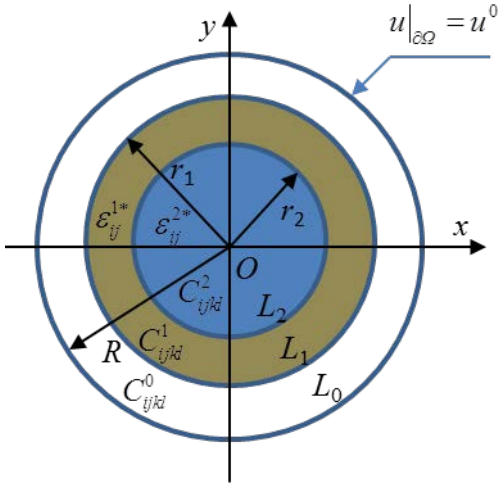

Figure 6.1. Illustration of a 3-phase concentric RVE in 2D domain

In the formulation of complex potentials for the 2D elastic problem, the displacements and tractions along the boundary or interface can be written in terms of two complex potential functions of complex variable $z = x + iy$ as

$$\begin{aligned} u + iv &= \frac{1}{2\mu}\left(\kappa\varphi(z) - z\overline{\varphi'(z)} - \overline{\psi(z)}\right) \\ \sigma_x + i\sigma_y &= \varphi(z) + z\overline{\varphi'(z)} + \overline{\psi(z)} \end{aligned} \tag{6.3}$$

where u, v, σ_x and σ_y are displacements and tractions in x and y direction, respectively; μ is shear modulus and κ is the Kolosov constant. Here μ_0 and κ_0 are the assigned material properties for exterior matrix; μ_1 and κ_1 the interfacial zone; and μ_2 and κ_2 the interior inclusion.

In order to find the complex potentials, the problem can be decomposed into three sequential steps to simplify the formulation. First the inclusion and the interfacial zone undergo stress-free deformation according to the given eigenstrain $\varepsilon_{ij}^{(2*)}$ and $\varepsilon_{ij}^{(1*)}$. This can be generally expressed as

$$u^{(2*)}=\varepsilon_1^{(2*)}x+\frac{\gamma_{12}^{(2*)}}{2}y,\ v^{(2*)}=\frac{\gamma_{12}^{(2*)}}{2}x+\varepsilon_2^{(2*)}y,\ (x,y)\in\Omega_2$$
$$u^{(1*)}=\varepsilon_1^{(1*)}x+\frac{\gamma_{12}^{(1*)}}{2}y,\ v^{1*}=\frac{\gamma_{12}^{(1*)}}{2}x+\varepsilon_2^{(1*)}y,\ \ (x,y)\in\Omega_1 \tag{6.4}$$

here rigid body translations and rotations are ignored again since they do not induce any elastic deformation. At this stage, no constraints are applied on the interior boundaries L_1 and L_2. Then surface tractions are applied to bring the inclusion as well as the interfacial zone back to their original shapes (strain-free state). At the last step, all the three phases are welded together and undergo deformation under the prescribed constraints on the exterior boundary L_0 as well as the surface tractions on L_1 and L_2, which are equal in value to what have been applied at the second step but in opposite directions. Obviously, the last step is the key and mathematical formulations are needed to construct the complex potentials to describe the elastic fields. Here, the potentials are denoted as $\varphi_2(z)$ and $\psi_2(z)$ for the inclusion, $\varphi_1(z)$ and $\psi_1(z)$ for the interfacial zone and $\varphi_0(z)$ and $\psi_0(z)$ for the matrix. For the displacement gap $g_1(t)$ and $g_2(t)$ at L_1 and L_2, which would happen if the inclusion and interfacial zone underwent the stress-free displacement shown in Eq. (6.4) and were not confined by other phases in the RVE, they can be expressed as

$$g_1(t)=-\frac{t}{2}\left(\varepsilon_1^{(1*)}+\varepsilon_2^{(1*)}\right)-\frac{\overline{t}}{2}\left(\varepsilon_1^{(1*)}-\varepsilon_2^{(1*)}+i\gamma_{12}^{(1*)}\right),\ t\in L_1 \text{ or } L_2$$
$$g_2(t)=-\frac{t}{2}\left(\varepsilon_1^{(2*)}+\varepsilon_2^{(2*)}\right)-\frac{\overline{t}}{2}\left(\varepsilon_1^{(2*)}-\varepsilon_2^{(2*)}+i\gamma_{12}^{(2*)}\right),\ t\in L_2 \tag{6.5}$$

where $\overline{t}=r_1^2/t$ or $\overline{t}=r_2^2/t$ for $t\in L_1$ or $t\in L_2$. Based on equilibrium and compatibility on the interfaces L_1 and L_2 as well as the imposed boundary condition on matrix, the complex potentials must satisfy the following equations:

$$\Gamma_2\left(\kappa_2\varphi_2(t)-t\overline{\varphi_2'(t)}-\overline{\psi_2(t)}\right)-2\mu_1\tilde{g}_2(t)=\kappa_1\varphi_1(t)-t\overline{\varphi_1'(t)}-\overline{\psi_1(t)} \text{ for}$$

$$t\in L_2 \tag{6.6a}$$

$$\varphi_1(t)+t\overline{\varphi_1'(t)}+\overline{\psi_1(t)}=\varphi_2(t)+t\overline{\varphi_2'(t)}+\overline{\psi_2(t)} \text{ for } t\in L_2 \tag{6.6b}$$

$$\Gamma_1\left(\kappa_1\varphi_1(t)-t\overline{\varphi_1'(t)}-\overline{\psi_1(t)}\right)-2\mu_0 g_1(t)=\kappa_0\varphi_0(t)-t\overline{\varphi_0'(t)}-\overline{\psi_0(t)} \text{ for}$$

$$t\in L_1 \tag{6.6c}$$

$$\varphi_2(t)+t\overline{\varphi_2'(t)}+\overline{\psi_2(t)}=\varphi_0(t)+t\overline{\varphi_0'(t)}+\overline{\psi_0(t)} \text{ for } t\in L_1 \tag{6.6d}$$

$$\frac{1}{2\mu_0}\left(\kappa_0\varphi_0(t)-t\overline{\varphi_0'(t)}-\overline{\psi_0(t)}\right)=f_0(t) \qquad \text{for } t\in L_0 \tag{6.6e}$$

Here $\Gamma_2=\mu_1/\mu_2$, $\Gamma_1=\mu_0/\mu_1$ and

$$\begin{aligned} f_0(t)&=\left(\varepsilon_1^{(0)}+\varepsilon_2^{(0)}-i\gamma_{12}^{(0)}\right)\frac{t}{2}+\left(\varepsilon_1^{(0)}-\varepsilon_2^{(0)}+i\gamma_{12}^{(0)}\right)\frac{R^2}{2t} \\ \tilde{g}_2(t)&=g_2(t)-g_1(t) \\ &=-\frac{t}{2}\left(\tilde{\varepsilon}_1^{(2*)}+\tilde{\varepsilon}_2^{(2*)}\right)-\frac{r_2^2}{2t}\left(\tilde{\varepsilon}_1^{(2*)}-\tilde{\varepsilon}_2^{(2*)}+i\tilde{\gamma}_{12}^{(2*)}\right) \end{aligned} \tag{6.7}$$

where $\tilde{\varepsilon}_1^{(2*)}=\left(\varepsilon_1^{(2*)}-\varepsilon_1^{(1*)}\right)$, $\tilde{\varepsilon}_2^{(2*)}=\left(\varepsilon_2^{(2*)}-\varepsilon_2^{(1*)}\right)$ and $\tilde{\gamma}_{12}^{(2*)}=\gamma_{12}^{(2*)}-\gamma_{12}^{(1*)}$.

To simplify the analysis, two auxiliary functions $w_2(t)=\sum_{n=-\infty}^{\infty}c_n t^n, t\in L_2$ and $w_1(t)=\sum_{n=-\infty}^{\infty}d_n t^n, t\in L_1$ are introduced to satisfy the following relation

$$\begin{aligned} \varphi_1(t)-t\overline{\varphi_1'(t)}-\overline{\psi_1(t)}&=\varphi_2(t)-t\overline{\varphi_2'(t)}-\overline{\psi_2(t)}-2w_2(t) \\ \varphi_0(t)-t\overline{\varphi_0'(t)}-\overline{\psi_0(t)}&=\varphi_1(t)-t\overline{\varphi_1'(t)}-\overline{\psi_1(t)}-2w_1(t) \end{aligned} \tag{6.8}$$

Then, after straightforward algebraic operations, Eq. (6.8) combined with Eqs (6.6b) and (6.6d) leads to

$$\begin{aligned}
&\varphi_2(t)-\varphi_1(t)=w_2(t), \text{ and } \psi_2(t)-\psi_1(t)=-\left(\overline{w_2(t)}+\overline{t}\left(w_2'(t)\right)\right) \text{ for } t\in L_2\\
&\varphi_1(t)-\varphi_0(t)=w_1(t), \text{ and } \psi_1(t)-\psi_0(t)=-\left(\overline{w_1(t)}+\overline{t}\left(w_1'(t)\right)\right) \text{ for } t\in L_1
\end{aligned} \tag{6.9}$$

Therefore, according to Sokhotski-Plemelj Theorem (Muskhelishvili and Radok 1953, Sherman 1959), Cauchy Integral evaluation can be established as follows

$$\begin{aligned}
&\frac{1}{2\pi i}\int_{L_2}\frac{w_2(t)}{t-z}dt+\hat{\varphi}(z)=\begin{cases}\varphi_2(z) & z\in\Omega_2\\ \varphi_1(z) & z\in\Omega_1\end{cases}\\
&\frac{1}{2\pi i}\int_{L_2}\frac{-\left(\overline{w_2(t)}+\overline{t}\left(w_2(t)\right)\right)}{t-z}dt+\hat{\psi}(z)=\begin{cases}\psi_2(z) & z\in\Omega_2\\ \psi_1(z) & z\in\Omega_1\end{cases}\\
&\frac{1}{2\pi i}\int_{L_1}\frac{w_1(t)}{t-z}dt+\tilde{\varphi}(z)=\begin{cases}\varphi_1(z) & z\in\Omega_1\\ \varphi_0(z) & z\in\Omega_0\end{cases}\\
&\frac{1}{2\pi i}\int_{L_1}\frac{-\left(\overline{w_1(t)}+\overline{t}\left(w_1(t)\right)\right)}{t-z}dt+\tilde{\psi}(z)=\begin{cases}\psi_1(z) & z\in\Omega_1\\ \psi_0(z) & z\in\Omega_0\end{cases}
\end{aligned} \tag{6.10}$$

where the holomorphic functions $\hat{\varphi}(z)$, $\hat{\psi}(z)$, $\tilde{\varphi}(z)$ and $\tilde{\psi}(z)$ in the corresponding domains could be expressed uniquely by their Laurent Series: $\hat{\varphi}(z)=\sum_{n=0}^{+\infty}a_n z^n$, $\hat{\psi}(z)=\sum_{n=0}^{+\infty}b_n z^n$, $\tilde{\varphi}(z)=\sum_{n=-\infty}^{+\infty}p_n z^n$ and $\tilde{\psi}(z)=\sum_{n=-\infty}^{+\infty}q_n z^n$. Based on the evaluation of the Cauchy Integrals expressed in Eq. (6.10), the complex potentials can be expressed as:

$$\varphi_2(z)=\sum_{n=0}^{\infty}c_n z^n+\hat{\varphi}(z) \tag{6.11}$$

$$\varphi_1(z) = -\sum_{n=-\infty}^{-1} c_n z^n + \hat{\varphi}(z) \tag{6.12}$$

$$\psi_2(z) = -\left(\sum_{n=-\infty}^{0} r_2^{2n} \overline{c}_n z^{-n} + \sum_{n=2}^{\infty} n r_2^2 c_n z^{n-2} \right) + \hat{\psi}(z) \tag{6.13}$$

$$\psi_1(z) = \left(\sum_{n=1}^{+\infty} r_2^{2n} \overline{c}_n z^{-n} + \sum_{n=-\infty}^{1} n r_2^2 c_n z^{n-2} \right) + \hat{\psi}(z) \tag{6.14}$$

$$\varphi_1(z) = \sum_{n=0}^{\infty} d_n z^n + \tilde{\varphi}(z) \tag{6.15}$$

$$\varphi_0(z) = -\sum_{n=-\infty}^{-1} d_n z^n + \tilde{\varphi}(z) \tag{6.16}$$

$$\psi_1(z) = -\left(\sum_{n=-\infty}^{0} r_1^{2n} \overline{d}_n z^{-n} + \sum_{n=2}^{\infty} n r_1^2 d_n z^{n-2} \right) + \tilde{\psi}(z) \tag{6.17}$$

$$\psi_0(z) = \left(\sum_{n=1}^{+\infty} r_1^{2n} \overline{d}_n z^{-n} + \sum_{n=-\infty}^{1} n r_1^2 d_n z^{n-2} \right) + \tilde{\psi}(z) \tag{6.18}$$

It is worth mentioning here that Eq. (6.12) must be identical to Eq. (6.15), as well as Eq. (6.14) identical to Eq. (6.17), although expressed in different forms.

Substituting Equations (6.11) to (6.14) as well as Eq. (6.16) and Eq. (6.18) into the Eqs. (6.5), (6.6a) to (6.6e) and (6.7), the following equations could be obtained:

$$\Gamma_2\left(\kappa_2\left(\sum_{n=0}^{\infty}c_n r_2^n\,\mathrm{e}^{in\theta}\right)-\left(\sum_{n=0}^{\infty}n\overline{c}_n r_2^n\,\mathrm{e}^{-i(n-2)\theta}\right)+\left(\sum_{n=-\infty}^{0}r_2^n c_n\,\mathrm{e}^{in\theta}+\sum_{n=2}^{\infty}n\overline{c}_n r_2^n\,\mathrm{e}^{-i(n-2)\theta}\right)\right)$$

$$+\Gamma_2\left(\kappa_2\sum_{n=0}^{+\infty}a_n r_2^n\,\mathrm{e}^{in\theta}-\left(\sum_{n=0}^{+\infty}n\overline{a}_n r_2^n\,\mathrm{e}^{-i(n-2)\theta}\right)-\left(\sum_{n=0}^{+\infty}\overline{b}_n r_2^n\,\mathrm{e}^{-in\theta}\right)\right)$$

$$-2\mu_1\left(-\frac{r_2\,\mathrm{e}^{i\theta}}{2}\left(\tilde{\varepsilon}_1^{(2*)}+\tilde{\varepsilon}_2^{(2*)}\right)-\frac{r_2\,\mathrm{e}^{-i\theta}}{2}\left(\tilde{\varepsilon}_1^{(2*)}-\tilde{\varepsilon}_2^{(2*)}+i\tilde{\gamma}_{12}^{(2*)}\right)\right) \tag{6.19}$$

$$=\kappa_1\left(-\sum_{n=-\infty}^{-1}c_n r_2^n\,\mathrm{e}^{in\theta}\right)-\left(-\sum_{n=-\infty}^{-1}n\overline{c}_n r_2^n\,\mathrm{e}^{-i(n-2)\theta}\right)-\left(\sum_{n=1}^{+\infty}r_2^n c_n\,\mathrm{e}^{in\theta}+\sum_{n=-\infty}^{1}n\overline{c}_n r_2^n\,\mathrm{e}^{-i(n-2)\theta}\right)$$

$$+\left(\kappa_1\sum_{n=0}^{+\infty}a_n r_2^n\,\mathrm{e}^{in\theta}-\left(\sum_{n=0}^{+\infty}n\overline{a}_n r_2^n\,\mathrm{e}^{-i(n-2)\theta}\right)-\left(\sum_{n=0}^{+\infty}\overline{b}_n r_2^n\,\mathrm{e}^{-in\theta}\right)\right)$$

$$\Gamma_1\left(\kappa_1\left(\sum_{n=0}^{\infty}d_n r_1^n\,\mathrm{e}^{in\theta}\right)-\left(\sum_{n=0}^{\infty}n\overline{d}_n r_1^n\,\mathrm{e}^{-i(n-2)\theta}\right)+\left(\sum_{n=-\infty}^{0}r_2^n d_n\,\mathrm{e}^{in\theta}+\sum_{n=2}^{\infty}n\overline{d}_n r_2^n\,\mathrm{e}^{-i(n-2)\theta}\right)\right)$$

$$+\Gamma_1\left(\kappa_1\sum_{n=-\infty}^{+\infty}p_n r_1^n\,\mathrm{e}^{in\theta}-\left(\sum_{n=-\infty}^{+\infty}n\overline{p}_n r_1^n\,\mathrm{e}^{-i(n-2)\theta}\right)-\left(\sum_{n=-\infty}^{+\infty}\overline{q}_n r_1^n\,\mathrm{e}^{-in\theta}\right)\right)$$

$$-2\mu_0\left(-\frac{r_1\,\mathrm{e}^{i\theta}}{2}\left(\varepsilon_1^{(2*)}+\varepsilon_2^{(2*)}\right)-\frac{r_1\,\mathrm{e}^{-i\theta}}{2}\left(\varepsilon_1^{(2*)}-\varepsilon_2^{(2*)}+i\gamma_{12}^{(2*)}\right)\right) \tag{6.20}$$

$$=\kappa_0\left(-\sum_{n=-\infty}^{-1}d_n r_1^n\,\mathrm{e}^{in\theta}\right)-\left(-\sum_{n=-\infty}^{-1}n\overline{d}_n r_1^n\,\mathrm{e}^{-i(n-2)\theta}\right)-\left(\sum_{n=1}^{+\infty}r_1^n d_n\,\mathrm{e}^{in\theta}+\sum_{n=-\infty}^{1}n\overline{d}_n r_1^n\,\mathrm{e}^{-i(n-2)\theta}\right)$$

$$+\left(\kappa_0\sum_{n=-\infty}^{+\infty}p_n r_1^n\,\mathrm{e}^{in\theta}-\left(\sum_{n=-\infty}^{+\infty}n\overline{p}_n r_1^n\,\mathrm{e}^{-i(n-2)\theta}\right)-\left(\sum_{n=-\infty}^{+\infty}\overline{q}_n r_1^n\,\mathrm{e}^{-in\theta}\right)\right)$$

$$
\begin{aligned}
&\kappa_0\left(-\sum_{n=1}^{+\infty}R^{-n}d_{-n}e^{-in\theta}\right)+\sum_{n=3}^{+\infty}-(n-2)R^{-(n-2)}\overline{d}_{-(n-2)}e^{in\theta}\\
&-\left(\sum_{n=1}^{+\infty}R^{-n}r_1^{2n}d_ne^{in\theta}+\sum_{n=1}^{+\infty}-(n-2)R^{-n}r_1^{2}\overline{d}_{-(n-2)}e^{in\theta}\right)\\
&=-\kappa_0\sum_{n=-\infty}^{+\infty}R^{n}p_ne^{in\theta}+\sum_{n=-\infty}^{+\infty}\left((n+2)R^{n+2}\overline{p}_{n+2}+R^{n}\overline{q}_n\right)e^{-in\theta}\\
&+\mu_0\left(\varepsilon_1^{(0)}+\varepsilon_2^{(0)}-i\gamma_{12}^{(0)}\right)Re^{i\theta}+\mu_0\left(\varepsilon_1^{(0)}-\varepsilon_2^{(0)}+i\gamma_{12}^{(0)}\right)Re^{-i\theta}
\end{aligned}
\tag{6.21}
$$

To guarantee that Eq. (6.12) is identical to Eq. (6.15), as well as Eq. (6.14) identical to Eq. (6.17), the following relations must be enforced:

$$
\begin{aligned}
&-c_n=p_n \quad n\le -1\\
&a_n=d_n+p_n \quad n\ge 0\\
&r_2^{-2n}\overline{c}_{-n}+(n+2)r_2^2c_{n+2}=q_n \quad n\le -1\\
&r_1^{-2n}\overline{d}_{-n}+(n+2)r_1^2d_{n+2}+b_n=q_n \quad n\ge 0
\end{aligned}
\tag{6.22}
$$

According to the linear independency of the basis $e^{in\theta}$, $n=-\infty,\cdots,\infty$, the Eqs.(6.19) to (6.22) together lead to a system of equations of the unknown coefficients. Solving the equations will lead to the conclusion that $a_n=0$ and $b_n=0$, $n=0,\cdots,\infty$; $c_m=0$, $d_m=0$, $p_m=0$ and $q_m=0$, $m=-\infty,\cdots,\infty$, except for some special terms listed below.

Denote $\boldsymbol{\alpha}_1=\{a_3 \quad b_1 \quad c_{-1} \quad c_3 \quad d_{-1} \quad d_3\}^T$ and $\boldsymbol{\alpha}_2=\{a_1 \quad c_1 \quad d_1\}^T$, then we have

$$
\boldsymbol{\alpha}_1=\mathbf{A}_1^{-1}\mathbf{b}_1+\mathbf{A}_2^{-1}\mathbf{b}_2\,;\boldsymbol{\alpha}_2=\mathbf{A}_3^{-1}\mathbf{b}_3+\mathbf{A}_4^{-1}\mathbf{b}_4\,. \tag{6.23}
$$

where

$$\mathbf{A}_1=\begin{bmatrix} -3(\Gamma_2-1)r_2^3 & -(\Gamma_2-1)r_2 & (\Gamma_2+\kappa_1)r_2^{-1} & 0 & 0 & 0 \\ -3(\Gamma_1-1)r_1^3 & -(\Gamma_1-1)r_1 & -(\Gamma_1\kappa_1-\kappa_0)r_1^{-1} & 0 & (1+\kappa_0)r_1^{-1} & 0 \\ 3 & R^{-2} & \kappa_0 R^{-4} & 0 & R^{-2}r_1^{-2}+\kappa_0 R^{-4} & 3\left(R^{-2}r_1^2-1\right) \\ \Gamma_2\kappa_2-\kappa_1 & 0 & 0 & 1+\Gamma_2\kappa_2 & 0 & 0 \\ \Gamma_1\kappa_1-\kappa_0 & 0 & (\Gamma_1-1)\left(r_1^{-6}r_2^2-r_1^{-4}\right) & -(\Gamma_1-1)r_1^{-6}r_2^6 & 0 & 1+\kappa_0 \\ \kappa_0 & 0 & R^{-6}r_2^2-R^{-4} & -R^{-6}r_2^6 & R^{-6}r_1^2-R^{-4} & -\left(\kappa_0+R^{-6}r_1^6\right) \end{bmatrix}$$

$$\mathbf{A}_2=\begin{bmatrix} 3(\Gamma_2-1)r_2^3 & (\Gamma_2-1)r_2 & (\Gamma_2+\kappa_1)r_2^{-1} & 0 & 0 & 0 \\ 3(\Gamma_1-1)r_1^3 & (\Gamma_1-1)r_1 & -(\Gamma_1\kappa_1-\kappa_0)r_1^{-1} & 0 & (1+\kappa_0)r_1^{-1} & 0 \\ -3 & -R^{-2} & \kappa_0 R^{-4} & 0 & R^{-2}r_1^{-2}+\kappa_0 R^{-4} & -3\left(R^{-2}r_1^2-1\right) \\ \Gamma_2\kappa_2-\kappa_1 & 0 & 0 & 1+\Gamma_2\kappa_2 & 0 & 0 \\ \Gamma_1\kappa_1-\kappa_0 & 0 & -(\Gamma_1-1)\left(r_1^{-6}r_2^2-r_1^{-4}\right) & -(\Gamma_1-1)r_1^{-6}r_2^6 & 0 & 1+\kappa_0 \\ \kappa_0 & 0 & -\left(R^{-6}r_2^2-R^{-4}\right) & -R^{-6}r_2^6 & -\left(R^{-6}r_1^2-R^{-4}\right) & -\left(\kappa_0+R^{-6}r_1^6\right) \end{bmatrix} \tag{6.24}$$

$$\mathbf{A}_3=\begin{bmatrix} \kappa_1-1-\Gamma_2(\kappa_2-1) & -\left((\Gamma_2\kappa_2+1)-(\Gamma_2-1)\right) & 0 \\ \kappa_0-1-\Gamma_1(\kappa_1-1) & -2(1-\Gamma_1)r_1^{-2}r_2^2 & -(1+\kappa_0) \\ (-\kappa_0+1) & 2R^{-2}r_2^2 & \kappa_0-\left(1-2R^{-2}r_1^2\right) \end{bmatrix}$$

$$\mathbf{A}_4=\begin{bmatrix} \kappa_1+1-\Gamma_2(\kappa_2+1) & -\left((\Gamma_2\kappa_2+1)+(\Gamma_2-1)\right) & 0 \\ \kappa_0+1-\Gamma_1(\kappa_1+1) & 0 & -(1+\kappa_0) \\ -(\kappa_0+1) & 0 & \kappa_0+1 \end{bmatrix} \tag{6.25}$$

and

$$\mathbf{b}_1=\left\{-\mu_1 r_2\left(\tilde{\varepsilon}_1^{(2*)}-\tilde{\varepsilon}_2^{(2*)}\right) \quad -\mu_0 r_1\left(\varepsilon_1^{(1*)}-\varepsilon_2^{(1*)}\right) \quad -\mu_0\left(\varepsilon_1^{(0)}-\varepsilon_2^{(0)}\right)R^{-2} \quad 0 \quad 0 \quad 0\right\}^T$$

$$\mathbf{b}_2=\left\{-\mu_1 r_2\left(i\tilde{\gamma}_{12}^{(2*)}\right) \quad -\mu_0 r_1\left(i\gamma_{12}^{(1*)}\right) \quad -\mu_0\left(i\gamma_{12}^{(0)}\right)R^{-2} \quad 0 \quad 0 \quad 0\right\}^T \tag{6.26}$$

$$\mathbf{b}_3=\left\{\mu_1\left(\tilde{\varepsilon}_1^{(2*)}+\tilde{\varepsilon}_2^{(2*)}\right) \quad \mu_0\left(\varepsilon_1^{(1*)}+\varepsilon_2^{(1*)}\right) \quad -\mu_0\left(\varepsilon_1^{(0)}+\varepsilon_2^{(0)}\right)\right\}^T$$

$$\mathbf{b}_4=\left\{0 \quad 0 \quad \mu_0\left(i\gamma_{12}^{(0)}\right)\right\}^T$$

Besides, the following equations could be collected to determine the other non-zero coefficients in the formulation

$$
\begin{aligned}
p_{-1} &= -c_{-1} \\
p_1 &= a_1 - d_1 \\
p_3 &= a_3 - d_3 \\
q_{-1} &= r_2^2 \overline{c_1} + r_2^2 c_1 \\
q_{-3} &= r_2^6 \overline{c_3} - r_2^2 c_{-1} \\
q_1 &= r_1^{-2} \overline{d}_{-1} + 3 r_1^2 d_3 + b_1
\end{aligned}
\tag{6.27}
$$

and

$$
\begin{aligned}
&\kappa_1 a_0 - \overline{b_0} = 0 \\
&\kappa_2 a_0 - \overline{b_0} + (\kappa_2 + 1) c_0 = 0 \\
&-\kappa_0 a_0 + \overline{b_0} + (\kappa_0 + 1) d_0 = 0
\end{aligned}
\tag{6.28}
$$

Consequently, the complex potentials have been obtained as follows

$$
\begin{aligned}
\varphi_2(z) &= (c_1 + a_1) z + (c_3 + a_3) z^3 \\
\psi_2(z) &= -\left(r_2^{-2}\overline{c}_{-1} + 3r_2^{\,2}c_3 - b_1\right) z \\
\varphi_1(z) &= -c_{-1} z^{-1} + a_1 z + a_3 z^3 \\
\psi_1(z) &= r_2^2\left(\overline{c}_1 + c_1\right) z^{-1} + \left(r_2^6\overline{c}_3 - r_2^2 c_{-1}\right) z^{-3} + b_1 z \\
\varphi_0(z) &= \left(-d_{-1} + p_{-1}\right) z^{-1} + p_1 z + p_3 z^3 \\
\psi_0(z) &= \left(r_1^2\left(\overline{d}_1 + d_1\right) + q_{-1}\right) z^{-1} + \left(r_1^6\overline{d}_3 - r_1^2 d_{-1} + q_{-3}\right) z^{-3} + q_1 z
\end{aligned}
\tag{6.29}
$$

It is worth mentioning here that the coefficients corresponding to the constant terms in the potentials disappear in Eq. (6.29) because in fact they will cancel each other when the obtained complex potentials are combined together to give the analytical solution for the displacement field according to Eq. (6.28). In addition to the complex potentials obtained for the deformation happened at the third step, the initial stress-free displacement at the second step should be add to the final expression of the displacement field. It means

$$
u + iv = \begin{cases}
\dfrac{1}{2\mu_2}\left(\kappa_2\varphi_2 - z\overline{\varphi_2'} - \overline{\psi_2}\right) + u^{(2*)} + iv^{(2*)} & z \in \Omega_2 \\
\dfrac{1}{2\mu_1}\left(\kappa_1\varphi_1 - z\overline{\varphi_1'} - \overline{\psi_1}\right) + u^{(1*)} + iv^{(1*)} & z \in \Omega_1 \\
\dfrac{1}{2\mu_0}\left(\kappa_0\varphi_0 - z\overline{\varphi_0'} - \overline{\psi_0}\right) & z \in \Omega_0
\end{cases}
\tag{6.30}
$$

Subsequently, the strain fields could be determined after the straight-forward gradient operation on the displacement fields given in Eq. (6.30).

The obtained solution is a general expression for the elastic fields in the RVE with eigenstrains described in Eq. (6.1) under the prescribed boundary condition given in Eq. (6.2). Therefore, if valid, it must be able to reproduce solutions available for some special cases, e.g., the RVEs with unbounded matrix with similar eigenstrains and under same boundary conditions.

In addition, it should be able to predict the elastic response of the finite RVEs induced by the eignestrains under given conditions, which could be simulated numerically.

6.3 COMPARISON WITH THE ANALYTICAL SOLUTIONS AVAILABLE FOR INFINITE DOMAINS

Several analytical solutions are available for 3-phase inhomogeneous inclusions in unbounded domains. Luo and Weng (1989) solved the 3-phase inhomogeneous inclusion problem in an infinite domain via the stress function formulation proposed by Christenson and Lo (1979) with a uniform eigenstrain in the inclusion. Recently, Markenscoff and Dundurs (2014) obtained the solution of the elastic fields disturbed by an annulus (or a ring) inhomogeneity embedded in the infinite domain. In their work, the uniform eigenstrain happens in the interfacial zone. It is shown here that these solutions could be reproduced from the general solution obtained in this study.

First, only dilatational eigenstrain in the inclusion is considered, i.e. the non-zero terms are $\varepsilon_1^{(2*)} = \varepsilon_2^{(2*)} = \varepsilon^*$. When $R \to +\infty$ and $\varepsilon_{ij}^0 = 0$, the solution of the displacement fields inside the RVE could be obtained according to Eqs. (6.23) - (6.26), Eq. (6.29) and (6.30), which are listed as:

$$u+iv=\begin{cases}\dfrac{\dfrac{2}{\kappa_2-1}\left[\left(\dfrac{2}{\kappa_1-1}+\Gamma_1\right)-\dfrac{r_2^2}{r_1^2}\left(\Gamma_1-1\right)\right]z}{\left[\left(\dfrac{2}{\kappa_2-1}+\Gamma_2\right)\left(\dfrac{2}{\kappa_1-1}+\Gamma_1\right)-\dfrac{r_2^2}{r_1^2}\left(\dfrac{2}{\kappa_2-1}-\dfrac{2\Gamma_2}{\kappa_1-1}\right)\left(\Gamma_1-1\right)\right]}\varepsilon^* & z\in\Omega_2\\ \dfrac{-\dfrac{r_2^2}{r_1^2}\dfrac{2}{\kappa_2-1}\left(\Gamma_1-1\right)z+\dfrac{r_2^2}{r_1^2}\dfrac{2}{\kappa_2-1}\left(\dfrac{2}{\kappa_1-1}+\Gamma_1\right)\dfrac{r_1^2}{\overline{z}}}{\left[\left(\dfrac{2}{\kappa_2-1}+\Gamma_2\right)\left(\dfrac{2}{\kappa_1-1}+\Gamma_1\right)-\dfrac{r_2^2}{r_1^2}\left(\dfrac{2}{\kappa_2-1}-\dfrac{2\Gamma_2}{\kappa_1-1}\right)\left(\Gamma_1-1\right)\right]}\varepsilon^* & z\in\Omega_1\\ \dfrac{\dfrac{2}{\kappa_2-1}\left(\dfrac{2}{\kappa_1-1}+1\right)\dfrac{r_2^2}{\overline{z}}}{\left[\left(\dfrac{2}{\kappa_2-1}+\Gamma_2\right)\left(\dfrac{2}{\kappa_1-1}+\Gamma_1\right)-\dfrac{r_2^2}{r_1^2}\left(\dfrac{2}{\kappa_2-1}-\dfrac{2\Gamma_2}{\kappa_1-1}\right)\left(\Gamma_1-1\right)\right]}\varepsilon^* & z\in\Omega_0\end{cases}\tag{6.31}$$

This is identical to the solution obtained by Luo and Weng (1989) in the polar coordinates based on the observation that

$$u+iv=\left(u_r+iu_\theta\right)\frac{z}{r}\tag{6.32}$$

Here r and θ stand for the polar coordinates as well as u_r and u_θ the displacements in the corresponding directions.

Similarly, consider the dilatational eigenstrain in the interfacial zone of the RVE with unbounded matrix, which means $\varepsilon_{ij}^{(2*)}=0$ and $\varepsilon_{ij}^{(1*)}=0$ except for $\varepsilon_1^{(1*)}=\varepsilon_2^{(1*)}=e^*$. When $R\to+\infty$, $\varepsilon_{ij}^{(0)}=0$, the solution of the displacement fields inside the RVE could also be obtained as

$$u+iv=\begin{cases}\dfrac{2\Gamma_2\left(1-\Gamma_1\right)\left(\dfrac{r_2^2}{r_1^2}-1\right)z}{\left(\dfrac{\kappa_1-1}{\kappa_2-1}-\Gamma_2\right)\left(-2\left(1-\Gamma_1\right)\dfrac{r_2^2}{r_1^2}\right)+\left(\Gamma_2+\dfrac{2}{\kappa_2-1}\right)\left(-2-\Gamma_1\left(\kappa_1-1\right)\right)}e^* & z\in\Omega_2 \\ \dfrac{\left(\Gamma_1\Gamma_2\left(\kappa_2-1\right)+2\Gamma_1+2\left(1-\Gamma_1\right)\dfrac{r_2^2}{r_1^2}\right)z+\left(\Gamma_1\Gamma_2\dfrac{\kappa_2-1}{\kappa_1-1}+\dfrac{2}{\kappa_1-1}\right)\dfrac{2r_2^2}{\overline{z}}}{\left(1-\Gamma_2\dfrac{\kappa_2-1}{\kappa_1-1}\right)\left(-2\left(1-\Gamma_1\right)\dfrac{r_2^2}{r_1^2}\right)+\left(\Gamma_2\left(\kappa_2-1\right)+2\right)\left(-\dfrac{2}{\kappa_1-1}-\Gamma_1\right)}e^* & z\in\Omega_1 \\ \dfrac{-2\left(\dfrac{2}{\kappa_2-1}+\Gamma_2\right)\left(r_1^2-r_2^2\right)\dfrac{1}{\overline{z}}}{\left(\dfrac{\kappa_1-1}{\kappa_2-1}-\Gamma_2\right)\left(-2\left(1-\Gamma_1\right)\dfrac{r_2^2}{r_1^2}\right)+\left(\Gamma_2+\dfrac{2}{\kappa_2-1}\right)\left(-2-\Gamma_1\left(\kappa_1-1\right)\right)}e^* & z\in\Omega_0\end{cases} \tag{6.33}$$

It is identical to the solution obtained by Markenscoff and Dundurs (2014) once same elastic properties are assigned to inclusion and matrix, which means that $\Gamma_1\Gamma_2=1$.

When the deviatoric eigenstrains are considered in the inclusion or the interfacial zone and the boundary conditions are prescribed as $\varepsilon_{ij}^{(0)}=0$ at infinity, it is difficult to conduct the direct comparison because tedious calculation is needed to find out the inverse matrices in the theoretical solutions given by Luo and Weng (1989) and Markenscoff and Dundurs (2014). Alternatively, the displacements at 3 arbitrarily selected points are compared when the material properties of the constituent phases are specified.

To compare the obtained solution via complex potential method (denoted as CP) with the one via stress function (denoted as SF) formulation by Luo and Weng (1989), the deviatoric eigenstrain in the inclusion is selected as as $\varepsilon_1^{(2*)}=-\varepsilon_1^{(2*)}=0.02$. The geometry of the concentric RVE is characterized by $r_2=0.6\,\mathrm{m}$, $r_1=0.7\,\mathrm{m}$ and $R\to+\infty$. The parameters of material properties are assigned in four different groups sharing the common parameters of $E_2=100\,\mathrm{GPa}$,

$\nu_2 = 0.2$ for inclusion, $\nu_1 = 0.15$ for the interfacial zone and $\nu_0 = 0.2$ for the unbounded matrix. The results for the displacements at three arbitrary selected points are listed in Table 6.1.

Table 6.1. The comparison of displacements induced by deviatoric eigenstrain in the inclusion only.

Groups	**SF**	**CP**	**SF**	**CP**	**SF**	**CP**
Location	(0.2500, 0.4330)		(0.5259, 0.3821)		(0.2225, 0.9749)	
E_1/E_2=10	0.002917	0.002917	0.005748	0.005748	-0.0002158	-0.0002158
E_0/E_2=0.5	-0.006516	-0.006516	-0.002707	-0.002707	-0.006716	-0.006716
Location	(-0.2000, 0.3464)		(-0.1947, 0.5992)		(-0.8105, 1.0164)	
E_1/E_2=3	-0.003668	-0.003668	-0.001470	-0.001470	-0.001137	-0.001137
E_0/E_2=0.01	-0.007292	-0.007292	-0.01165	-0.01165	-0.003096	-0.003096
Location	(-0.1500, -0.2598)		(-0.5340, -0.3879)		(-1.3515, -0.6508)	
E_1/E_2=0.5	-0.001734	-0.001734	-0.004595	-0.004595	-0.002301	-0.002301
E_0/E_2=2	0.002923	0.002923	0.003187	0.003187	0.00008168	0.00008168
Location	(0.1000, -0.1732)		(0.2101, -0.6467)		(0.3783, -1.6574)	
E_1/E_2=0.02	0.001762	0.001762	0.0005255	0.0005255	-0.00000921	-0.00000921
E_0/E_2=5	0.003034	0.003034	0.002348	0.002348	0.0002644	0.0002644

Similarly, the CP solution is compared with the SF one by Markenscoff and Dunders (2014). Now the deviatoric eigenstrain in the interfacial zone is chosen as $\varepsilon_1^{(1*)} = -\varepsilon_1^{(1*)} = 0.03$. A different configuration is selected for the unbounded RVE, characterized by $r_2 = 0.65\,\mathrm{m}$, $r_1 = 0.75\,\mathrm{m}$ and $R \to +\infty$. The inclusion and the unbounded matrix are assigned with the same

material properties of $E_2 = 50\,\text{GPa}$ and $\nu_2 = 0.2$. For the interfacial zone, $\nu_1 = 0.15$ while E_1 has four different values. The results for the displacements at three arbitrarily selected points are listed in Table 6.2.

Table 6.2. The comparison of displacements induced by deviatoric eigenstrains in the interfacial zone only.

Groups	**S.F.**	**C.P.**	**S.F.**	**C.P.**	**S.F.**	**C.P.**
Location	(0.3000, 0.5196)		(0.5340, 0.3879)		(0.2448, 1.0724)	
E_1/E_2=2	0.003751	0.003751	0.006737	0.006737	0.0001470	0.0001470
	-0.006921	-0.006921	-0.004593	-0.004593	-0.006330	-0.006330
Location	(-0.2500, 0.4330)		(-0.2101, 0.6467)		(-1.1713, 0.5640)	
E_1/E_2=1.5	-0.003325	-0.003325	-0.002211	-0.002211	-0.004346	-0.004346
	-0.005901	-0.005901	-0.008282	-0.008282	-0.0004288	-0.0004288
Location	(-0.2000, -0.3464)		(-0.5744, -0.4173)		(-1.3515, -0.6508)	
E_1/E_2=0.5	-0.002865	-0.002865	-0.006526	-0.006526	-0.003720	-0.003720
	0.004877	0.004877	0.004448	0.004448	0.0003047	0.0003047
Location	(0.1500, -0.2598)		(0.2256, -0.6943)		(0.9976, -1.2509)	
E_1/E_2=0.4	0.002140	0.002140	0.002004	0.002004	0.001004	0.001004
	0.003662	0.003662	0.007721	0.007721	0.002165	0.002165

Based on the comparison shown in Table 6.1 and 6.2, the analytical solutions obtained in this study is able to reproduce the results of Luo and Weng (1989) as well as Markenscoff and Dundurs (2014) for unbounded RVEs.

6.4 COMPARISON WITH FEM RESULTS FOR FINITE DOMAINS

For finite domain, to the authors' best knowledge, no general solutions are available in the current literature. Therefore, the obtained analytical solution has to be compared with FEM results for finite concentric RVEs. In the comparison, arbitrary values are assigned to material properties and volume fractions, and firm agreements are always achieved. Here two plane strain examples of very different RVEs are illustrated; see Figure 6.2 and Figure 6.3.

In the first example, the Young's Modulus and Poisson's ratio of each phase are assigned as $E_2 = 100\ \text{GPa}$ and $\nu_2 = 0.2$ for the inclusion, $E_1 = 5\ \text{GPa}$ and $\nu_1 = 0.15$ for the interfacial zone, and $E_0 = 30\ \text{GPa}$ and $\nu_0 = 0.25$ for the matrix. The configuration of the RVE is set as $r_2 = 0.6\ \text{m}$, $r_1 = 0.7\ \text{m}$ and $R = 1\ \text{m}$. The eigenstrains are selected as $\left[\varepsilon_1^{(2*)} \quad \varepsilon_2^{(2*)} \quad \gamma_{12}^{(2*)}\right]^T = \left[0.01 \quad 0.02 \quad 0.03\right]^T$ for the inclusion and $\left[\varepsilon_1^{(1*)} \quad \varepsilon_2^{(1*)} \quad \gamma_{12}^{(1*)}\right]^T = \left[-0.02 \quad -0.04 \quad -0.05\right]^T$ for the interfacial zone. The boundary condition on the exterior matrix is given as $\left[\varepsilon_1^{(0)} \quad \varepsilon_2^{(0)} \quad \gamma_{12}^{(0)}\right]^T = \left[-0.01 \quad 0.01 \quad -0.05\right]^T$.

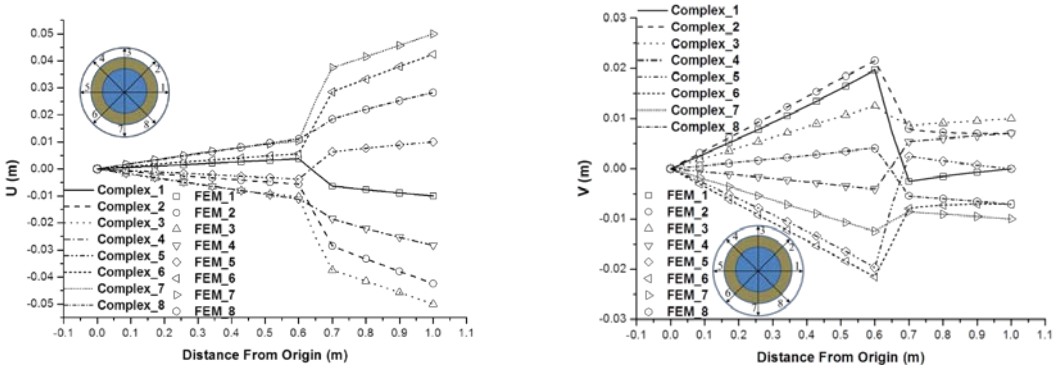

Figure 6.2. Comparison of the analytical solutions of displacement field based on complex potential Method (lines) with FEM (symbols) for a three-phase concentric inhomogeneous RVE with a weak interfacial zone

In the second example, a stronger interfacial zone is selected compared to the inclusion and the matrix. Similarly, the Young's Modulus and Poisson's ratio for each phase are assigned as $E_2 = 10\,\text{GPa}$ and $\nu_2 = 0.25$, $E_1 = 50\,\text{GPa}$ and $\nu_1 = 0.3$, and $E_0 = 25\,\text{GPa}$ and $\nu_0 = 0.2$. A different configuration is chosen for the finite RVE characterized by $r_2 = 0.5\,\text{m}$, $r_1 = 0.8\,\text{m}$ and $R = 1\,\text{m}$. The eigenstrains are selected as $\left[\varepsilon_1^{(2*)} \quad \varepsilon_2^{(2*)} \quad \gamma_{12}^{(2*)}\right]^T = \left[-0.016 \quad -0.034 \quad 0.029\right]^T$ and $\left[\varepsilon_1^{(1*)} \quad \varepsilon_2^{(1*)} \quad \gamma_{12}^{(1*)}\right]^T = \left[-0.019 \quad 0.030 \quad -0.033\right]^T$. The boundary condition on the exterior matrix is given as $\left[\varepsilon_1^{(0)} \quad \varepsilon_2^{(0)} \quad \gamma_{12}^{(0)}\right]^T = \left[0.010 \quad -0.024 \quad 0.015\right]^T$.

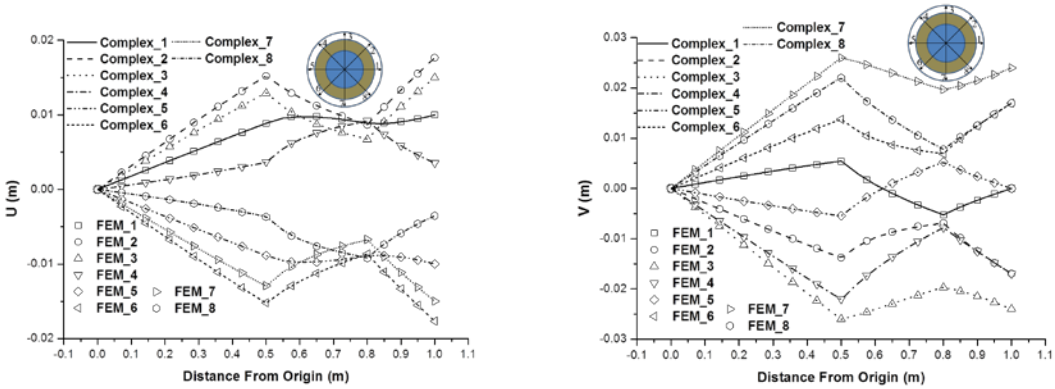

Figure 6.3. Comparison of the analytical solutions of displacement field based on complex potential Method (lines) with FEM (symbols) for a three-phase concentric inhomogeneous RVE with a strong interfacial zone

The displacement fields obtained from FEM utilizing ABAQUS are compared with the analytical solutions. As shown in Figure 6.2 and Figure 6.3, firm agreements are achieved between the analytical solution and the numerical simulation along eight main directions in each RVE. The disturbance induced by the eigenstrains and inhomogeneity is characterized by the

slope change of the displacement curve when it enters a different phase in the RVE despite the uniform boundary conditions imposed on the exterior matrix. The comparison demonstrates that the analytical solution via complex potential method can accurately predict the elastic fields in the 3-phase inhomogeneous concentric RVE in a finite domain with independent eigenstrains in the interfacial zone and inclusion and arbitrary uniform boundary condition on the exterior matrix.

6.5 DISCUSSION AND CONCLUSION

In this study, analytical solutions of elastic fields for 3-phase inhomogeneous inclusion problem are obtained for concentric 2D finite RVEs. Without conducting dilatational and deviatoric decomposition based on the Airy stress function, a different but more general approach utilizing complex potential method is employed to construct potential functions satisfying the equilibrium and compatibility along the interfaces between the constituent phases. The closed-form expression of the displacement field is shown to accurately predict the disturbance induced by independent eigenstrains in the inclusion and its surrounding interfacial zone as well as the material mismatch of different phases in a finite RVE.

In addition, the mathematical formulation of complex potentials in this study is purely based upon equilibrium and compatibility, which leads to a system of equations to identify the coefficients of the complex potentials. Therefore, the current study provides an analytical way to systematically tackle multi-phase REVs and may be extended to eccentric configurations and non-uniform eigenstrains.

7.0 APPLICATION OF THE ANALYTICAL INCLUSION SOLUTION IN NUMERICAL SIMULATION

In this chapter, an upgraded patch recovery method of finite element simulation is proposed as a direct application of the analytical solution obtained in previous research. This numerical methodology is developed based on the essential ideas of Hughes' variational multiscale formulation (Hughes et al 1995, 1998) with Zienkiewicz-Zhu feedback mechanism (Zienkiewicz and Zhu 1992a, 1992b) and Li's error homogenization formulation (Li et al 2005, Wang et al 2005) via eigenstrain in finite space. The accurate solution of an arbitrary homogeneous inclusion inside a finite domain obtained in this research is mounted onto this computational scheme to achieve a great improvement compared to the pioneer work of Li et al. Moreover, the mesh shape sensitive problem of Li's method has been overcome. In general, this upgraded method automatically homogenizes the discretization errors of FEM and improves the computational results without increasing the calculation burden significantly. The details of this application is demonstrated in the following sections.

7.1 BACKGROUND AND MOTIVATION

Since the beginning of the FEM era, the discretization error in calculation has been always a significant concern, especially for the derivative of the physical fields. This error is intrinsically

embedded in the simulations. The digital model manageable by the computer is utilized to replace the continuum model of mechanical behaviors, and therefore some information possessed by the partial differential equations describing the phenomena itself is in general ignored. To mitigate the errors, guided by the error estimation methodology, h-p simulation can always be employed which either decreases the mesh size or increases the order of approximation. This can cause a significant increase of computational cost and sometimes produce solutions with unexpected fluctuation in dealing with some particular problems, e.g. Runge Problem. A computational method with higher accuracy with acceptable computational cost is always in high demand, even though the improvement of computational hardware has been significant.

The variational multiscale simulation method proposed by Hughes et al (1995, 1998) gives an inspirational thought about how to keep the coarse scale mesh and remedy the solution by analytical analysis of the discretization error. The basic logic of this method is to explore the possibility of solving the discretization error analytically and consider its contribution within the coarse scale solution by revising the coefficient matrices to give a much better coarse scale solution.

However, if the error is not estimated in a systematic manner, there is no solid fundament to develop the error recovery method. In order to deal with this topic, many error estimation method has been developed (Demkowicz et al 1985, Szabo 1986, Zienkiewicz and Zhu 1987, 1992a, 1992b) among which the Zienkiewicz-Zhu feedback mechanism is a very feasible one for error recovery. In this estimation, Zienkiewicz and Zhu proposed a higher order derivative field based on the interpolation in the neighborhood of the nodes of interest, despite of the fact that in FEM simulation the derivatives of the fields have much lower accuracy. Although the exact solution is not obtained, the interpolated derivative fields can serve as an alternative solution to

give a quite good approximation of the exact one. The accuracy of this approximation is improved by enforcing the minimum difference between the interpolated derivate fields and the FEM solution at the Gaussian points, where the FEM solution of derivatives are with higher order accuracy.

By employing Zienkiewicz and Zhu's feedback mechanism, Li et al (2005) and Wang et al (2005) proposed an error recovery method treating the error as an eigenstrain inside the inclusion which is in fact the element of interest. Then the effect of the error in each element on the area containing this element is equivalently treated as the disturbance in the RVE by the eigenstrain inside the inclusion. The RVE size in this method is selected in an artificial way, and in the discussion part, Li proposed a certain value to achieve a good accuracy. The accuracy of this method is demonstrated in some problems for traditional FEM where significant improvement can be seen. For example, the locking phenomena is tackled by this improved simulation scheme.

However, this recovery method proposed by Li et al has a rather serious intrinsic defect. In this method, the inclusion has to be a circle circumscribed this element no matter what shape the element exhibits. This is due to the fact that when the method was proposed, there was no analytical solution available for the finite RVE containing a polygonal inclusion which is able to represent the FEM mesh. Li et al has to seek help from the concentric circle-circle RVE. In that case, if two elements of significantly different shapes share the same circumcircle, the errors solved in fine scale are expected to be the same, which is a contradiction to the common sense. In addition, the method shows more severe problem when dealing with the elements near the boundary. This is due to the fact that the assumption of concentric configuration differs substantially from the real geometrical conditions.

Luckily the solution obtained in this research for an arbitrary shaped inclusion can be used to remedy this intrinsic defect in this novel and effective element error recovery method. This solution can physically consider the effect of shape and position of the inclusion on the disturbed fields inside the RVE, and therefore give a more reliable solution for the elements with varies shapes and positions. The details of this method is discussed in the following sections.

7.2 THEORETICAL FORMULATION OF THE ERROR HOMOGENIZATION SCHEME

To make this discussion self-contained, some fundamental details of Hughes (1998), Zienkwicz and Zhu (1992) and Li et al (2004, 2005) and Wang et al (2005b) are also explained below. Considering partial differential equations describing the Continuum mechanics problem in 2D space,

$$\sigma_{ji,j} + b_i = 0 \quad \forall \mathbf{x} \in \Omega \tag{7.1}$$

$$u_i = u_i^0 \quad \forall \mathbf{x} \in \Gamma_u \tag{7.2}$$

$$\sigma_{ij} n_j = t_i^0 \quad \forall \mathbf{x} \in \Gamma_t \tag{7.3}$$

where σ_{ij} is the Cauchy stress tensor, b_i is the body force, u_i is the displacement component, n_j is the outward-normal of the boundary, and u_i^0 and t_i^0 stand for the prescribed displacement and traction vector correspondingly. According to the generalized Hooke's Law, the stress tensor will be linked to the infinitesimal strain tensor as:

$$\sigma_{ij} = C_{ijkl} \varepsilon_{kl} \tag{7.4}$$

where C_{ijkl} is the elastic tensor. The compatibility of the continuum requires that

$$\varepsilon_{ij} = \frac{1}{2}\left(u_{i,j} + u_{j,i}\right) \tag{7.5}$$

Here it is necessary to introduce the trial and test function spaces

$$J = \left\{ \mathbf{u}(\mathbf{x}) \middle| \mathbf{u}(\mathbf{x}) \in \left[H^1(\Omega) \right]^2, \mathbf{u} = \mathbf{u}^0, \forall\, \mathbf{x} \in \Gamma_u \right\} \tag{7.6}$$

$$V = \left\{ \mathbf{w}(\mathbf{x}) \middle| \mathbf{w}(\mathbf{x}) \in \left[H^1(\Omega) \right]^2, \mathbf{u} = \mathbf{0}, \forall\, \mathbf{x} \in \Gamma_u \right\} \tag{7.7}$$

where $\left[H^1(\Omega) \right]^2$ is a two dimensional Hilbert Space. Accordingly, the variational formulation for this boundary-value problem is to find $\mathbf{u} \in J$ such that

$$a(\mathbf{w}, \mathbf{u}) = (\mathbf{w}, \mathbf{b})_\Omega + \left(\mathbf{w}, \mathbf{t}^0\right)_{\Gamma_t} \qquad \forall \mathbf{w} \in V \tag{7.8}$$

where

$$a(\mathbf{w}, \mathbf{u}) := \int_\Omega (\nabla \otimes \mathbf{w}) : \mathbf{C} : (\nabla \otimes \mathbf{u})\, d\Omega \tag{7.9}$$

$$(\mathbf{w}, \mathbf{b})_\Omega := \int_\Omega \mathbf{w} \cdot \mathbf{b}\, d\Omega \tag{7.10}$$

$$(\mathbf{w}, \mathbf{t})_{\Gamma_t} := \int_{\Gamma_t} \mathbf{w} \cdot \mathbf{t}\, dS \tag{7.11}$$

7.2.1 Multiscale formulation.

The variational multiscale method is based on the fact that there exist a decomposition of the real solution as follows

$$\mathbf{u} = \bar{\mathbf{u}} + \mathbf{u}' \tag{7.12}$$

where $\bar{\mathbf{u}}$ represent the coarse scale solution and it is expected that the fine scale solution $\mathbf{u}'$ is solved from the analytical analysis of the original problem and eliminated from the problem of $\bar{\mathbf{u}}$. Correspondingly, the test function in the FEM scheme can also be expressed in a similar decomposition as

$$\mathbf{w} = \bar{\mathbf{w}} + \mathbf{w}' \tag{7.13}$$

According to the assumptions of Hughes et al (1996) that the fine scale solution and test function all disappear on the boundary where displacement fields are prescribed, the weak form of Eq (7.8) can be expressed at different scales as follows

$$a\left(\bar{\mathbf{w}}, \bar{\mathbf{u}}\right) + a\left(\bar{\mathbf{w}}, \mathbf{u}'\right) = \left(\bar{\mathbf{w}}, \mathbf{b}\right)_{\Omega} + \left(\bar{\mathbf{w}}, \mathbf{t}^0\right)_{\Gamma_t} \tag{7.14}$$

$$a\left(\mathbf{w}', \bar{\mathbf{u}}\right) + a\left(\mathbf{w}', \mathbf{u}'\right) = \left(\mathbf{w}', \mathbf{b}\right)_{\Omega} + \left(\mathbf{w}', \mathbf{t}^0\right)_{\Gamma_t} \tag{7.15}$$

Following the assumption that the linear form $\left(\mathbf{w}', \mathbf{t}^0\right)_{\Gamma_t}$ is negligible, then the solution of Eq. (7.15) is in fact the weak solution of the equivalent boundary value problem:

$$C_{ijkl} u'_{k,lj} + C_{ijkl} \bar{u}_{k,lj} + b_i = 0 \quad \forall \mathbf{x} \in \Omega \tag{7.16}$$

$$u'_i = 0 \quad \forall \mathbf{x} \in \Gamma_u \tag{7.17}$$

$$\sigma'_{ij} n_j = t_i^0 \quad \forall \mathbf{x} \in \Gamma_t \tag{7.18}$$

Here Eqs. (7.16) to (7.18) can be treated alternatively as an inclusion problem if the residue of the coarse scale solution $C_{ijkl} \bar{u}_{k,lj} + b_i$ can be replaced by the "equivalent eigenstrain" as following:

$$C_{ijkl} \bar{u}_{k,lj} + b_i =: -C_{ijkl} \varepsilon^*_{kl,j} \quad \forall \mathbf{x} \in \Omega \tag{7.19}$$

It is worth mentioning here that the equivalent eigestrain employed is different from the terminology used in EIM which is proposed to deal with material mismatch. In fact, it is straightforward to write out that

$$\varepsilon^*_{kl} = u_{k,l} - \bar{u}_{k,l} \tag{7.20}$$

Consequently the fine scale solution can be treated as the disturbance driven by the equivalent eigenstrain which represents the residual of the coarse scale solution. That is to say the solution of Eq. (7.16)-(7.18) can be expressed directly as

$$u'_{i,j}(\mathbf{x}) = S_{ijkl}\varepsilon^*_{kl} \quad \forall \mathbf{x} \in \Omega \tag{7.21}$$

Based on the fact that the equivalent eigenstrain ε^*_{ij} is related to the coarse scale solution $\bar{\mathbf{u}}$ as shown in Eq. (7.19), and with the help of Eq. (7.21), the fine scale solution $\mathbf{u}'$ can be analytically expressed as a function of $\bar{\mathbf{u}}$, and as a result be eliminated from the equation for $\bar{\mathbf{u}}$. The details can be found in Hughes (1998), Li et al (2004, 2005) and Wang et al (2005). It is stated that this multiscale revision of the equation for $\bar{\mathbf{u}}$ can significantly improve the accuracy of the solution.

7.2.2 Zienkiewicz-Zhu feedback and its implementation

In Eq. (7.20), it can be seen that the equivalent eigenstrain depends on the exact solution of the original problem which is unknown in advance. To overcome the difficulty lies in determination of the equivalent eigenstrain, the Zienkiewecz-Zhu feedback mechanism is employed to give an alternative evaluation of the coarse scale error with high efficiency. This evaluation is realized by replacing the exact solution in Eq. (7.20) by a higher order interpolation of the strain field inside the whole domain, which is enforced to be accurate at the Gaussian points in the sense of least squares. The details are described below.

First, the higher order strain field can be interpolated by the following equation,

$$u^Z_{i,j}(\mathbf{x}) = \sum_{n=1}^{n_{ed}} N^n(\mathbf{x})\tilde{u}^{Z,n}_{i,j}(\mathbf{x}) \qquad \forall \mathbf{x} \in \Omega_e \tag{7.22}$$

where n_{ed} is the number of nodes in element Ω_e; $N^n(\mathbf{x})$ is the same shape function for displacement fields; $\tilde{u}^{Z,n}_{i,j}(\mathbf{x})$ is the nodal value of the strain field. This interpolation produces a

displacement gradient field with the same order as the finite element displacement fields, which means the result strain field will be smoother than the original approximation.

Second, the nodal displacement gradient is assumed to be the nodal value of a polynomial field function with the same order of the shape function. This function also controls the displacement gradient field in the neighborhood of the node of interest, and can be expressed as

$$\tilde{u}^{p}_{i,j}(\mathbf{x}) = \mathbf{P}(\mathbf{x})\mathbf{a} \qquad \forall \mathbf{x} \in \Omega_e \tag{7.23}$$

where $\mathbf{P}(\mathbf{x})$ is the standard polynomial basis vector with the order of shape function, and **a** is an unknown vector for the (*i*, *j*) component of the displacement gradient. This unknown vector can be determined by a least-square operation, namely minimizing the functional $E(\mathbf{a})$ defined in the following expression,

$$E(\mathbf{a}) = \int_{\Omega^n_E} \left(\tilde{u}^{p}_{i,j}(\mathbf{x}) - \overline{u}_{i,j}(\mathbf{x}) \right)^2 d\Omega = \int_{\Omega^n_E} \left(\mathbf{P}(\mathbf{x})\mathbf{a} - \overline{u}_{i,j}(\mathbf{x}) \right)^2 d\Omega \tag{7.24}$$

The minimization resultes in

$$\mathbf{a} = \left(\int_{\Omega^n_E} \mathbf{P}^{\mathrm{T}}\mathbf{P} d\Omega \right)^{-1} \int_{\Omega^n_E} \mathbf{P}^{\mathrm{T}} \overline{u}_{i,j} d\Omega \tag{7.25}$$

Therefore substituting Eq. (7.25) into (7.23) will lead to

$$\tilde{u}^{Z,n}_{i,j} = \mathbf{P}(\mathbf{x}^n) \left(\int_{\Omega^n_E} \mathbf{P}^{\mathrm{T}}\mathbf{P} d\Omega \right)^{-1} \int_{\Omega^n_E} \mathbf{P}^{\mathrm{T}} \overline{u}_{i,j} d\Omega \tag{7.26}$$

which can be combined with Eq. (7.22) to give the interpolated displacement gradient fields. It is reported that this displacement gradient has an O(h^2) convergence for both linear triangle and bilinear quadrilateral elements. And as a result, it can replace the exact displacement gradient in Eq. (7.20) to give an accurate estimation of the equivalent eigenstrain.

Once the equivalent eigenstrain is obtained, following the formulation of Li et al (2005) for the local element Ω_e, the critical equation (7.19) and (7.20) can be further expressed as

$$\varepsilon'_{ij}(\mathbf{y}) = S^{I,F}_{ijkl}(\mathbf{y})\varepsilon^{*}_{kl}(\mathbf{y}) + \sum_{\mathbf{x}\notin\Omega_e} S^{E,F}_{ijkl}(\mathbf{y}-\mathbf{x})\varepsilon^{*}_{kl}(\mathbf{x}) \quad \forall \mathbf{y}\in\Omega_e \tag{7.27}$$

This equation states that, the contribution to the fine scale strain inside element Ω_e can be decomposed into two parts. The first part is the disturbance driven by the equivalent eigenstrain inside the element itself, while the second one considers the effect of the equivalent eigenstrain inside the elements close to Ω_e. The former eigenstrain will be mapped into the disturbance by the interior Eshelby tensor $S^{I,F}_{ijkl}$ and correspondingly the latter exterior Eshelby tensor $S^{E,F}_{ijkl}$.

In addition, based on the fact that the exterior tensor decays quite fast when the point of interest is away from Ω_e, a further simplification is made to ignore the contribution from the exterior elements. It indeed ignors the interaction of the errors inside each element, and leads to the expression as

$$\varepsilon'_{ij}(\mathbf{y}) = S^{I,F}_{ijkl}(\mathbf{y})\varepsilon^{*}_{kl}(\mathbf{y}) \quad \forall \mathbf{y}\in\Omega_e \tag{7.28}$$

Finally, the fine scale solution over element Ω_e can be expressed in terms of the coarse scale solution as:

$$\varepsilon'_{ij}(\mathbf{x}) = S^{I,F}_{ijkl}(\mathbf{x})\left\{\sum_{n=1}^{n_{ed}} N^{n}(\mathbf{x})\left[\mathbf{P}(\mathbf{x}^{n})\left(\int_{\Omega^{n}_{E}}\mathbf{P}^{\mathrm{T}}\mathbf{P}d\Omega\right)^{-1}\int_{\Omega^{n}_{E}}\mathbf{P}^{\mathrm{T}}\bar{u}_{k,l}d\Omega\right] - \bar{u}_{k,l}(\mathbf{x})\right\} \quad \forall \mathbf{x}\in\Omega_e \tag{7.29}$$

As a result, the fine scale solution can be eliminated from Eq. (7.14), and lead to the modified finite element formulation for $\bar{\mathbf{u}}$, which is the smart element method proposed by Li since the method can automatically detect and homogenize the numerical errors and made the modification of the stiffness matrix in one step.

7.2.3 Upgrade from Li's Smart Element Formulation

In Li et al's smart element formulation, the element of interest is always approximated by a concentric circle at the center of the virtual RVE which physically represents the range of the disturbance induced by the equivalent eigenstrain. This approximation has produced good results as demonstrated in Li et al (2005). However, the intrinsic defects can sometimes undermine the improvement of this variational multiscale method. First, the smallest circle encompass the element highly depends on the distance between vertices, which sometimes could result in an ill-posed situation where a big circular inclusion are employed for an element with small area. Second, the concentric configuration of that virtual RVE cannot capture the real influence of the elements close to boundary.

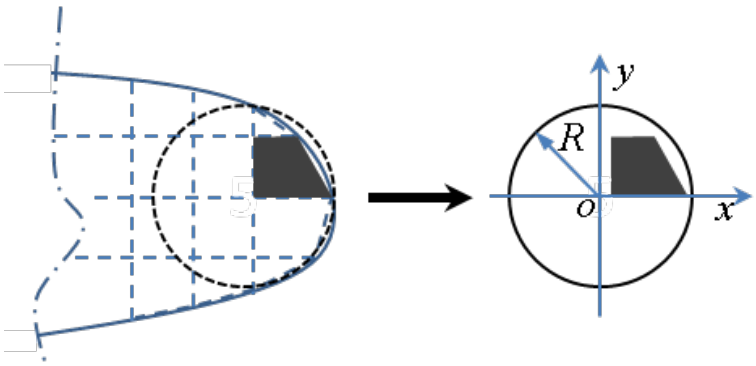

Figure 7.1. A cantilever beam with rectangular or triangular mesh sharing the same nodes

To demonstrate this problem, here the domain with a curved boundary is taken as an example. As depicted in Figure 7.1, a typical element closed to the boundary is not a square and not located at the center of a circular virtual RVE which encompasses the neighbors. However, in Li's formulation, this configuration has to be simplified as a concentric circular RVE, which

obviously ignores the topological characteristics of this element inside the domain and is not able to capture the local behavior of this disturbance field.

In fact, the reason Li et al has to stick with that rough approximation is that there existed no analytical solution for inclusions with arbitrary shape embedded in a finite domain at that time. Currently this gap is filled by the solution provided in Chapter 4 which analyzes the polygonal inclusion arbitrarily located inside a finite circular domain. Observing that the newly developed solution can capture the difference in the shapes and locations of elements inside the whole domain, it is natural to implement it to the smart element formulation to make improvement. This can be done by simply replacing the average interior Eshelby tensor in the in Eq. (7.29) by the upgraded one, which is discussed in Section 4.6. The improvement can be demonstrated in the following section by several classic examples.

7.3 NUMERICAL EXAMPLES

To demonstrate the application of the updated smart element method, three numerical examples have been studied. The first one is about a rectangular cantilever beam under the vertical line load along the free edge, and the second one is the Cook Panel problem in 2D space. In both examples, the conventional FEM results, Li's smart element simulation and the updated one are all employed for investigation.

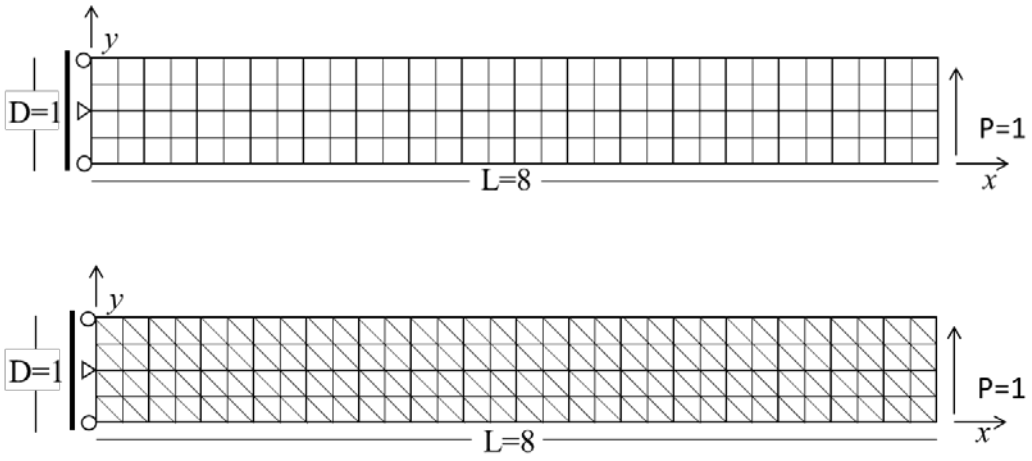

Figure 7.2. A cantilever beam with rectangular or triangular mesh sharing the same nodes

As shown in the Figure 7.2, the cantilever beam in plane strain condition has a span of 8 and the depth of 1. Young's modulus and Poisson ratio is assigned as 1000 and 0.25. A line load P = 1 is applied vertically along the free edge; see Figure 7.2. Here all the parameters are dimensionless and can be scaled whenever needed since this is a linear elastic problem. The exact solution of such a problem can be found in Timeoshenko and Goodier (1963) as

$$u_x = -\frac{Py}{6\bar{E}I}\left(y-\frac{D}{2}\right)\left[3x(2L-x)+(2+\bar{\nu})y(y-D)\right] \tag{7.30}$$

$$u_y = -\frac{Py}{6\bar{E}I}\left[x^2(3L-x)+3\bar{\nu}(L-x)\left(y-\frac{D}{2}\right)^2+\frac{4+5\bar{\nu}}{4}D^2x\right] \tag{7.31}$$

where $I = D^3/12$, $\bar{E} = E/(1-\nu^2)$ and $\bar{\nu} = \nu/(1-\nu)$ as for plain strain.

As a demonstration of the improvement in the coarse scale solution, two different coarse meshes are investigated, one with 25 nodes the other 50 nodes. In each simulation both rectangular and triangular elements sharing the same nodes are employed respectively, see Figure 7.2. The vertical displacement along the bottom line of the beam from conventional FEM,

Li's Smart Element Method and the updated Smart Element Method is plotted against the exact solution in Figure 7.3 and Figure 7.4.

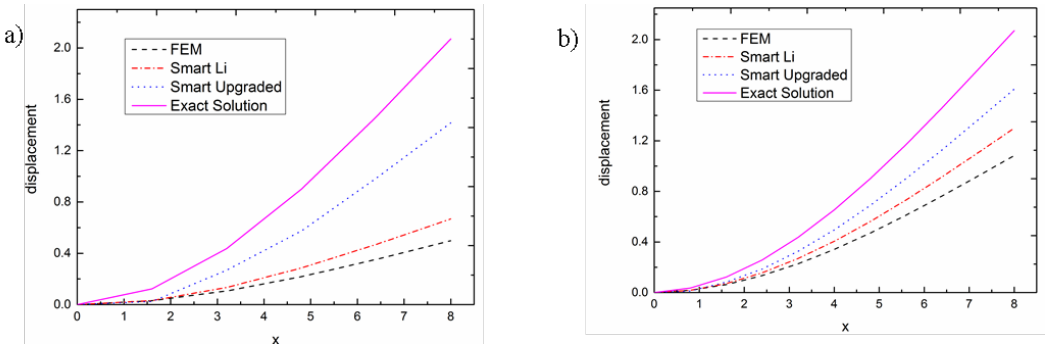

Figure 7.3. Solutions obtained via triangular elements discretization using a) 25 nodes and b) 50 nodes

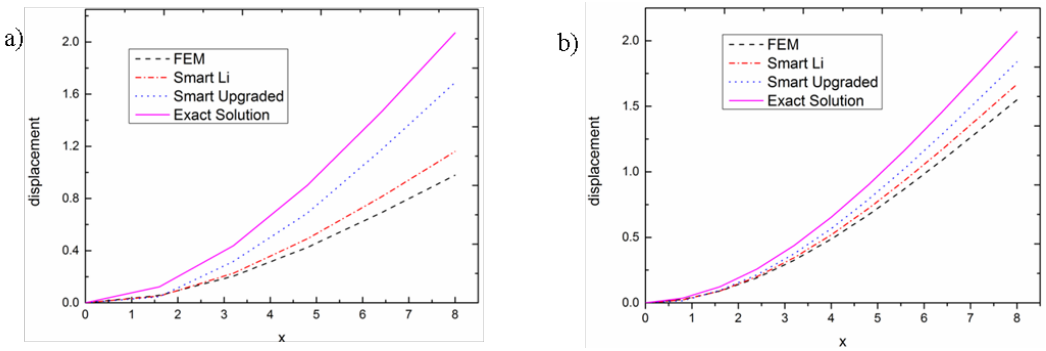

Figure 7.4. Solutions obtained via rectangular elements discretization using a) 25 nodes and b) 50 nodes

It is found in the comparison of the two coarse scale simulations, the updated smart element simulation leads to a result much closer to the exact solution when compared to the conventional FEM solution and Li's smart element method. It has produced a noticeable improvement from Li et al's original method, e.g., for the 5x5 mesh, the improvement being as much as 35% at the free end.

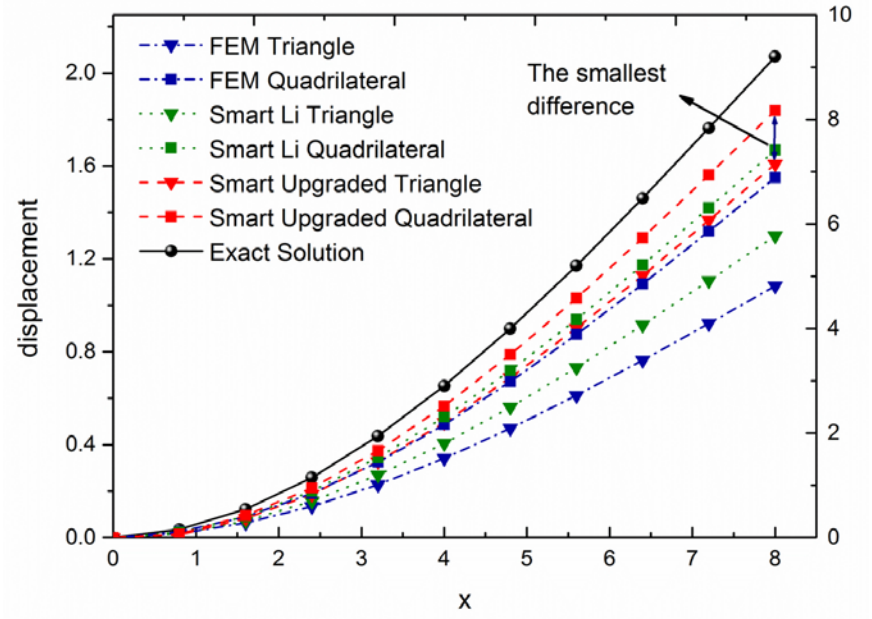

Figure 7.5. Comparison of the numerical simulation of vertical displacement along the beam bottom for triangular and rectangular (symbols) elements in 10 x 5 mesh discretization of the cantilever beam

Another significant advantage of this updated smart element method is that it is less element shape sensitive than the conventional FEM and Li's method. The numerical results for the same meshes different element shapes are plotted against the exact solution in Figure 7.5 for comparison. As demonstrated in the Figure, the results based on triangular and rectangular elements from the updated smart element method stay much closer than Li et al's method and the conventional FEM simulation. This is because that the updated smart element method considers the shape effect of the inclusion on the disturbance, and therefore produces results less dependent on the element shape. This characteristic of the updated smart element method can be further demonstrated in the following Figure.

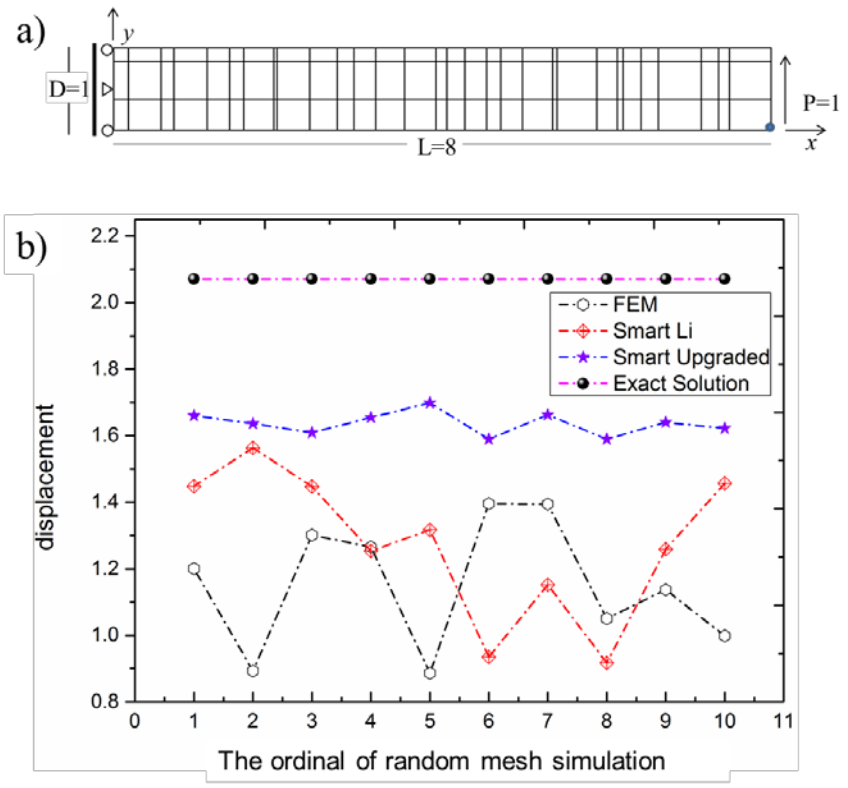

Figure 7.6. a) an example of random mesh; b) the numerical results obtained in 10 randomly selected mesh for the vertical displacement at the bottom of the free end

As shown in Figure 7.6, ten randomly selected meshes generated by a random number generator are used to simulate the vertical displacement at the bottom point of the right end on the cantilever beam (highlighted in Figure 7.6a). Similarly the results via conventional FEM, Li et al's smart element method and the updated smart element method are plotted against the exact solution. It can be seen that although the mesh structures are randomly selected, the solution from the updated smart element method is much more consistent and accurate than FEM and Li's smart element method. This updated smart element method is shown to be more reliable despite of the artificial mesh randomness in engineering practice.

In addition to the cantilever beam studied above, a frequently met engineering problem, the Cook Panel under the concentrated force on the bottom of the free end is investigated in 2D plane strain. This problem is known to have no analytical solution and therefore need to be analyzed numerically in practice. Here the details of the panel is shown in Figure 7.7, while the material properties is assigned as E=1000, v=0.25 or v=0.40. The vertical displacement along the bottom edge of this panel is being investigated.

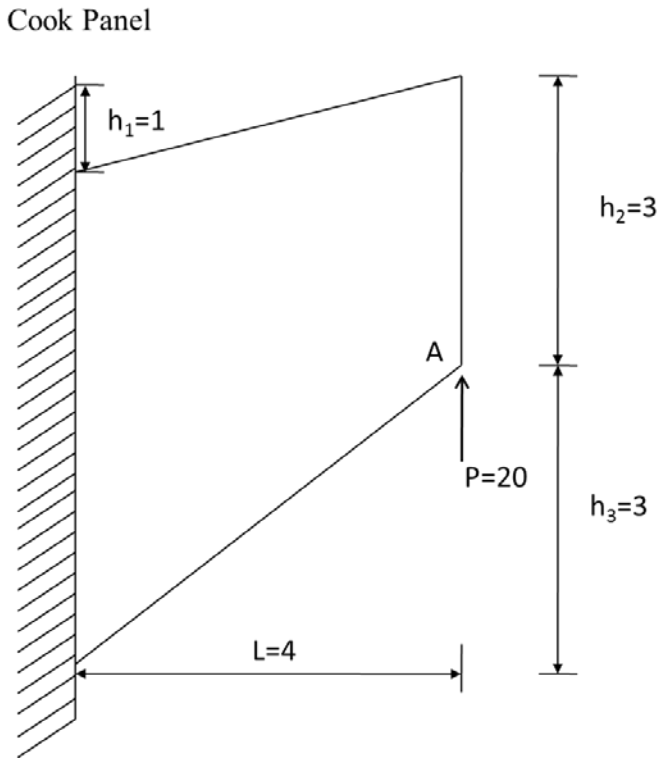

Figure 7.7. The Cook Panel under investigation

The numerical results of the vertical displacement along the bottom edge via a 4x4 coarse mesh for two different Poisson ratios are plotted in Figure 7.8 against the FEM solutions, which serve as a benchmarks here. As shown in Figure 7.8, the updated smart element simulation always shows a better performance over Li's method and the conventional FEM. This is

especially obvious when the Poisson ration is set closer to the incompressible limit v=0.5. This has been discussed in Li et al's work (2005) that the smart element scheme is free of volumetric locking, which is also inherited by the updated smart element method. It is safe to draw the conclusion that the updated smart element method can have a good application in practice.

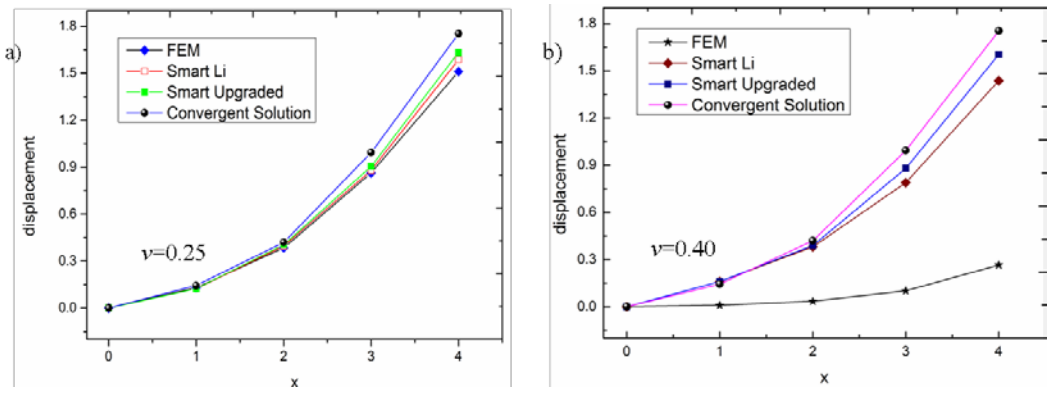

Figure 7.8. Numerical results obtained for the Cook Panel via 4x4 quadrilateral mesh for a) v=0.25 and b) v=0.40

7.4 DISCUSSION AND CONCLUSION

In this chapter, the proposed variational multiscale method has been updated by introducing the newly developed solution for a homogeneous RVE containing a polygonal inclusion. This modification brings in significant improvement of the numerical results, which is resulted from the consideration of the mesh shapes and the positions of the elements close to boundary. In some particular cases the improvement can be as great as 30%. Besides, the upgraded method behaves in a much more consistent way compared to the conventional FEM and the original version of this method. It means this upgrading introduces a more reliable and efficient method compared to the original version.

8.0 SUMMARY AND DISCUSSION OF FUTURE WORK

In this dissertation, the traditional complex potential method has been applied to deal with the inclusion problems in 2D finite domains. The framework is equipped with the Laurent series expansion of holomorphic functions, Fourier Transform of analytic functions and conformal mapping strategy. Starting from the simplest problem with a concentric circular configuration, the shape effect of inclusion as well as matrix has also been studied for the homogeneous inclusion problems. Following the methodology developed, RVEs with arbitrarily shaped inclusions and matrices can be analyzed theoretically. For the inhomogeneous inclusion problems, the obtained analytic solution for the concentric configuration lead to a theoretical discussion of the applicability of the commonly adopted Equivalent Inclusion Method (EIM) for composite RVEs. A specified volume fraction limit is suggested for the proper application of EIM. The developed approach is then extended to study the multi-inhomogeneous inclusion problem which could serve in the theoretical analysis of composites with inter-phase layers where non-elastic strain could happen.

The analytical solution documented in this dissertation has some direct applications in science and engineering analysis. Just as discussed in Chapter 7, the analytical solution of bounded homogeneous domain with an arbitrary inclusion can be applied to upgrade the smart element method proposed by Li and his colleague (Le et al 2005, Wang et al 2005). This upgraded smart element method produces much better results compared to the original one,

being able to take into the account the effect from the shape difference of elements and their relative position in the “virtual” RVEs. This is a typical example showing that how a significant improvement can be made via accurate prediction of the disturbance induced by the inclusions inside a finite domain.

In spite of the progress has been made in seeking for the analytical solution of finite domain inclusion problem, there is still some work left for further investigation. As an example, in the inhomogeneous RVEs, the shape effect of the inclusions and matrices deserve more attentions. Different from the homogeneous inclusion problem, it is mainly hindered by the convergence problem of the generalized binomial expansions of holomorphic functions in handling the interface and the exterior boundary simultaneously. Although some initial results are obtained for some simple shapes, to develop a systematic methodology to deal with such problems still need more effort. In fact, the progressing conformal mapping study in computational geometry and image recognition might provide an insightful guidance for solving this problem, just as the help from Schwarz-Christoffel mapping strategy in handling polygonal boundaries.

APPENDIX A

DETAILS FOR EVALUATION OF CAUCHY INTEGRALS IN 3.

In order to construct the potential $\psi_1(\zeta)$ for curved square, the following Cauchy integrals besides (3.43) are needed.

$$
\begin{aligned}
I_1 &= \frac{1}{2\pi i}\cdot\int_\gamma \frac{1}{\left(C_1 t + C_5 t^5 + C_9 t^9\right)^3}\cdot\frac{dt}{t-\zeta} \\
&= \frac{-3{C_1}^2 C_5\zeta - \left(3C_1{C_5}^2 + 3{C_1}^2 C_9\right)\zeta^5 - \left({C_5}^3 + 6C_1 C_5 C_9\right)\zeta^9}{{C_1}^3\left(C_1 + C_5\zeta^4 + C_9\zeta^8\right)^3} \\
&\quad + \frac{-\left(3{C_5}^2 C_9 + 3C_1{C_9}^2\right)\zeta^{13} - 3C_5{C_9}^2\zeta^{17} - {C_9}^3\zeta^{21}}{{C_1}^3\left(C_1 + C_5\zeta^4 + C_9\zeta^8\right)^3}
\end{aligned}
\tag{A.1}
$$

$$I_2 = \frac{1}{2\pi i}\int_\gamma \frac{dt}{t-\xi}\cdot\frac{\bar{C}_1\frac{1}{t}+\bar{C}_5\frac{1}{t^5}+\bar{C}_9\frac{1}{t^9}}{\left(C_1 t + C_5 t^5 + C_9 t^9\right)^2}$$

$$= \bar{C}_1\left(\frac{-\frac{C_5^{\,2}}{C_1^{\,2}}\zeta^5 - \frac{C_9^{\,2}}{C_1^{\,2}}\zeta^{13} - \frac{2C_1C_5}{C_1^{\,2}}\zeta - \frac{2C_1C_9}{C_1^{\,2}}\zeta^5 - \frac{2C_5C_9}{C_1^{\,2}}\zeta^9}{\left(C_1^{\,2} + C_5^{\,2}\zeta^8 + C_9^{\,2}\zeta^{16} + 2C_1C_5\zeta^4 + 2C_1C_9\zeta^8 + 2C_5C_9\zeta^{12}\right)}\right)$$

$$+ \bar{C}_5\left(\frac{-\frac{C_5^{\,2}}{C_1^{\,2}}\zeta - \frac{C_9^{\,2}}{C_1^{\,2}}\zeta^9 - \frac{2C_1C_9}{C_1^{\,2}}\zeta - \frac{2C_5C_9}{C_1^{\,2}}\zeta^5}{\left(C_1^{\,2} + C_5^{\,2}\zeta^8 + C_9^{\,2}\zeta^{16} + 2C_1C_5\zeta^4 + 2C_1C_9\zeta^8 + 2C_5C_9\zeta^{12}\right)}\right.$$

$$\left. + \left(-\frac{2C_1C_5}{C_1^{\,2}}\right)\left(\frac{-\frac{C_5^{\,2}}{C_1^{\,2}}\zeta^5 - \frac{C_9^{\,2}}{C_1^{\,2}}\zeta^{13} - \frac{2C_1C_5}{C_1^{\,2}}\zeta - \frac{2C_1C_9}{C_1^{\,2}}\zeta^5 - \frac{2C_5C_9}{C_1^{\,2}}\zeta^9}{\left(C_1^{\,2} + C_5^{\,2}\zeta^8 + C_9^{\,2}\zeta^{16} + 2C_1C_5\zeta^4 + 2C_1C_9\zeta^8 + 2C_5C_9\zeta^{12}\right)}\right)\right)$$

$$+ \bar{C}_9\left(\frac{-\frac{C_9^{\,2}}{C_1^{\,2}}\zeta^5 - \frac{2C_5C_9}{C_1^{\,2}}\zeta}{\left(C_1^{\,2} + C_5^{\,2}\zeta^8 + C_9^{\,2}\zeta^{16} + 2C_1C_5\zeta^4 + 2C_1C_9\zeta^8 + 2C_5C_9\zeta^{12}\right)}\right. \qquad \text{(A.2)}$$

$$\left. + \left(-\frac{C_5^{\,2}}{C_1^{\,2}} - \frac{2C_1C_9}{C_1^{\,2}}\right)\left(\frac{-\frac{C_5^{\,2}}{C_1^{\,2}}\zeta^5 - \frac{C_9^{\,2}}{C_1^{\,2}}\zeta^{13} - \frac{2C_1C_5}{C_1^{\,2}}\zeta - \frac{2C_1C_9}{C_1^{\,2}}\zeta^5 - \frac{2C_5C_9}{C_1^{\,2}}\zeta^9}{\left(C_1^{\,2} + C_5^{\,2}\zeta^8 + C_9^{\,2}\zeta^{16} + 2C_1C_5\zeta^4 + 2C_1C_9\zeta^8 + 2C_5C_9\zeta^{12}\right)}\right)\right.$$

$$\left. + \left(-\frac{2C_1C_5}{C_1^{\,2}}\right)\left(\frac{-\frac{C_5^{\,2}}{C_1^{\,2}}\zeta - \frac{C_9^{\,2}}{C_1^{\,2}}\zeta^9 - \frac{2C_1C_9}{C_1^{\,2}}\zeta - \frac{2C_5C_9}{C_1^{\,2}}\zeta^5}{\left(C_1^{\,2} + C_5^{\,2}\zeta^8 + C_9^{\,2}\zeta^{16} + 2C_1C_5\zeta^4 + 2C_1C_9\zeta^8 + 2C_5C_9\zeta^{12}\right)}\right)\right.$$

$$\left. + \left(-\frac{2C_1C_5}{C_1^{\,2}}\right)\left(\left(-\frac{2C_1C_5}{C_1^{\,2}}\right)\left(\frac{-\frac{C_5^{\,2}}{C_1^{\,2}}\zeta^5 - \frac{C_9^{\,2}}{C_1^{\,2}}\zeta^{13} - \frac{2C_1C_5}{C_1^{\,2}}\zeta - \frac{2C_1C_9}{C_1^{\,2}}\zeta^5 - \frac{2C_5C_9}{C_1^{\,2}}\zeta^9}{\left(C_1^{\,2} + C_5^{\,2}\zeta^8 + C_9^{\,2}\zeta^{16} + 2C_1C_5\zeta^4 + 2C_1C_9\zeta^8 + 2C_5C_9\zeta^{12}\right)}\right)\right)\right)$$

$$I_3 = \frac{1}{2\pi i}\int_\gamma \frac{\overline{\omega(t)}}{\omega'(t)}\frac{\varphi'(t)dt}{t-\zeta}$$

$$\begin{aligned}
&= a_1\overline{C}_1(\mathrm{TO1}) + \sum_{n=2}^{\infty} n a_n \overline{C}_1 \cdot \frac{\zeta^{n-2}}{C_1 + 5C_5\zeta^4 + 9C_9\zeta^8} \\
&\quad + a_1\overline{C}_5(\mathrm{TO5}) + 2a_2\overline{C}_5(\mathrm{TO4}) + 3a_3\overline{C}_5(\mathrm{TO3}) + 4a_4\overline{C}_5(\mathrm{TO2}) + 5a_5\overline{C}_5(\mathrm{TO1}) \\
&\quad + \sum_{n=6}^{\infty} n a_n \overline{C}_1 \cdot \frac{\zeta^{n-6}}{C_1 + 5C_5\zeta^4 + 9C_9\zeta^8} \\
&\quad + a_1\overline{C}_9(\mathrm{TO9}) + 2a_2\overline{C}_9(\mathrm{TO8}) + 3a_3\overline{C}_9(\mathrm{TO7}) + 4a_4\overline{C}_9(\mathrm{TO6}) + 5a_5\overline{C}_9(\mathrm{TO5}) \\
&\quad + 6a_6\overline{C}_9(\mathrm{TO4}) + 7a_7\overline{C}_9(\mathrm{TO3}) + 8a_8\overline{C}_9(\mathrm{TO2}) + 9a_9\overline{C}_9(\mathrm{TO1}) \\
&\quad + \sum_{n=10}^{\infty} n a_n \overline{C}_1 \cdot \frac{\zeta^{n-10}}{C_1 + 5C_5\zeta^4 + 9C_9\zeta^8}
\end{aligned} \tag{A.3}$$

where

$$\begin{aligned}
\mathrm{TO1} &= \frac{1}{2\pi i}\cdot\int_\gamma \frac{1}{t}\cdot\frac{1}{C_1 + 5C_5t^4 + 9C_9t^8}\cdot\frac{dt}{t-\zeta} \\
&= \frac{-\frac{5C_5}{C_1}\zeta^3 - \frac{9C_9}{C_1}\zeta^7}{C_1 + 5C_5\zeta^4 + 9C_9\zeta^8}
\end{aligned} \tag{A.4}$$

$$\begin{aligned}
\mathrm{TO2} &= \frac{1}{2\pi i}\cdot\int_\gamma \frac{1}{t^2}\cdot\frac{1}{C_1 + 5C_5t^4 + 9C_9t^8}\cdot\frac{dt}{t-\zeta} \\
&= \frac{-\frac{5C_5}{C_1}\zeta^2 - \frac{9C_9}{C_1}\zeta^6}{C_1 + 5C_5\zeta^4 + 9C_9\zeta^8}
\end{aligned} \tag{A.5}$$

$$\begin{aligned}
\mathrm{TO3} &= \frac{1}{2\pi i}\cdot\int_\gamma \frac{1}{t^3}\cdot\frac{1}{C_1 + 5C_5t^4 + 9C_9t^8}\cdot\frac{dt}{t-\zeta} \\
&= \frac{-\frac{5C_5}{C_1}\zeta - \frac{9C_9}{C_1}\zeta^5}{C_1 + 5C_5\zeta^4 + 9C_9\zeta^8}
\end{aligned} \tag{A.6}$$

$$\mathrm{TO4}=\frac{1}{2\pi i}\cdot\int_{\gamma}\frac{1}{t^4}\cdot\frac{1}{C_1+5C_5t^4+9C_9t^8}\cdot\frac{dt}{t-\zeta}$$

$$=\frac{-\frac{5C_5}{C_1}-\frac{9C_9}{C_1}\zeta^4}{C_1+5C_5\zeta^4+9C_9\zeta^8} \tag{A.7}$$

$$\mathrm{TO5}=\frac{1}{2\pi i}\cdot\int_{\gamma}\frac{1}{t^5}\cdot\frac{1}{C_1+5C_5t^4+9C_9t^8}\cdot\frac{dt}{t-\zeta}$$

$$=-\frac{5C_5}{C_1}(\mathrm{TO1})+\frac{-\frac{9C_9}{C_1}\zeta^3}{C_1+5C_5\zeta^4+9C_9\zeta^8} \tag{A.8}$$

$$\mathrm{TO6}=\frac{1}{2\pi i}\cdot\int_{\gamma}\frac{1}{t^6}\cdot\frac{1}{C_1+5C_5t^4+9C_9t^8}\cdot\frac{dt}{t-\zeta}$$

$$=-\frac{5C_5}{C_1}(TO2)+\frac{-\frac{9C_9}{C_1}\zeta^2}{C_1+5C_5\zeta^4+9C_9\zeta^8} \tag{A.9}$$

$$\mathrm{TO7}=\frac{1}{2\pi i}\cdot\int_{\gamma}\frac{1}{t^7}\cdot\frac{1}{C_1+5C_5t^4+9C_9t^8}\cdot\frac{dt}{t-\zeta}$$

$$=-\frac{5C_5}{C_1}(\mathrm{TO3})+\frac{-\frac{9C_9}{C_1}\zeta}{C_1+5C_5\zeta^4+9C_9\zeta^8} \tag{A.10}$$

$$\mathrm{TO8}=\frac{1}{2\pi i}\cdot\int_{\gamma}\frac{1}{t^8}\cdot\frac{1}{C_1+5C_5t^4+9C_9t^8}\cdot\frac{dt}{t-\zeta}$$

$$=-\frac{5C_5}{C_1}(\mathrm{TO4})+\frac{-\frac{9C_9}{C_1}}{C_1+5C_5\zeta^4+9C_9\zeta^8} \tag{A.11}$$

$$\mathrm{TO9}=\frac{1}{2\pi i}\cdot\int_{\gamma}\frac{1}{t^9}\cdot\frac{1}{C_1+5C_5t^4+9C_9t^8}\cdot\frac{dt}{t-\zeta}$$

$$=-\frac{5C_5}{C_1}(\mathrm{TO5})-\frac{9C_9}{C_1}(\mathrm{TO1}) \tag{A.12}$$

Finally,

$$\psi_1(\zeta) = \kappa \frac{\mu r^2}{\kappa+1}\left(\varepsilon_1^* - \varepsilon_2^* - i\gamma_{12}^*\right)\frac{\zeta}{\overline{C}_1} + \frac{\mu r^2}{\kappa+1}\left(\varepsilon_1^* - \varepsilon_2^* + i\gamma_{12}^*\right) I_2$$
$$+ \frac{2\mu r^2}{\kappa+1}\left(\varepsilon_1^* + \varepsilon_2^*\right)\left(-\frac{C_5\zeta^3 + C_9\zeta^7}{C_1^2 + C_1C_5\zeta^4 + C_1C_9\zeta^8}\right) - \frac{\mu r^4}{\kappa+1}\left(\varepsilon_1^* - \varepsilon_2^* + i\gamma_{12}^*\right) I_1 - I_3 \tag{A.13}$$

APPENDIX B

THE DEFINITE INTEGRALS IN EQS. (4.19)-(4.23) FOR A CIRCULAR DOMAIN

The results for the circular domain are listed below:

$$\begin{aligned} I_n^F &= \frac{1}{2\pi i}\int_{\partial\tilde{\Omega}} \frac{F(\zeta)d\zeta}{\zeta^n} \\ &= \frac{1}{2\pi i}\left(-C_2 \sum_{k=1}^{L}\left(\overline{\theta}_k \tilde{I}_{n-1}(k) + \overline{\theta}_k R^2 I_n'(k) + \overline{\delta}_k I_{n-1}'(k)\right)\right) \\ &\quad -\frac{1}{2\pi i}\left(2\overline{C}_1 \sum_{k=1}^{L}\left(\overline{\theta}_k R^2 \tilde{I}_{n+1}(k) + \overline{\delta}_k \tilde{I}_n(k)\right) - C_2\left(\sum_{k=1}^{L}\left(\overline{\theta}_k \overline{\theta}_k R^2 \tilde{I}_{n+1}(k) + \overline{\theta}_k \overline{\delta}_k \tilde{I}_n(k)\right)\right)\right) \end{aligned} \tag{B.1}$$

where $n \geq 2$, and

$$\begin{aligned} I_n^{Fc} &= \frac{1}{2\pi i}\int_{\partial\tilde{\Omega}} \frac{\overline{F(\zeta)}d\zeta}{\zeta^n} \\ &= -\kappa\left(\frac{1}{2\pi i}\left(-C_2 \sum_{k=1}^{L}\left(\overline{\theta}_k R^2 \tilde{I}_{n+1}(k) + \overline{\delta}_k \tilde{I}_n(k)\right)\right)\right) \end{aligned} \tag{B.2}$$

where $n \geq 1$. And in the above equations,

$$\tilde{I}_n(k) = \frac{1}{-n+1}\left(\frac{\overline{z}_{k+1}}{R^2}\right)^{n-1} - \frac{1}{-n+1}\left(\frac{\overline{z}_k}{R^2}\right)^{n-1} \quad \text{for } n > 1 \tag{B.3}$$

$$I_n'(k) = \frac{1}{\overline{z}_{k+1}}\left(R^2/\overline{z}_{k+1}\right)^{-n+1} - \frac{1}{\overline{z}_k}\left(R^2/\overline{z}_k\right)^{-n+1} \text{ for } n \geq 2 \tag{B.4}$$

and

$$\tilde{I}_1 = 0\,,\ I_1' = 0\,. \tag{B.5}$$

APPENDIX C

THE EXPLICIT EXPRESSION FOR DISPLACEMENT FIELDS IN 5.3

According to Eq. (5.25), the displacement fields and strain field could be expressed as functions of the Cartesian coordinates *x* and *y*.

$$\begin{Bmatrix} u \\ v \end{Bmatrix} = \begin{cases} \begin{Bmatrix} u_2^1 + u_2^2 \\ v_2^1 + v_2^2 \end{Bmatrix} & (x, y) \in \Omega_e \\ \begin{Bmatrix} u_1^1 + u_1^2 \\ v_1^1 + v_1^2 \end{Bmatrix} & (x, y) \in \Omega / \Omega_e \end{cases} \tag{C.1}$$

and

$$\begin{Bmatrix} \varepsilon_1 \\ \varepsilon_2 \\ \gamma_{12} \end{Bmatrix} = \begin{bmatrix} \dfrac{\partial}{\partial x} & 0 \\ 0 & \dfrac{\partial}{\partial y} \\ \dfrac{\partial}{\partial y} & \dfrac{\partial}{\partial x} \end{bmatrix} \begin{Bmatrix} u \\ v \end{Bmatrix} \tag{C.2}$$

Here

$$u_2^1 = \frac{\Gamma}{2}\left\{\left(\frac{(\kappa_2-1)(\varepsilon_1^0+\varepsilon_2^0)}{C_0} - \frac{C_4(\varepsilon_1^0-\varepsilon_2^0)}{C_1C_4-C_2C_3}\right)x + \left(\frac{\gamma_{12}^0}{\Gamma} - \frac{C_4\gamma_{12}^0}{C_1C_4-C_2C_3}\right)y \right.$$
$$+ \frac{(3-\kappa_2)C_3(\varepsilon_1^0-\varepsilon_2^0)}{C_1C_4-C_2C_3}x^3 + \frac{3(\kappa_2+1)C_3(\varepsilon_1^0-\varepsilon_2^0)}{C_1C_4-C_2C_3}xy^2 \qquad \text{(C.3)}$$
$$\left. - \frac{3(\kappa_2-1)C_3\gamma_{12}^0}{C_1C_4-C_2C_3}x^2y + \frac{(\kappa_2+3)C_3\gamma_{12}^0}{C_1C_4-C_2C_3}y^3\right\}$$

$$v_2^1 = \frac{\Gamma}{2}\left\{\left(\frac{(\kappa_2-1)(\varepsilon_1^0+\varepsilon_2^0)}{C_0} + \frac{C_4(\varepsilon_1^0-\varepsilon_2^0)}{C_1C_4-C_2C_3}\right)y - \left(\frac{\gamma_{12}^0}{\Gamma} + \frac{C_4\gamma_{12}^0}{C_1C_4-C_2C_3}\right)x \right.$$
$$+ \frac{(\kappa_2-3)C_3(\varepsilon_1^0-\varepsilon_2^0)}{C_1C_4-C_2C_3}y^3 + \frac{(\kappa_2+3)C_3\gamma_{12}^0}{C_1C_4-C_2C_3}x^3 \qquad \text{(C.4)}$$
$$\left. - \frac{3(\kappa_2+1)C_3(\varepsilon_1^0-\varepsilon_y)}{C_1C_4-C_2C_3}x^2y - \frac{3(\kappa_2-1)C_3\gamma_{12}^0}{C_1C_4-C_2C_3}xy^2\right\}$$

$$u_2^2 = \frac{1}{2}\left(\frac{\Gamma(\kappa_2-1)}{M_5+M_6} + \frac{(\kappa_2-1)}{(\kappa_1-1)}\left(\frac{r}{R}\right)^2\frac{2\Gamma}{M_5+M_6} + 1\right)(\varepsilon_1^*+\varepsilon_2^*)x$$
$$- \frac{1}{2}\left(\frac{\Gamma r^2 M_3}{M_1M_4-M_2M_3} + \frac{\Gamma}{-\kappa_1}\cdot\frac{-3M_4R^4+M_3R^2}{M_1M_4-M_2M_3}\right)\left((\varepsilon_1^*-\varepsilon_2^*)x+\gamma_{12}^*y\right)$$
$$+ \left(\frac{3}{2}\Gamma r^4\cdot\frac{(\kappa_1-\Gamma\kappa_2)}{(1+\Gamma\kappa_2)}\cdot\frac{M_4}{M_1M_4-M_2M_3} + \frac{1}{2}\right)\left((\varepsilon_1^*-\varepsilon_2^*)x+\gamma_{12}^*y\right) \qquad \text{(C.5)}$$
$$+ \frac{1}{2}\kappa_2\left(\frac{\Gamma r^2(\kappa_1+1)}{1+\Gamma\kappa_2}\cdot\frac{M_4}{M_1M_4-M_2M_3}\right)\left((\varepsilon_1^*-\varepsilon_2^*)(x^3-xy^2)+\gamma_{12}^*(x^2y-y^3)\right)$$
$$- \frac{3}{2}\left(\Gamma r^2\cdot\frac{\kappa_1+1}{1+\Gamma\kappa_2}\cdot\frac{M_4}{M_1M_4-M_2M_3}\right)\left((\varepsilon_1^*-\varepsilon_2^*)(x^3+xy^2)+\gamma_{12}^*(x^2y+y^3)\right)$$

$$
\begin{aligned}
v_2^2 = & \frac{1}{2}\left(\frac{\Gamma\left(\kappa_2-1\right)}{M_5+M_6}+\frac{\left(\kappa_2-1\right)}{\left(\kappa_1-1\right)}\left(\frac{r}{R}\right)^2\frac{2\Gamma}{M_5+M_6}+1\right)\left(\varepsilon_1^*+\varepsilon_2^*\right)y \\
& -\frac{1}{2}\left(\frac{\Gamma r^2 M_3}{M_1M_4-M_2M_3}+\frac{\Gamma}{-\kappa_1}\frac{-3M_4R^4+M_3R^2}{M_1M_4-M_2M_3}\right)\left(-\left(\varepsilon_1^*-\varepsilon_2^*\right)y+\gamma_{12}^*x\right) \\
& +\left(\frac{3}{2}\Gamma r^4\cdot\frac{\left(\kappa_1-\Gamma\kappa_2\right)}{\left(1+\Gamma\kappa_2\right)}\cdot\frac{M_4}{M_1M_4-M_2M_3}+\frac{1}{2}\right)\left(-\left(\varepsilon_1^*-\varepsilon_2^*\right)y+\gamma_{12}^*x\right) \\
& +\frac{1}{2}\kappa_2\left(\frac{\Gamma r^2\left(\kappa_1+1\right)}{1+\Gamma\kappa_2}\cdot\frac{M_4}{M_1M_4-M_2M_3}\right)\left(\left(\varepsilon_1^*-\varepsilon_2^*\right)\left(x^2y-y^3\right)-\gamma_{12}^*\left(x^3-xy^2\right)\right) \\
& -\frac{3}{2}\left(\Gamma r^2\cdot\frac{\kappa_1+1}{1+\Gamma\kappa_2}\cdot\frac{M_4}{M_1M_4-M_2M_3}\right)\left(\left(\varepsilon_1^*-\varepsilon_2^*\right)\left(-x^2y-y^3\right)+\gamma_{12}^*\left(x^3+xy^2\right)\right)
\end{aligned}
\tag{C.6}
$$

$$
\begin{aligned}
u_1^1 = {} & \frac{1}{2}\left(\frac{(\kappa_1-1)(1+\Gamma\kappa_2)}{(\kappa_1+1)}+\frac{(\kappa_1-1)(1-\Gamma)}{(\kappa_1+1)}\right)\frac{\left(\varepsilon_1^0+\varepsilon_2^0\right)}{C_0}x+\frac{1}{2}\gamma_{12}^0 y \\
& +\frac{1}{2}\left(\left(-1+\frac{(1-\Gamma)}{(\kappa_1+1)}\right)C_4+\left(1-\frac{(1+\Gamma\kappa_2)}{(\kappa_1+1)}-\frac{(1-\Gamma)}{(\kappa_1+1)}\right)3r^2C_3\right)\frac{\left(\varepsilon_1^0-\varepsilon_2^0\right)}{C_1C_4-C_2C_3}x \\
& +\frac{1}{2}\left(\left(-1+\frac{(1-\Gamma)}{(\kappa_1+1)}\right)C_4+\left(1-\frac{(1+\Gamma\kappa_2)}{(\kappa_1+1)}-\frac{(1-\Gamma)}{(\kappa_1+1)}\right)3r^2C_3\right)\frac{\gamma_{12}^0}{C_1C_4-C_2C_3}y \\
& -r^2\left(1-\frac{(1+\Gamma\kappa_2)}{(\kappa_1+1)}-\frac{(1-\Gamma)}{(\kappa_1+1)}\right)\cdot\frac{\left(\varepsilon_1^0+\varepsilon_2^0\right)}{C_0}\cdot\frac{x}{x^2+y^2} \\
& -\frac{1}{2}\cdot\frac{\kappa_1(1+\Gamma\kappa_2)}{(\kappa_1+1)}\cdot\frac{C_3\left(\varepsilon_1^0-\varepsilon_2^0\right)}{C_1C_4-C_2C_3}\left(x^3-3xy^2\right) \\
& +\frac{1}{2}\cdot\frac{(1-\Gamma)}{(\kappa_1+1)}\cdot\frac{C_5\left(\varepsilon_1^0-\varepsilon_2^0\right)}{C_1C_4-C_2C_3}\cdot\frac{\left(x^3-3xy^2\right)}{\left(x^2+y^2\right)^2} \\
& -\frac{1}{2}\cdot\frac{\kappa_1(1+\Gamma\kappa_2)}{(\kappa_1+1)}\cdot\frac{C_3\gamma_{12}^0}{C_1C_4-C_2C_3}\left(3x^2y-y^3\right) \\
& +\frac{1}{2}\cdot\frac{(1-\Gamma)}{(\kappa_1+1)}\cdot\frac{C_5\gamma_{12}^0}{C_1C_4-C_2C_3}\cdot\frac{\left(3x^2y-y^3\right)}{\left(x^2+y^2\right)^2} \\
& +\frac{1}{2}\left(\left(1-\frac{(1+\Gamma\kappa_2)}{(\kappa_1+1)}+3\frac{(1-\Gamma)}{(\kappa_1+1)}\right)r^6C_3-\frac{(1-\Gamma)}{(\kappa_1+1)}r^4C_4\right)\cdot\frac{\left(\varepsilon_1^0-\varepsilon_2^0\right)}{C_1C_4-C_2C_3}\cdot\frac{\left(x^3-3xy^2\right)}{\left(x^2+y^2\right)^3} \\
& +\frac{1}{2}\left(\left(1-\frac{(1+\Gamma\kappa_2)}{(\kappa_1+1)}+3\frac{(1-\Gamma)}{(\kappa_1+1)}\right)r^6C_3-\frac{(1-\Gamma)}{(\kappa_1+1)}r^4C_4\right)\cdot\frac{\gamma_{12}^0}{C_1C_4-C_2C_3}\cdot\frac{\left(3x^2y-y^3\right)}{\left(x^2+y^2\right)^3} \\
& +\frac{1}{2}\cdot\frac{\kappa_1(1-\Gamma)}{(\kappa_1+1)}\cdot\frac{C_5\left(\varepsilon_1^0-\varepsilon_2^0\right)}{C_1C_4-C_2C_3}\cdot\frac{x}{x^2+y^2} \\
& +\frac{3}{2}\cdot\frac{(1+\Gamma\kappa_2)}{(\kappa_1+1)}\cdot\frac{C_3\left(\varepsilon_1^0-\varepsilon_2^0\right)}{C_1C_4-C_2C_3}\left(x^2+y^2\right)x \\
& +\frac{1}{2}\cdot\frac{\kappa_1(1-\Gamma)}{(\kappa_1+1)}\cdot\frac{C_5\gamma_{12}^0}{C_1C_4-C_2C_3}\cdot\frac{y}{x^2+y^2} \\
& +\frac{3}{2}\cdot\frac{(1+\Gamma\kappa_2)}{(\kappa_1+1)}\cdot\frac{C_3\gamma_{12}^0}{C_1C_4-C_2C_3}\left(x^2+y^2\right)y
\end{aligned}
\tag{C.7}
$$

$$
\begin{aligned}
v_1^1 = {} & \frac{1}{2}\left(\frac{(\kappa_1-1)(1+\Gamma\kappa_2)}{(\kappa_1+1)}+\frac{(\kappa_1-1)(1-\Gamma)}{(\kappa_1+1)}\right)\cdot\frac{\left(\varepsilon_1^0+\varepsilon_2^0\right)}{C_0}y-\gamma_{12}^0 x \\
& +\frac{1}{2}\left(\left(1-\frac{(1-\Gamma)}{(\kappa_1+1)}\right)C_4-\left(1-\frac{(1+\Gamma\kappa_2)}{(\kappa_1+1)}-\frac{(1-\Gamma)}{(\kappa_1+1)}\right)3r^2C_3\right)\cdot\frac{\left(\varepsilon_1^0-\varepsilon_2^0\right)}{C_1C_4-C_2C_3}y \\
& +\frac{1}{2}\left(\left(-1+\frac{(1-\Gamma)}{(\kappa_1+1)}\right)C_4+\left(1-\frac{(1+\Gamma\kappa_2)}{(\kappa_1+1)}-\frac{(1-\Gamma)}{(\kappa_1+1)}\right)3r^2C_3\right)\cdot\frac{\gamma_{12}^0}{C_1C_4-C_2C_3}x \\
& -\left(1-\frac{(1+\Gamma\kappa_2)}{(\kappa_1+1)}-\frac{(1-\Gamma)}{(\kappa_1+1)}\right)\cdot\frac{\left(\varepsilon_1^0+\varepsilon_2^0\right)}{C_0}\cdot r^2\cdot\frac{y}{x^2+y^2} \\
& -\frac{1}{2}\cdot\frac{\kappa_1(1+\Gamma\kappa_2)}{(\kappa_1+1)}\cdot\frac{C_3\left(\varepsilon_1^0-\varepsilon_2^0\right)}{C_1C_4-C_2C_3}\left(3x^2y-y^3\right) \\
& +\frac{1}{2}\cdot\frac{(1-\Gamma)}{(\kappa_1+1)}\cdot\frac{C_5\left(\varepsilon_1^0-\varepsilon_2^0\right)}{C_1C_4-C_2C_3}\cdot\frac{\left(3x^2y-y^3\right)}{\left(x^2+y^2\right)^2} \\
& +\frac{1}{2}\cdot\frac{\kappa_1(1+\Gamma\kappa_2)}{(\kappa_1+1)}\cdot\frac{C_3\gamma_{12}^0}{C_1C_4-C_2C_3}\cdot\left(x^3-3xy^2\right) \\
& -\frac{1}{2}\cdot\frac{(1-\Gamma)}{(\kappa_1+1)}\cdot\frac{C_5\gamma_{12}^0}{C_1C_4-C_2C_3}\cdot\frac{\left(x^3-3xy^2\right)}{\left(x^2+y^2\right)^2} \\
& +\frac{1}{2}\left(\left(1-\frac{(1+\Gamma\kappa_2)}{(\kappa_1+1)}+3\cdot\frac{(1-\Gamma)}{(\kappa_1+1)}\right)r^6C_3-\frac{(1-\Gamma)}{(\kappa_1+1)}r^4C_4\right)\cdot\frac{\left(\varepsilon_1^0-\varepsilon_2^0\right)}{C_1C_4-C_2C_3}\cdot\frac{\left(3x^2y-y^3\right)}{\left(x^2+y^2\right)^3} \\
& +\frac{1}{2}\left(-\left(1-\frac{(1+\Gamma\kappa_2)}{(\kappa_1+1)}+3\cdot\frac{(1-\Gamma)}{(\kappa_1+1)}\right)r^6C_3+\frac{(1-\Gamma)}{(\kappa_1+1)}r^4C_4\right)\cdot\frac{\gamma_{12}^0}{C_1C_4-C_2C_3}\cdot\frac{\left(x^3-3xy^2\right)}{\left(x^2+y^2\right)^3} \\
& -\frac{1}{2}\cdot\frac{\kappa_1(1-\Gamma)}{(\kappa_1+1)}\cdot\frac{C_5\left(\varepsilon_1^0-\varepsilon_2^0\right)}{C_1C_4-C_2C_3}\cdot\frac{y}{x^2+y^2} \\
& -\frac{3}{2}\cdot\frac{(1+\Gamma\kappa_2)}{(\kappa_1+1)}\cdot\frac{C_3\left(\varepsilon_1^0-\varepsilon_2^0\right)}{C_1C_4-C_2C_3}\cdot\left(x^2+y^2\right)y \\
& +\frac{1}{2}\cdot\frac{\kappa_1(1-\Gamma)}{(\kappa_1+1)}\cdot\frac{C_5\gamma_{12}^0}{C_1C_4-C_2C_3}\cdot\frac{x}{x^2+y^2} \\
& +\frac{3}{2}\cdot\frac{(1+\Gamma\kappa_2)}{(\kappa_1+1)}\cdot\frac{C_3\gamma_{12}^0}{C_1C_4-C_2C_3}\cdot\left(x^2+y^2\right)x
\end{aligned}
\tag{C.8}
$$

$$u_1^2 = \left(\frac{r}{R}\right)^2 \cdot \frac{\left(\varepsilon_1^* + \varepsilon_2^*\right)}{M_5 + M_6} x - \frac{1}{2}\left(-r^2 \cdot \frac{M_3}{M_1 M_4 - M_2 M_3}\right)\left(\left(\varepsilon_1^* - \varepsilon_2^*\right) x + \gamma_{12}^* y\right)$$

$$+\frac{1}{2}\kappa_1 r^2 \cdot \frac{M_4}{M_1 M_4 - M_2 M_3}\left(\left(\varepsilon_1^* - \varepsilon_2^*\right)\left(x^3 - xy^2\right) + \gamma_{12}^*\left(x^2 y - y^3\right)\right)$$

$$-\frac{1}{2} r^2 \cdot \frac{-3M_4 R^4 + M_3 R^2}{M_1 M_4 - M_2 M_3}\left(\left(\varepsilon_1^* - \varepsilon_2^*\right)\left(\frac{x}{x^2 + y^2}\right) + \gamma_{12}^*\left(\frac{y}{x^2 + y^2}\right)\right)$$

$$-\frac{3}{2} r^2 \cdot \frac{M_4}{M_1 M_4 - M_2 M_3}\left(\left(\varepsilon_1^* - \varepsilon_2^*\right)\left(x^3 + xy^2\right) + \gamma_{12}^*\left(x^2 y + y^3\right)\right)$$

$$-\frac{1}{2} r^2 \cdot \frac{1}{\kappa_1} \cdot \frac{-3M_4 R^4 + M_3 R^2}{M_1 M_4 - M_2 M_3}\left(\left(\varepsilon_1^* - \varepsilon_2^*\right)\frac{x^3 - xy^2}{\left(x^2 + y^2\right)^2} + \gamma_{12}^* \frac{x^2 y - y^3}{\left(x^2 + y^2\right)^2}\right) \qquad \text{(C.9)}$$

$$-r^2 \cdot \frac{\varepsilon_1^* + \varepsilon_2^*}{M_5 + M_6} \cdot \frac{x}{x^2 + y^2}$$

$$-\frac{1}{2}\left(\frac{\kappa_1 - \Gamma\kappa_2}{1 + \Gamma\kappa_2} \cdot \frac{M_4 r^8}{M_1 M_4 - M_2 M_3}\right)\left(\left(\varepsilon_1^* - \varepsilon_2^*\right)\frac{x^3 - xy^2}{\left(x^2 + y^2\right)^3} + \gamma_{12}^* \frac{x^2 y - y^3}{\left(x^2 + y^2\right)^3}\right)$$

$$-\frac{1}{2}\left(\frac{r^4}{\kappa_1} \cdot \frac{-3M_4 R^4 + M_3 R^2}{M_1 M_4 - M_2 M_3}\right)\left(\left(\varepsilon_1^* - \varepsilon_2^*\right)\frac{x^3 - xy^2}{\left(x^2 + y^2\right)^3} + \gamma_{12}^* \frac{x^2 y - y^3}{\left(x^2 + y^2\right)^3}\right)$$

$$
\begin{aligned}
v_1^2 &= \left(\frac{r}{R}\right)^2 \cdot \frac{\left(\varepsilon_1^* + \varepsilon_2^*\right)}{M_5 + M_6} y - \frac{1}{2}\left(-r^2 \cdot \frac{M_3}{M_1 M_4 - M_2 M_3}\right)\left(\left(\varepsilon_1^* - \varepsilon_2^*\right) x + \gamma_{12}^* y\right) \\
&+ \frac{1}{2}\kappa_1 r^2 \cdot \frac{M_4}{M_1 M_4 - M_2 M_3}\left(\left(\varepsilon_1^* - \varepsilon_2^*\right)\left(x^2 y - y^3\right) - \gamma_{12}^*\left(x^3 - x y^2\right)\right) \\
&- \frac{1}{2} r^2 \cdot \frac{-3M_4 R^4 + M_3 R^2}{M_1 M_4 - M_2 M_3}\left(\gamma_{12}^*\left(\frac{x}{x^2 + y^2}\right) - \left(\varepsilon_1^* - \varepsilon_2^*\right)\frac{y}{x^2 + y^2}\right) \\
&- \frac{3}{2} r^2 \cdot \frac{M_4}{M_1 M_4 - M_2 M_3}\left(\left(\varepsilon_1^* - \varepsilon_2^*\right)\left(-x^2 y - y^3\right) + \gamma_{12}^*\left(x^3 + x y^2\right)\right) \\
&- \frac{1}{2} r^2 \cdot \frac{1}{\kappa_1} \cdot \frac{-3M_4 R^4 + M_3 R^2}{M_1 M_4 - M_2 M_3}\left(\left(\varepsilon_1^* - \varepsilon_2^*\right)\frac{x^2 y - y^3}{\left(x^2 + y^2\right)^2} - \gamma_{12}^* \frac{x^3 - x y^2}{\left(x^2 + y^2\right)^2}\right) \\
&- r^2 \cdot \frac{\varepsilon_1^* + \varepsilon_2^*}{M_5 + M_6} \cdot \frac{y}{x^2 + y^2} \\
&- \frac{1}{2}\left(\frac{\kappa_1 - \Gamma\kappa_2}{1 + \Gamma\kappa_2} \cdot \frac{M_4 r^8}{M_1 M_4 - M_2 M_3}\right)\left(\left(\varepsilon_1^* - \varepsilon_2^*\right)\frac{x^2 y - y^3}{\left(x^2 + y^2\right)^3} - \gamma_{12}^* \frac{x^3 - x y^2}{\left(x^2 + y^2\right)^3}\right) \\
&- \frac{1}{2}\left(\frac{r^4}{\kappa_1} \cdot \frac{-3M_4 R^4 + M_3 R^2}{M_1 M_4 - M_2 M_3}\right)\left(\left(\varepsilon_1^* - \varepsilon_2^*\right)\frac{x^2 y - y^3}{\left(x^2 + y^2\right)^3} - \gamma_{12}^* \frac{x^3 - x y^2}{\left(x^2 + y^2\right)^3}\right)
\end{aligned}
\tag{C.10}
$$

The parameters $C_0, C_1 ..., C_4$ and $M_1, M_2 ..., M_6$ are defined in Eq. (5.10) and (5.23). In addition,

$$
C_5 = \kappa_1 \frac{\left(1 + \Gamma\kappa_2\right)}{\left(\kappa_1 + 1\right)} r^2 R^2 + \left(\frac{\left(1 + \Gamma\kappa_2\right)}{\left(\kappa_1 + 1\right)} - 1\right) r^8 R^{-4} \tag{C.11}
$$

BIBLIOGRAPHY

Andreev, A.D., O'Reilly, E.P. (2000). "Theory of the electronic structure of GaN/AlN hexagonal quantum dots." *Physical Review B*, 62(23), 15851.

Demkowicz, L., Devloo, P., Oden, J.T. (1985). "On an h-type mesh-refinement strategy based on minimization of interpolation errors." *Computer Methods in Applied Mechanics and Engineering*, 53(1), 67-89.

Eshelby, J.D. (1957). "The determination of the elastic field of an ellipsoidal inclusion, and related problems." *Proc. R. Soc. Lond. A*, 241, 376-396.

Eshelby, J.D. (1959). "The elastic field outside an ellipsoidal inclusion." *Proc. R. Soc. Lond. A*, 241, 376-396.

Eshelby, J.D. (1962). "The interaction of kinks and elastic waves". *Proc. R. Soc. Lond. A*, 266(1325), 222-246.

Franciosi, P., Lormand, G. (2004). Using the radon transform to solve inclusion problems in elasticity. International Journal of Solids and Structures, 41(3), 585-606.

Frenkel, J. (1946). *Kinetic theory of liquids*, Oxf. Univ. Press.

Gao, X-L., Ma, H.M. (2010) "Solution of Eshelby's inclusion problem with a bounded domain and Eshelby's tensor for a spherical inclusion in a finite spherical matrix based on a simplified strain gradient elasticity theory." *Journal of the Mechanics and Physics of Solids* 58(5), 779-797.

Hashin, Z., Shtrikman, S. (1962). "On some variational principles in anisotropic and nonhomogeneous elasticity." *Journal of the Mechanics and Physics of Solids*, 10(4), 335-342.

Hashin, Z., Shtrikman, S. (1963). "A variational approach to the theory of the elastic behaviour of multiphase materials." *Journal of the Mechanics and Physics of Solids*, 11(2), 127-140.

Hill, R1. (1965). "A self-consistent mechanics of composite materials." *Journal of the Mechanics and Physics of Solids*, 13, 213-222.

Huang, Y., Hu, K.X., Wei, X., Chandra, A. (1994). “A generalized self-consistent mechanics method for composite materials with multiphase inclusions.” *Journal of the Mechanics and Physics of Solids*. 42(3), 491-504.

Hughes, T.J. (1995). “Multiscale phenomena: Green's functions, the Dirichlet-to-Neumann formulation, subgrid scale models, bubbles and the origins of stabilized methods.” *Computer methods in applied mechanics and engineering*, 127(1), 387-401.

Hughes, T.J., Feijóo, G.R., Mazzei, L., Quincy, J.B. (1998). “The variational multiscale method—a paradigm for computational mechanics.” *Computer methods in applied mechanics and engineering*, 166(1), 3-24.

Jasiuk, I., Chen, J., Thorpe, M.F., (1992). “Elastic moduli of composites with rigid sliding inclusions.” *Journal of the Mechanics and Physics of Solids*. 40(2), 373-391.

Jaswon, M.A., Bhargava, R.D. (1961). “Two-dimensional elastic inclusion problems.” *Proc. Camb. Phil. Soc.*, 57, 669-680.

Jin, X., Keer, L. M., Wang, Q. (2011). “A closed-form solution for the Eshelby tensor and the elastic field outside an elliptic cylindrical inclusion.” *Journal of Applied Mechanics*, 78(3), 031009.

Kim, H., Cho, J. (2008). “Superior lithium electroactive mesoporous Si@ Carbon core− shell nanowires for lithium battery anode material.” *Nano Letters*, 8(11), 3688-3691.

Kinoshita, N., Mura, T. (1984). “Eigenstrain problems in a finite elastic body.” *SIAM Journal on Applied Mathematics*. 44(3), 524-535.

Kirchner, H.O.K., Ni, L. (1993). “Domain dependence of elastic Green's, Hadamard's and Bergmann's functions.” *Journal of the Mechanics and Physics of Solids* 41(9), 1461-1478.

Kuvshinov, B.N. (2008). “Elastic and piezoelectric fields due to polyhedral inclusions.” *International Journal of Solids and Structures*, *45*(5), 1352-1384.

Kolosov, G.V. (1909). *On an application of complex function theory to a plane problem of the mathematical theory of elasticity*. Yuriev, Russia.

Kröner, E. (1986). “Statistical modelling.” In *Modelling small deformations of polycrystals* (pp. 229-291). Springer Netherlands.

Kröner, E. (1990). “Modified Green functions in the theory of heterogeneous and/or anisotropic linearly elastic media.” In *Micromechanics and inhomogeneity* (pp. 197-211). Springer New York.

Li, Q., Anderson, P.M. (2001). “A compact solution for the stress field from a cuboidal region with a uniform transformation strain.” *Journal of elasticity and the physical science of solids*, 64(2-3), 237-245.

Li, S., Sauer, R.A., Wang, G. (2005). “A circular inclusion in a finite domain I. The Dirichlet-Eshelby problem.” *Acta mechanica* 179, 67-90.

Li, S., Sauer, R.A., Wang, G. (2007a) “The Eshelby tensors in a finite spherical domain—Part I: theoretical formulations.” *J. Appl. Mech*. 74, 770-781

Li, S., Wang, G., Sauer, R.A. (2007b) “The Eshelby tensors in a finite spherical domain—Part I: applications to homogenization.” *J. Appl. Mech*. 74, 784-797

List, R.D., Silberstein, J.P.O. (1966). “Two-dimensional elastic inclusion problems.” *Proc. Camb. Phil. Soc.*, 62, 303-311

Luo, H.A., Weng, G.J. (1987) “On Eshelby's inclusion problem in a three-phase spherically concentric solid, and a modification of Mori-Tanaka's method.” *Mechanics of Materials*. 6(4), 347-361

Ma, H. M., Gao, X.-L. (2011). “Strain gradient solution for a finite-domain Eshelby-type plane strain inclusion problem and Eshelby’s tensor for a cylindrical inclusion in a finite elastic matrix.” *Int. J. Solids. Strut.* 48(1), 44-55

Makeev, M.A., Yu, W., Madhukar, A. (2003). “Stress distributions and energetics in the laterally ordered systems of buried pyramidal Ge/Si (001) islands: An atomistic simulation study.” *Physical Review B*, 68(19), 195301.

Maranganti, R., Sharma, P. (2001). “A review of strain field calculations in embedded quantum dots and wires.” *Adv. Mater*, 13, 1673.

Markenscoff, X., Dundurs, J. (2014). “Annular inhomogeneities with eigenstrain and interphase modeling.” *Journal of the Mechanics and Physics of Solids*, 64, 468-482.

Mura, T. (1987). *Micromechanics of Defects in Solids (2nd ed.).* The Netherlands: Martinus Nijhoff.

Muskhelishvili, N.I., *Some basic problems of the mathematical theory of elasticity*. Groningen: Noordhoff, 1953.

Mori, T., Tanaka, K. (1973). “Average stress in matrix and average elastic energy of materials with misfitting inclusions.” *Acta Metallurgica*, 21(5), 571-574.

Mott, N.F., Nabarro, F.R.N. (1940). “An attempt to estimate the degree of precipitation hardening, with a simple model.” *Proc. Phys. Soc.*, 52, 86-89.

Nemat-Nasser, S., Hori, M. (1999). *Micromechanics: overall properties of heterogeneous solids*. Elsevier, Amsterdam.

Nozaki, H., Taya, M. (1997). “Elastic fields in a polygon-shaped inclusion with uniform eigenstrains.” *Journal of Applied Mechanics*, 64, 495-502.

Nozaki, H., Taya, M. (2001). “Elastic fields in a polyhedral inclusion with uniform eigenstrains and related problems.” *Journal of Applied Mechanics*, 68, 441-452.

Pan, C., Yu, Q. (2014). “Inclusion problem of a two-dimensional finite domain: The shape effect of matrix”. *Mechanics of Materials*, 77, 86-97.

Pan, C., Yu, Q. (2015). “Disturbed Elastic Fields in A Circular 2D Finite Domain Containing A Circular Inhomogeneity and A Finite Interfacial Zone”. *Acta Mechanica*

Priestley, H.A. (2003). *Introduction to complex analysis*. Oxford University Press.

Prochazka, W. (1983). “Conformal mapping of the unit circle or of the upper half plane onto a polygon.” *Computing*. 31(2), 155-172.

Rodin, G.J. (1996). “Eshelby’s inclusion problem for polygons and polyhedral.” *Journal of the Mechanics and Physics of Solids*, 44, 1977-1995.

Rodin, G.J. (1998), “Discussion: Elastic fields in a polygon-shaped inclusion with uniform eigenstrains, by N. Nozaki and M. Taya” *J. Appl. Mech*. 65, 278.

Ru, C.Q. (1999). “Analytic solution for Eshelby’s problem of an inclusion of arbitrary shape in a plane or half-plane.” *Journal of applied mechanics*, 66(2), 315-322.

Ru, C.Q. (2000). “Eshelby's problem for two–dimensional piezoelectric inclusions of arbitrary shape.” *Proc. R. Soc. Lond. A*, 456(1997), 1051-1068.

Ru, C.Q. (2001). “A two–dimensional Eshelby problem for two bonded piezoelectric half–planes.” *Proc. R. Soc. Lond. A*, 457(2008), 865-883.

Ru, C.Q. (2003). “Eshelby inclusion of arbitrary shape in an anisotropic plane or half-plane.” *Acta mechanica*, 160(3-4), 219-234.

Ryu, I., Choi, J.W., Cui, Y., Nix, W.D. (2011): “Size-dependent fracture of Si nanowire battery anodes.” *Journal of the Mechanics and Physics of Solids*, 59(9), 1717-1730.

Scrivener, K.L. (1989): *The Microstructure of Concrete. Material Science of Concrete*, Vol. 1, Edited by SKalny, Westerville, OH, pp. 127-162.

Sendeckyj, G.P. (1970). “Elastic inclusion problems in plane elastostatics.” *International Journal of Solids and Structures*, 6(12), 1535-1543

Sun, Z.H., Garboczi, E.J., Shah, S.P. (2006): “Modeling The Elastic Properties of Concrete Composites: Experiment, Differential Effective Medium Theory, and Numerical Simulation.” *Cement & Concrete Composites*, 29, 22-38.

Sharma, P., Ganti, S. (2004). “Size-dependent Eshelby’s tensor for embedded nano-inclusions incorporating surface/interface energies.” *Journal of Applied Mechanics*, 71(5), 663-671.

Sharma, P., Wheeler, L.T. (2007). "Size-Dependent Elastic State of Ellipsoidal Nano-Inclusions Incorporating Surface⁄ Interface Tension." *Journal of Applied Mechanics*, 74(3), 447-454.

Sherman, D.I. (1940). "One problem of the elasticity theory." *In Dokl. Akad. Nauk SSSR*, 27(9), 907-910.

Sherman, D.I., 1959. "On the problem of plane strain in non-homogeneous media." Non-homogeneity in Elasticity and Plasticity, 3-20.

Shodja, H.M., Tabatabaei, S.M., Kamali, M.T. (2006). "A piezoelectric-inhomogeneity system with imperfect interface." *International journal of engineering science*, *44*(5), 291-311.

Stenlund, H. (2010). "Inversion Formula". *math.GM*. arXiv:1008.0183.

Szabó, B.A. (1986). "Mesh design for the p-version of the finite element method." *Computer Methods in Applied Mechanics and Engineering*, 55(1-2), 181-197.

Theocaris, P.S., Ioakimidis, N.I. (1977). "The inclusion problem in plane elasticity." *The Quarterly Journal of Mechanics and Applied Mathematics*, 30(4), 437-448.

Timoshenko, S.P., Goodier, J.N. 1970. Theory of Elasticity, McGraw-Hill, New York.

Wang, G., Li, S., Sauer, R. (2005). "A circular inclusion in a finite domain II. The Neumann-Eshelby problem." *Acta mechanica* 179, 91-110.

Waldvogel, J. (1979). "The Newtonian potential of homogeneous polyhedra." *Zeitschrift für angewandte Mathematik und Physik ZAMP*, 30(2), 388-398.

Weng, G.J. (1990). "The theoretical connection between Mori-Tanaka's theory and the Hashin-Shtrikman-Walpole bounds." *International Journal of Engineering Science*, 28, 1111-1120.

Zienkiewicz, O.C., Zhu, J.Z. (1987). "A simple error estimator and adaptive procedure for practical engineerng analysis." *International Journal for Numerical Methods in Engineering*, 24(2), 337-357.

Zienkiewicz, O.C., Zhu, J.Z. (1992). "The superconvergent patch recovery and a posteriori error estimates. Part 1: The recovery technique." *International Journal for Numerical Methods in Engineering*, 33(7), 1331-1364.

Zienkiewicz, O.C., Zhu, J.Z. (1992). "The superconvergent patch recovery and a posteriori error estimates. Part 2: Error estimates and adaptivity." *International Journal for Numerical Methods in Engineering*, 33(7), 1365-1382.

Zou, W.N., He, Q.C., Zheng, Q.S., (2012). "Inclusions in a finite elastic body." *International Journal of Solids and Structures*. 49(13), 1627-1636.